REMARKS

The Office Action mailed February 13, 2003 has been reviewed and the comments of the Patent and Trademark Office have been considered. Claims 1-42 were pending in the application. Claims 1-28, 30-37, and 40-42 have been amended. No claims have been canceled, and no claims have been newly added. Therefore, claims 1-42 are pending in the application and submitted for reconsideration.

This amendment changes claims in this application. A detailed listing of all claims that are, or were, in the application, irrespective of whether the claim(s) remain under examination in the application, are presented, with an appropriate defined status identifier.

§ 112, second paragraph rejections

Claims 1-42 are rejected under 35 U.S.C. § 112, second paragraph, as being indefinite. In particular, the examiner questions the meanings of the terms "compactly" sintered, dense, skeletal part, the relationship between the skeletal part and calcium phosphate, the relationship between the pores, globular shape, % porosity and its measurement, and grain growth. The examiner also questions the meaning of "active" material, glass for a living body and microstructure.

In response, claims 1-37 and 40-42 have been amended to correct minor informalities, to clarify awkward phrasing and to remove element numbers to place the claims in proper U.S. format. No new matter has been added. In addition, Applicant has included Chapters 10 (Grain Growth, Sintering and Vitrification) and 11 (Mircostructure of Ceramics) of Kingery's Introduction to Ceramics and a web page introduction to a Business Communications Company report on Biocompatible Materials for the Human Body to assist the Examiner in understanding the above terms and phrases.

Applicant submits that the phrases microstructure, compactly sintered, densely sintered, % porosity, and grain growth are terms of art. For an understanding of globular shaped porosity, please see Chapter 10, section 10.2, specifically Figure 10.17. Regarding the definition of "% porosity", please see Chapter 11, section 11.1. Note, it is customary to define the % porosity as the volume of the pores divided by the total volume of the sample.

Regarding the measurement of % porosity, the resin embedding process may be used. See paragraphs [0042] and [0109] of the instant application.

Regarding skeletal part, this refers to a densely compacted, structural portion of a biomember. See paragraphs [0034] and [0059]. Additionally, Applicant notes that this terminology is the same as that used in U.S. Patent No. 6,340,648 cited by the Examiner. The relationship between calcium phosphate and the skeletal part is that calcium phosphate is the ceramic material, which when sintered forms the skeletal part of the claimed invention.

Regarding the definition of an "active" material, these include cell adhesion promoting, cell proliferation promoting materials as well as other materials. Please see paragraphs [0020] and [0123] of the instant application. Regarding glass for a living body, these are glass materials which are particularly compatible with an animal or human body. Please see paragraph [0054] of the instant application and the enclosed web page report on Biocompatible Materials for the Human Body, especially Table of Contents entries 47 and 48 (page 8 of 28).

§ 102 rejections

In the Office Action, claims 1-10, 16-21, 25-28, and 33-35 are rejected under 35 U.S.C. § 102(b) as being anticipated by International Application WO 93/04013 (hereafter "WO '013"). Claims 1-10, 16-21, 25-28, and 33-35 are rejected under 35 U.S.C. § 102(b) as being anticipated by International Application WO 98/38948 (hereafter "WO '948"). Claims 1-10, 16-21, 25-28, and 33-42 are rejected under 35 U.S.C. § 102(b) as being anticipated by International Application WO 98/20549 (hereafter "WO '549"). Claims 1-10, 12, 13, 15-22, 25-29, and 32-42 are rejected under 35 U.S.C. § 102(e) as being anticipated by U.S. patent 6,340,648 to Imura et al. (hereafter "Imura"). Applicant respectfully traverses these rejections for the following reasons.

"A claim is anticipated only if each and every element as set forth in the claim is found, either expressly or inherently described, in a single prior art reference." *Verdegall Bros. V. Union Oil Co. of California*, 814 F.2d 628, 631, 2 USPQ2d 1051, 1053 (Fed. Cir. 1987). In the present case, the independent claims include the following features:

claim 1: wherein the globular pores include a plurality of large pores having a size larger than the mean pore diameter, wherein the large pores have at least three communicating pores having a diameter of not less than 5 μm, on the average, and at least one of the communicating pores has-a diameter of not less than 25 μm,

claim 2: wherein the globular pores include a plurality of large pores having a size larger than the mean pore diameter, wherein the large pores have at least four communicating pores having a diameter of not less than 5μm, on the average, and at least one of the communicating pores has a diameter of not less than 50μm,

claim 16: wherein the large pores have at least three communicating pores having a diameter of not less than 5 μm, on the average, and at least one of the communicating pores has a diameter of not less than 25 μm,

claim 25: wherein large pores having a size larger than the mean pore diameter have at least three communicating pores having a diameter of not less than 5μm, on the average, wherein a pore among the three communicating pores has at least one communicating pore having a diameter of not less than 25 μm.

None of the references applied by the Examiner teach these features. WO '013 only discloses the final % porosity of an article made by the process taught in the reference. It is silent as to the pore size and distribution. There is nothing in the reference to indicate that the material of WO '013 meets the claimed limitations. Applicant submits that WO '013 does not anticipate claims 1, 2, 16, 25 or any of the claims which depend on these claims.

WO '948 teaches a bone implant made by process uses heat decomposable particles (page 3, line 24 to page 4, line 15). As discussed in paragraph [0045] of the instant application, this type of process results in small, sharp (non-globular) pores having communicating pores no greater than 10 μm. Thus, WO '948 does not anticipate independent claims 1, 2, 16, 25 or any of the claims which depend on these claims.

WO '549 teaches a bone substitute material which is made by combining ceramic powder with foams made of polyurathane or similar materials and heating to pyrolize the foam

to make the pores (page 5, lines 10-30). As discussed in paragraph [0045] of the instant application, this process results in small, sharp (non-globular) pores having communicating pores no greater than 10 μm. Thus, WO '549 does not anticipate independent claims 1, 2, 16, 25 or any of the claims which depend on these claims.

Imura discloses a method of making a calcium phosphate sintered body. However, Imura does not disclose a calcium phosphate sintered body having features discussed above. Further, there is nothing in the reference to indicate that the material of Imura meets the claimed limitations. Applicant submits that Imura does not anticipate claims 1, 2, 16, 25 or any of the claims which depend on these claims.

§ 103(a) rejections

Claims 11-15, 22-24, and 29-32 are rejected under 35 U.S.C. § 103(a) as being unpatentable WO '549 or WO '948 or Imura in combination with the Chistolini or Itokazu articles. Applicant respectfully traverses this rejection for the following reasons.

As discussed above, none of the primary references relied upon by Examiner teach the limitations on the communicating pores. Further, neither Chistolini nor Itokazu teach or suggest these features. Therefore, no combination of the applied references could possibly render the claims of the instant application obvious.

Conclusion

The dependent claims are also patentable for at least the same reasons as the respective independent claims on which they ultimately depend. In addition, they recite additional patentable features when considered as a whole.

In view of the foregoing, applicant respectfully submits that the application is in condition for allowance and an early notice to this effect is earnestly solicited. If there are any questions regarding the application or if an examiner's amendment or an interview would facilitate the allowance of one or more of the claims, the examiner is courteously invited to contact the undersigned attorney at the local number below.

Respectfully submitted,

Date August 13, 2003

By Martin Sulsky

FOLEY & LARDNER
Customer Number: 22428
22428
PATENT TRADEMARK OFFICE
Telephone: (202) 945-6162
Facsimile: (202) 672-5399

Richard L. Schwaab
Attorney for Applicant
Registration No. 25,479

Martin S. Sulsky
Registration No. 45,403

Attached: Three references

Should additional fees be necessary in connection with the filing of this paper, or if a petition for extension of time is required for timely acceptance of same, the Commissioner is hereby authorized to charge deposit account No. 19-0741 for any such fees; and applicant hereby petitions for any needed extension of time.

Business Communications Company, Inc.
25 Van Zant Street, Suite 13, Norwalk, Connecticut 06855-1781.
Telephone: 203.853-4266. Fax: 203.853-0348

B-072N Biocompatible Materials for the Human Body

Barbara Breindel

Published July 2003
$3,650.00 for full report (add 15% for PDF version)

INTRODUCTION

STUDY GOAL AND OBJECTIVES

This study, *Biocompatible Materials for the Human Body*, examines the market for biocompatible materials used in medical devices on or within the human body. Biocompatible materials used in the worldwide $50 billion end-use device market account for current annual sales of approximately $1 billion. This study focuses on the current major materials, including medical-grade polymers, metals, advanced ceramics, pyrolytic carbon, composites, and natural materials. End-use devices include implants, valves, grafts, pacemakers, bone repair and replacement devices, artificial organs, dental materials, drug-delivery systems, dialysis/separation/filtration systems, and catheters and stents.

This report provides the reader with a comprehensive description and evaluation of this dynamic marketplace so that its significance to the practice of modern medicine can be understood. It will supply information on the structure, size, and dynamics of the major end-market segments, as well as provide a full description of the materials markets, including corporate strategies. Other areas covered include technological and research advances, regulatory impact, and international developments. Particular emphasis is placed on technological advances, and research and development activities that will yield the products of the future.

REASONS FOR DOING THIS STUDY

The market for biocompatible materials has expanded dramatically since Business Communications Co. (BCC) last looked at it in 1990. The market has seen advances resulting from new technologies, and demand for end-use devices has increased as the result of the wider use of improved devices. It is BCC's goal to identify and examine these trends and to forecast future market changes through the year 2008.

SCOPE AND FORMAT

This study will provide a description of the market for biocompatible materials in the U.S. and will also include an overview of the worldwide nature of the industry. It focuses on key market segments and important industry players within these segments. Specifically, this report will cover the following:

- Describe the biocompatible materials industry, the end-user segments, and their changing demands;
- Analyze market influences in the industry and predict the changes that will shape the future market;
- Discuss trends within the market segments and provide a future outlook for each segment;
- Review business activities of market leaders in each segment; and
- Highlight emerging and leading technologies that are likely to have an impact in the future.

CONTRIBUTIONS OF THE STUDY AND AUDIENCE

This study of the changing biocompatible materials for the human body market will prove particularly beneficial to those involved in the medical and medical device industries. Participants holding marketing, management, and technical development positions will find it of particular interest. It will also benefit readers who are suppliers to this industry, as well as investors, venture capitalists, reimbursers, and those interested biocompatible devices.

METHODOLOGY AND INFORMATION SOURCES

The primary data collection methodology for this report focuses on interviews with industry personnel, government agency personnel, industry observers, scientists, and industry professional organizations. In addition to these primary data sources, secondary data research techniques include a literature search of BCC's extensive library, as well as medical and business libraries.

All data collected were analyzed by BCC personnel to determine specific findings and make forecasts. Once these forecasts were obtained, they were validated by consultation with industry experts. Consequently, all estimates provided in this report represent a consensus opinion of BCC personnel, industry participants, and industry observers. Growth forecasts are made in constant dollars based on the U.S. manufacturers' (wholesale) price level unless otherwise noted.

ABOUT THE AUTHOR AND RELATED BCC WORK CREDENTIALS

Barbara Breindel, the author and project director of this report, holds both medical technology and advanced marketing degrees. Further supporting the analyst's knowledge in this area is an extensive experience in the pharmaceutical industry, the medical device industry, and other high-technology markets. Other published and related BCC studies include:

- C-088R The Dynamic Antibody Industry
- C-103 Expanding Horizons for Gene Probes
- C-060 New Directions in Diagnostic Testing
- C-084 Microorganism Testing
- C-104 Drug Monitoring and Drug-Abuse Testing
- C-140R Trends in the Noninvasive and Minimally Invasive Medical Device Market
- GB-157 The Dental Market
- C-181R New Strategies in Drug Marketing
- B-108 Bulk Pharmaceutical Actives
- GA-056N Sterilization Technology Advancing into the Twenty-First Century
- B-111R Drugs & Cosmetics for Aging Boomers: A Surging Market
- C-045X Medical Diagnostic Kits & Products
- C-181R The Evolving Drug Industry: New Strategies, New Products
- B-168 The Changing U.S. Clinical Diagnostics Equipment Market
- B-170 Antisense Products: Technologies, Markets
- B-122R Telemedicine: Opportunities for Medical and Electronics Providers
- B-177 The Market for Antifungal Drugs
- B-130R The Expanding Market for Psychotherapeutic Drugs - Updated Edition
- C-141N New Treatments and Advances in Immune Diseases
- B-142R Genomics-based Approaches to Drug Target Validation
- B-188 Analysis of New Marketing Strategies to Expand Drug Markets
- C-140N Trends in the Noninvasive and Minimally Invasive Medical Device Market
- B-166 Biological, Chemical and Nuclear Terrorism: Potential Diagnostic and Treatment Costs to the U.S.
- B-103R The Market for Tissue and Organ Transplantation
- C-184R Biomaterials from Marine Sources
- B-121N Plant-Derived Drugs: Products, Technology, Applications
- B-176 Biological Response Modifiers
- C-068U Inert Ingredients for Drugs
- B-159 Biosensors and Bioelectronics
- Bimolecular Diagnostics News, *a monthly newsletter*

TABLE OF CONTENTS

Back

WILEY SERIES ON THE SCIENCE AND TECHNOLOGY OF MATERIALS
Advisory Editors: **E. Burke, B. Chalmers, James A. Krumhansl**

INTRODUCTION TO CERAMICS, SECOND EDITION
W. D. Kingery, H. K. Bowen, and D. R. Uhlmann
ANALYSIS OF METALLURGICAL FAILURES
V. J. Colangelo and F. A. Heiser
THERMODYNAMICS OF SOLIDS: SECOND EDITION
Richard A. Swalin
GLASS SCIENCE
Robert H. Doremus
THE SUPERALLOYS
Chester T. Sims and William C. Hagel, editors
X-RAY DIFFRACTION METHODS IN POLYMER SCIENCE
L. E. Alexander
PHYSICAL PROPERTIES OF MOLECULAR CRYSTALS, LIQUIDS, AND GLASSES
A. Bondi
FRACTURE OF STRUCTURAL MATERIALS
A. S. Tetelman and A. J. McEvily, Jr.
ORGANIC SEMICONDUCTORS
F. Gutmann and L. E. Lyons
INTERMETALLIC COMPOUNDS
J. H. Westbrook, editor
THE PHYSICAL PRINCIPLES OF MAGNETISM
Allan H. Morrish
PHYSICS OF MAGNETISM
Sōshin Chikazumi
PHYSICS OF III-V COMPOUNDS
Otfried Madelung (translation by D. Meyerhofer)
PRINCIPLES OF SOLIDIFICATION
Bruce Chalmers
THE MECHANICAL PROPERTIES OF MATTER
A. H. Cottrell
THE ART AND SCIENCE OF GROWING CRYSTALS
J. J. Gilman, editor
SELECTED VALUES OF THERMODYNAMIC PROPERTIES OF METALS AND ALLOYS
Ralph Hultgren, Raymond L. Orr, Philip D. Anderson and Kenneth K. Kelly
PROCESSES OF CREEP AND FATIGUE IN METALS
A. J. Kennedy
COLUMBIUM AND TANTALUM
Frank T. Sisco and Edward Epremian, editors
TRANSMISSION ELECTRON MICROSCOPY OF METALS
Gareth Thomas
PLASTICITY AND CREEP OF METALS
J. D. Lubahn and R. P. Felgar
PHYSICAL METALLURGY
Bruce Chalmers
ZONE MELTING, SECOND EDITION
William G. Pfann

Introduction to Ceramics

Second Edition

W. D. Kingery
PROFESSOR OF CERAMICS
MASSACHUSETTS INSTITUTE OF TECHNOLOGY

H. K. Bowen
ASSOCIATE PROFESSOR OF CERAMICS
MASSACHUSETTS INSTITUTE OF TECHNOLOGY

D. R. Uhlmann
PROFESSOR OF CERAMICS AND POLYMERS
MASSACHUSETTS INSTITUTE OF TECHNOLOGY

A Wiley–Interscience Publication
JOHN WILEY & SONS, New York • Chichester • Brisbane • Toronto

Library of Congress Cataloging in Publication Data:

Kingery, W. D.

Introduction to ceramics.

(Wiley series on the science and technology of materials)

"A Wiley-Interscience publication."

Includes bibliographical references and index.

I. Ceramics. I. Bowen, Harvey Kent, joint author. II. Uhlmann, Donald Robert, joint author. III. Title.

TP807.K52 1975 666 75-22248

ISBN 0-471-47860-1

Printed in the United States of America

10 9 8 7 6 5 4

Preface to the Second Edition

During the fifteen years which have passed since the first edition was published, the approach described has been widely accepted and practiced. However, the advances made in understanding and controlling and developing new ceramic processes and products have required substantial modifications in the text and the introduction of a considerable amount of new material.

In particular, new and deeper understanding of the structure of noncrystalline solids and the characteristics of structural imperfections, new insight into the nature of surfaces and interfaces, recognition of spinodal decomposition as a viable alternative to classical nucleation, recognition of the widespread occurrence of phase separation, development of glass-ceramics, clearer understanding of some of the nuances of sintering phenomena, development of scanning electron microscope and transmission electron microscope techniques for the observation of microstructure, a better understanding of fracture and thermal stresses, and a myriad of developments relative to electrical, dielectric, and magnetic ceramics have been included. The breadth and importance of these advances has made a single author text beyond any individual's competence.

The necessary expansion of material related to physical ceramics, and the recent availability of excellent texts aimed at processing and manufacturing methods [F. N. Norton, *Fine Ceramics*, McGraw-Hill, New York (1970); F. H. Norton, *Refractories*, McGraw-Hill, New York (1961); F. H. Norton, *Elements of Ceramics*, second ed., Addison Wesley Publ. Co. (1974); F. V. Tooley, ed., *Handbook of Glass Manufacture*, 2 Vols., Ogden Publ. Co. (1961); A. Davidson, ed., *Handbook of Precision*

11

Microstructure of Ceramics

One of the main principles on which this introduction to ceramics is based is that the properties of ceramic products are determined not only by the composition and structure of the phases present but also by the arrangement of the phases. The phase distribution or microstructure in the final ware depends on the initial fabrication techniques, raw materials used, phase-equilibrium relations, and kinetics of phase changes, grain growth, and sintering. In this chapter the resulting structures for a number of different systems are discussed.

11.1 Characteristics of Microstructure

The observation and interpretation of microstructure have a long history in geology, metallurgy, and ceramics. Many of the most fruitful analyses of ceramic microstructures were carried out in the period 1910–1930, so that this is by no means a new subject. However, new developments in techniques and the understanding of factors affecting microstructure development have provided a more complete picture of what the structure is actually like and better interpretation of its origin.

The characteristics of microstructure that can be determined are (1) the number and identification of phases present, including porosity, (2) the relative amounts of each phase present, and (3) characteristics of each phase, such as size, shape, and orientation.

Techniques of Studying Microstructure. Many different techniques of studying microstructure have been used; the two most widely used optical methods are observations of thin sections with transmitted light and observations of polished sections with reflected light. Thin-section techniques use light passing through a section that is 0.015 to 0.03 mm thick. The section is prepared by cutting a thin slice of material, polishing one side, cementing this side to a microscope slide, and then grinding and polishing

the other side to obtain a section of the required uniform thickness. The method is advantageous in that the optical properties of each phase present can be determined and the phases thus identified. It suffers from two main disadvantages: first, specimens are difficult to prepare, and, second, the individual grains in many fine-grained ceramic materials are smaller in size than the section thickness, which leads to confusion, particularly for those who are not experts. In general, considerable experience is necessary to use thin-section techniques to best advantage.

Polished sections are usually prepared by mounting a cut specimen in Bakelite or Lucite plastic and then grinding and polishing one face smooth, using a series of abrasive papers followed by abrasive powders on cloth wheels. Polished surfaces can be observed directly with reflected light in a metallurgical microscope to distinguish pore structure and, in some ceramics, to distinguish differences in relief or reflectivity between different phases. Usually, however, different phases are best distinguished after chemical etching. When the sample is subjected to a chemical reagent, some phases are more rapidly attacked than others; grain boundaries are usually the most rapidly dissolved. Resulting differences in relief and surface roughness allow a distinction among the phases present. Polished sections are advantageous in that they are relatively easy to prepare and are simpler to interpret, particularly for a beginner. Phases present cannot be identified by their optical properties but can be distinguished and sometimes identified by their etching characteristics. Suitable etchants must be developed for each class of material. As discussed in Chapter 13, the reflectivity of a transparent material depends on its index of refraction; for a silicate with a refractive index of 1.5 only about 4% of normal incident light is reflected. For these materials a xenon or arc-light source is preferred; as an alternative a thin layer of highly reflective gold may be evaporated from a tungsten filament onto the sample surface.

The resolution obtainable in a microscope is limited by the wavelength of light used, and in practice optical microscopy is limited to a magnification of about 1000×. By using an electron beam with a wavelength measured in angstroms, the resolution can be improved to some tens of angstroms (or less with special techniques), and magnifications of 50,000× can be readily achieved. As with light microscopy, thin sections can be viewed with transmitted electrons. In this mode a sample thickness of less than about 10,000 Å (1 micron) is required, preferably less than 1000 Å (0.1 micron). Samples this thin cannot usually be prepared by grinding but require in addition either chemical thinning or thinning by argon ion bombardment. For survey studies it is often possible to shatter a specimen and then use the thin edges of the resulting particles for

transmission electron microscopy. One of the powerful advantages of electron microscopy is that selected area electron diffraction patterns can serve to identify and characterize phases just as they are seen in the microstructure.

Scanning electron microscopy uses an electron beam which scans the surface, causing the emission of secondary electrons suitable for viewing. A wide range of magnifications is possible, 20× to 50,000×, and a smooth surface is not required. To prevent electrostatic charging of the surface of ceramic insulators, they must be coated with a thin layer of gold evaporated from a tungsten filament onto the sample surface. Scanning electron microscopy is particularly useful for observing surface features and fracture surfaces but is widely applicable to general microstructure observations as well. A special advantage of this method is that by analysis of the electron emission energy spectrum from a point on the sample, its approximate chemical composition can be determined in situ.

Many other techniques are useful for determining phase distribution, morphology, and characteristics in ceramic materials. Phase microscopy allows greatly increased depth resolution. Use of polarized light with polished or thin sections aids in phase identification. Stereoscopic microscopy, X-ray microscopy, dark-field electron microscopy, and many other special methods are useful and should be considered as possible techniques for each particular problem. The best methods vary from sample to sample, and any general rule would be subject to many exceptions. For most purposes preparation and examination of polished sections by optical or scanning electron microscopy together with X-ray diffraction or microscopic phase identification constitutes a good basic procedure.

Porosity. A phase that is almost always present in ceramics prepared by powder compaction and heat treatment is porosity. Porosity can be characterized by the volume fraction of pores present and their size, shape, and distribution compared with other phases. The amount of porosity can vary from zero to more than 90% of the total volume; this is the basic measurement required, but it is not sufficient. Many properties are also strongly dependent on pore shape and distribution. For example, the direct-current electrical conductivity and also thermal conductivity change with porosity between wide limits (Fig. 11.1). These limits can perhaps be best visualized by considering an idealized case of parallel slabs, as shown in Fig. 11.2. Here the low conductivity (high resistance) of the porosity is in series with the solid for electrical or heat flow normal to the slabs and

$$\frac{1}{k_t} = \frac{f_s}{k_s} + \frac{f_p}{k_p} \qquad (11.1)$$

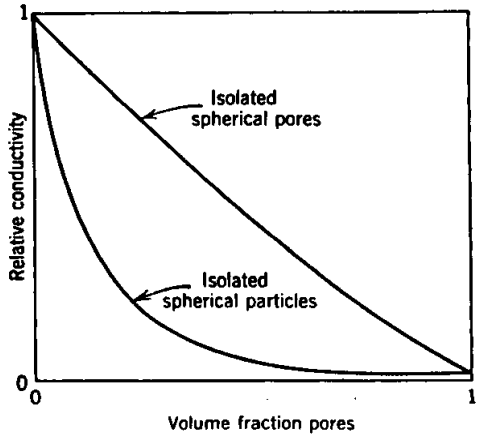

Fig. 11.1. Effect of porosity on direct-current electrical conductivity or on thermal conductivity. Upper curve, isolated spherical pores in a continuous solid matrix; lower curve, isolated solid particles in a continuous pore matrix.

where k_p and k_s are the conductivity of the pore and solid phases and f is the volume fraction for each phase. If k_p is much less than k_s, then k_t nearly equals k_p/f_p. In contrast, for flow parallel to the slabs each conducts heat or electricity with the same thermal or potential gradient and

$$k_t = f_s k_s + f_p k_p \qquad (11.2)$$

If k_p is much less than k_s, then k_t nearly equals $f_s k_s$.

In general, samples with low porosity nearly approach a continuous

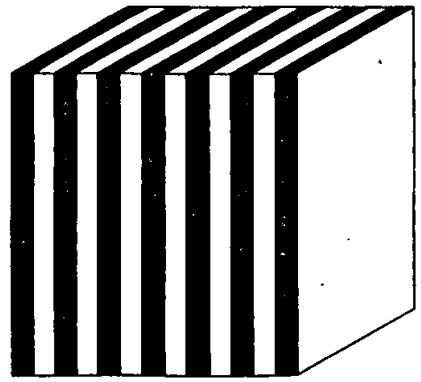

Fig. 11.2. Parallel slabs of pore space and solid material.

solid phase, and samples with high porosity tend to approach a continuous pore phase to give an S-shaped property-variation curve (Fig. 11.1). However, this does not always happen. Although a high-fired porcelain such as that shown in Fig. 11.3 closely approaches having isolated

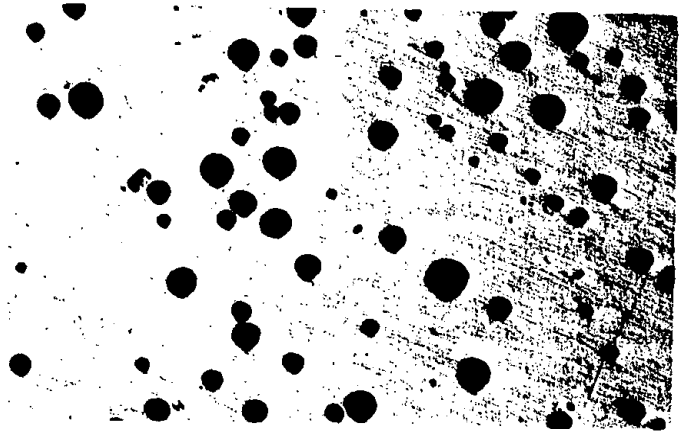

Fig. 11.3. Pore structure in high-fired Japanese hard porcelain (95×, unetched).

spherical pores, the low-porosity large-grain Al_2O_3 sample shown in Fig. 5.15 has flat cracks along many grain boundaries that closely approach a continuous pore phase, even though the fraction porosity is low. Similarly, a foam glass structure is essentially a continuous-solid-phase–isolated-pore-phase structure, even though the porosity is high.

Porosity can also be characterized by its relation to other phases. The nearly spherical pores in Fig. 11.3 are considerably larger than the other constituents. In contrast, the fine pores in the recrystallized alumina shown in Fig. 10.16*b* are similar in shape but are nearly all inside individual grains. The same-size pores in Fig. 10.16*a* are nearly all on grain boundaries. These distinctions can have an important effect on sintering, grain growth, and high-temperature deformation properties. As already mentioned, the shape of pores also affects properties. An interesting example of porosity with crystallographic orientation and crystallographic faces developed is given in Fig. 11.4.

One of the common methods of characterizing porosity is as *apparent porosity*—those pores connected to the surface, or *open pores*. In contrast the *total porosity* includes both the open and the *closed pores*—those not connected to the surface. Obviously, the open pores

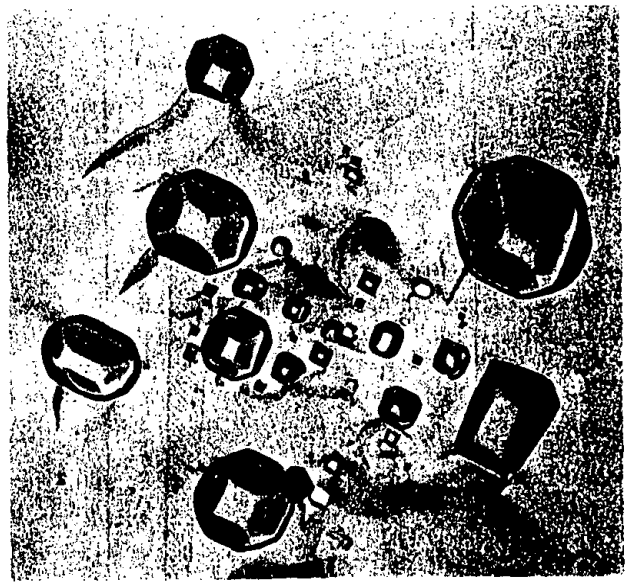

Fig. 11.4. Pores which have formed "negative" crystals in UO_2; (100) planes are parallel to surface (18,000×). Courtesy T. R. Padden.

directly affect properties such as permeability, vacuum tightness, and surface available for catalytic reactions and chemical attack, whereas closed pores have little effect on these properties.

Before firing, almost the entire porosity is present as open pores. During firing, the volume fraction porosity decreases, as discussed in Chapter 10. Although some open pores are eliminated directly, many are transformed into closed pores. As a result, the volume fraction of closed pores increases initially and only decreases toward the end of the firing process. Open pores are generally eliminated when the porosity has decreased to 5%. This is illustrated for the permeability of ceramics to gas flow in Fig. 11.5. By the time 95% of theoretical density is reached, the ware is gastight.

Single-Phase Polycrystalline Ceramics. In addition to porosity it is necessary to determine the amount, size, shape, and distribution of other constituents present in order to characterize a microstructure completely. In the simplest case this is a single phase. The microstructure of a polycrystalline ceramic normally develops as grains that meet at *faces* whose intersections form angles of 120° (discussed in Chapters 5 and 10).

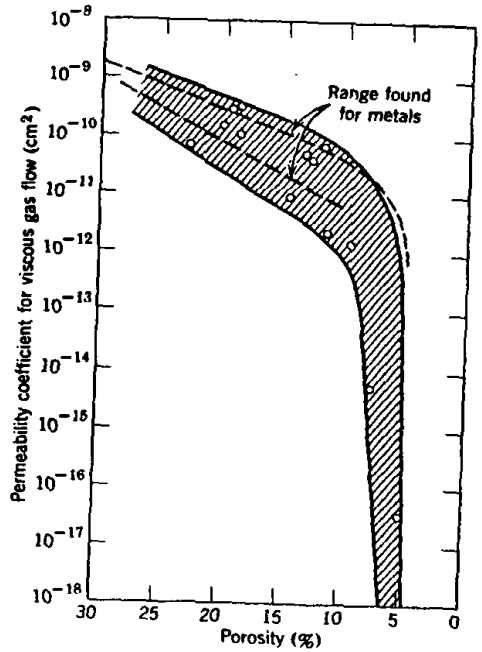

Fig. 11.5. Permeability coefficient for viscous gas flow in beryllia ware of differing porosity. Permeability drops rapidly when the porosity is below 5 to 8%. After J. S. O'Neil, A. W. Hey, and D. T. Livey, U.K. AERE-R3007.

Viewed in a polished section we cannot see the three-dimensional form which is apparent in Fig. 5.15. However, there are only a limited number of ways in which grains satisfying the 120°-angle requirement at the intersection of three grains to form a common boundary can be shaped to fit together and fill space. It is found that grains of many different materials usually have nine to eighteen faces, each face with four to six edges, as discussed in the next section. However, in some materials a duplex structure is developed in which some large grains grow in a fine-grained matrix (Figs. 10.12, 10.13, and 10.15). Also, grains are sometimes columnar, prismatic, cubic, spheroidal, or acicular or have some other special habit of growth; these shapes can give rise to special properties such as those of the oriented ferrites.

In single-phase ceramics the nature and composition of dislocations, subgrain boundaries, and grain boundaries (Figs. 4.23 and 4.24) are frequently important. These often have definite structural characteristics

such as specific orientation, concentration, and impurity segregations. However, they are more difficult to investigate than the gross microstructure.

Multiphase Ceramics. In multiphase compositions we must also consider the relationships among the amount, distribution, and orientation of separate phases. Perhaps the most common structure is one or more phases dispersed in a continuous matrix. These can be prismatic crystals in a glass, such as the forsterite-glass ceramic shown in Fig. 7.33, or they can be crystals precipitated on a crystalline matrix, as shown in Figs. 9.40 to 9.43. The crystalline habit may be cubic, prismatic, columnar, dendritic, acicular, or parallel plates or be formed in other specific shapes. They can be orientated with regard to the matrix and in some ceramics are preferentially found along grain boundaries, subgrain boundaries, or other preferred sites. Another common structure is large particles held together with a bond forming lenses between the grains.

The multiplicity of possible phase relations in complex systems makes the microstructure of ceramics a fascinating and valuable study, essential for understanding the effects of processing or environmental variables on properties.

11.2 Quantitative Analysis

Space Filling. Much of our understanding and interpretation of microstructures are based on the interface energy relationships discussed in Chapter 5 and the rate processes discussed in Chapters 8, 9, and 10. However, even the effects of these are limited by geometrical restrictions to the way in which an area or volume can be filled. If we consider a plane surface, for example, the only regular polygons that can fill an area are triangles, rectangles, or hexagons. Various irregular polygons can also fill space. In this case there is a definite relationship between the number of polygons P, edges between polygons E, and corners C which is given by Euler's law:

$$C - E + P = 1 \tag{11.3}$$

This law applies equally well to grain boundaries seen in a polished section and craze marks on a teacup. If the number of sides on an average polygon is $n = 2E/P$, from Eq. 11.3

$$n = 2\frac{C}{P} + 2 - \frac{2}{P} \tag{11.4}$$

The most common corners are those where three edges meet ($C/P = 1/3n$); much less common are corners where four edges meet ($C/P =$

$1/4n$). If we restrict the structure to one with the simplest corners with three grains meeting, the *average polygon* must be a hexagon.

As discussed in Chapter 5, a balance of the grain-boundary energies where three grain corners come together requires that the boundaries meet at an angle of 120°. If this requirement is met, the only equilibrium shape is a hexagon. Polygons with fewer or more than six sides, have curved faces and a pressure difference across these curved faces, and the boundaries tend to migrate. Grains with fewer than six sides shrink, and grains with more than six sides grow (Chapter 10).

In three dimensions there are similar geometric restrictions to filling space with regular polyhedra. For any system the number of corners, edges, faces, and polyhedra must obey a relation:

$$C - E + F - P = 1 \tag{11.5}$$

In addition, if interface energy relationships are to be fulfilled, there must be an angle of 120° between faces where three grains meet along a common boundary and angles of 109½° where four faces meet at a point. These relationships are nearly met, and space is filled by the packing of truncated octahedra (tetrakaidecahedra) (Fig. 11.6). This shape has six square faces and eight hexahedron faces with twenty-four vertices, each having two angles of 120° and one of 90°. These can be distorted to give a lower total interface energy by having all corners meeting at 109° and all edges at 120°. This sort of ideal grain is not observed exactly; studies of soap foams, plant cells, and polycrystalline metals, using stereoscopic microradiography, have shown that the number of faces in a three-dimensional grain ranges from nine to eighteen. The number of edges on

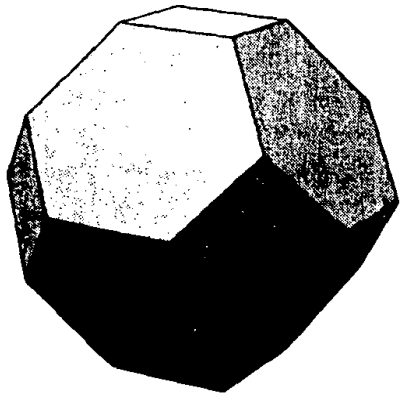

Fig. 11.6. *Truncated octahedron (tetrakaidecahedron).*

each face is most commonly five and is seldom less than four or more than six (Fig. 11.7).

As illustrated in Fig. 5.27, when a small amount of second phase is added, it can either be dispersed as isolated spherical particles or ideomorphic inclusions (Figs. 11.3 and 11.4), completely penetrate between and separate grains of the major phase (Fig. 7.11), or form between grain junctions with some equilibrium dihedral angle (observe the triangles of boundary phase with ϕ approximately 60° in Fig. 7.18). In a transparent section these angles can be measured with stereoscopic techniques or proper sample orientation. With plane sections, which often are all that are available, the plane of the polished section may lie at any angle to the line of the boundary. Consequently, a number of apparent angles is observed for any true angle present. From geometrical consider-

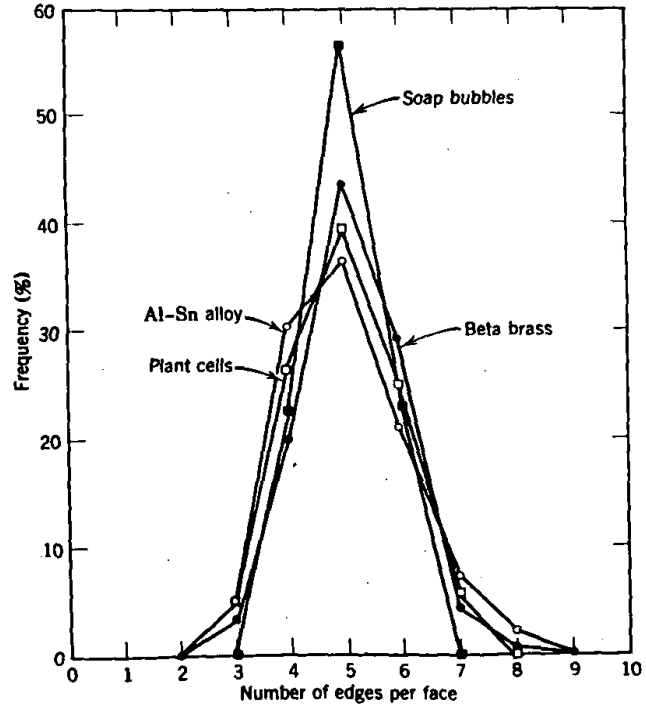

Fig. 11.7. Experimentally observed frequency distribution of the number of edges per face in various systems (reference 7).

ations D. Harker and E. R. Parker* have derived relationships between observed and true angles. A main result is that the most frequently observed angle is always equal to the average true angle. For quantitative measurements a large number of angles must be observed. From a histogram such as that shown in Fig. 11.8 the true angle can be determined; this dihedral angle characterizes one of the special relationships between phases.

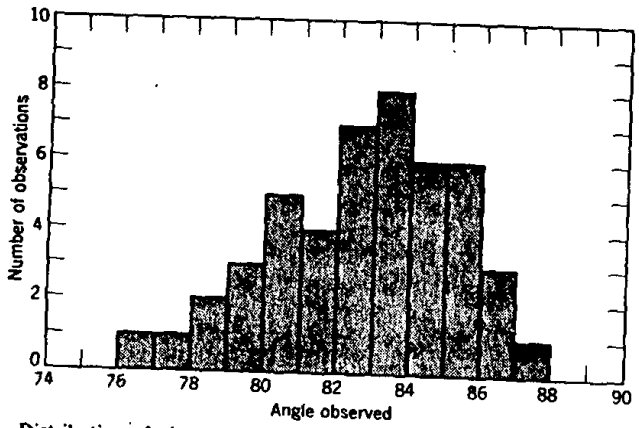

Fig. 11.8. Distribution of observed boundary angles in a polished section of the system Ni–Al_2O_3.

Relative Amounts of Phases Present. The information most frequently desired from microscopic analysis is the relative amounts of different phases present. For a random sample it can be shown that the volume fraction of a phase is equal to the cross-sectional area fraction of the phase in a random plane through the sample; it is also equal to the linear fraction of the phase intersecting a random line drawn through the sample; it is also equal to the fraction of points randomly distributed along a line over a cross-sectional area or throughout a volume that falls within the phase. Using the symbols defined in Table 11.1,

$$V_V = A_A = L_L = P_P \tag{11.6}$$

The experimental measurements on a ceramographic sample, which is a thin section (relative to particle size) or a polished plane taken from a three-dimensional sample, are usually done by a form of area, lineal, or

*Trans. Am. Soc. Met., 34, 156 (1945).

Table 11.1. Basic Symbols Used in Microstructure Analysis and Their Definitions

Symbol	Dimensions[a]	Definition
P		Number of point elements, or test points
P_P		Point fraction. Number of points (in areal features) per test point
P_L	mm^{-1}	Number of point intersections per unit length of test line
P_A	mm^{-2}	Number of points per unit test area
P_V	mm^{-3}	Number of points per unit test volume
L	mm	Length of lineal elements, or test line length
L_L	mm/mm	Lineal fraction. Length of lineal intercepts per unit length of test line
L_A	mm/mm^2	Length of lineal elements per unit test area
L_V	mm/mm^3	Length of lineal elements per unit test volume
A	mm^2	Planar area of intercepted features, or test area
S	mm^2	Surface or interface area (not necessarily planar)
A_A	mm^2/mm^2	Area fraction. Area of intercepted features per unit test area
S_V	mm^2/mm^3	Surface area per unit test volume
V	mm^3	Volume of three-dimensional features, or test volume
V_V	mm^3/mm^3	Volume fraction. Volume of features per unit test volume
N		Number of features (as opposed to points)
N_L	mm^{-1}	Number of interceptions of features per unit length of test line
N_A	mm^{-2}	Number of interceptions of features per unit test area
N_V	mm^{-3}	Number of features per unit test volume
$\bar{L}$	mm	Average lineal intercept, L_L/N_L
$\bar{A}$	mm^2	Average areal intercept, A_A/N_A
$\bar{S}$	mm^2	Average surface area, S_V/N_V
$\bar{V}$	mm^3	Average volume, V_V/N_V

[a] Arbitrarily shown in millimeters.

Source. E. E. Underwood, *Quantitative Stereology*, Addison-Wesley Publishing Company, Inc., Reading, Mass., 1970.

point analysis. *Point counting* is done by randomly distributing a grid of points over a sample in the microscope or on a photomicrograph or randomly moving a microscope cross hair and counting the fraction of the total point count that falls in a given phase P_P, which gives the volume fraction of the phases directly, as indicated in Eq. 11.6. In lineal analysis, a line in the microscope objective or one drawn across a micrograph is used, and the fractional length intercepting each phase L_L is measured. This can be done manually or with an integrating stage micrometer, which is more convenient. Areal analysis to determine the relative area of each phase A_A in the planar section is less commonly done, because it is slower than point counting or lineal analysis. Relative areas can be determined from tracings with a planimeter, by cutting out the separate phases from a micrograph and weighing them, or by counting squares on a grid placed over the micrograph. Modern developments in electronic scanning instrumentation may well bring back the importance of areal analysis.

In addition to determining the volume fraction of the phases present, relatively simple measurements and statistical analyses give a range of additional information about microstructure characteristics important for special purposes. The basic measurements with a known length of test line L, for which the magnification must be known, are the number of intersections of a particular feature such as phase boundaries along the line P_L and the number of interceptions of objects such as particles along the line N_L. Related measurements can be made of the number of points, such as three-grain intersections observed in a known area A, which is P_A, or the number of objects, such as grains, in a known area N_A. From these measurements, one can calculate directly the surface area per unit volume S_V, the length of lineal elements per unit volume L_V, and the number of point elements per unit volume P_V:

$$S_V = \left(\frac{4}{\pi}\right) L_A = 2P_L \tag{11.7}$$

$$L_V = 2P_A \tag{11.8}$$

$$P_V = \left(\frac{1}{2}\right) L_V S_V = 2P_A P_L \tag{11.9}$$

Sizes and Spacing of Structure Constituents. In observing microstructures, it is frequently found that there are two or more levels of structure. There is first a structure associated with the distribution of relatively large pores, grog (prefired clay) particles, or other grains in a matrix phase. Second, there is a structure of phase distribution within the large grains and within the bond phase. Also we are often concerned with the distribution of dislocations and the separation between various structure

constituents. It is often necessary to use different techniques for a study of each of these characteristics. For example, we may use a thin or polished section to study the larger-scale structure together with scanning electron microscopy to study a fine-clay matrix. Which level of structure is most important depends on the particular ceramic and the particular property of interest, and it is necessary to be selective about what is critical for a particular problem.

As a particle parameter, the mean intercept length $\bar{L} = L_L/N_L$ is a simple and convenient measurement to characterize particle size. For spherical particles or rods of uniform size, the mean intercept length gives a measure of the particle radius r:

$$\bar{L} = \frac{4}{3} r \qquad \text{sphere} \tag{11.10}$$

$$\bar{L} = 2r \qquad \text{rod} \tag{11.11}$$

and the thickness t of a plate-shaped phase

$$\bar{L} = 2t \qquad \text{plate} \tag{11.12}$$

In addition, for space-filling grains, since $\bar{L} = 1/N_L$ and $P_L = N_L$, the surface area per unit volume is given by

$$S_V = 2P_L = 2N_L = \frac{2}{\bar{L}} \tag{11.13}$$

For separated particles, $P_L = 2N_L$, and

$$S_V = 2P_L = 4N_L = \frac{4(V_V)}{\bar{L}} \tag{11.14}$$

Another important parameter in determining spatial distributions is the mean free distance between particles λ, the mean edge-to-edge distance along a straight line between the particles or phases. It is given by

$$\lambda = \frac{1 - V_V}{N_L} \tag{11.15}$$

This value is related to the mean intercept length:

$$\lambda = \frac{\bar{L}(1 - V_V)}{V_V} \tag{11.16}$$

and if the mean spacing between particle centers is S,

$$S = \frac{1}{N_L} \tag{11.17}$$

and

$$\bar{L} = S - \lambda \tag{11.18}$$

Thus, from relatively simple methods of point counting and lineal analysis, not only the volume fraction of phases present but a good deal of information about their size and spacial distribution can be determined. From a histogram of the mean intercept lengths, a calculation of the particle-size distribution can be made (reference 1). Special precautions are necessary in evaluating nonrandom-oriented and anisometric samples (references 1 and 2).

Porosity. A quantitative measurement of the porosity present is one of the characteristics of ceramics formed by compacting a powder and firing. The pores can occur in widely different sizes, shapes, and distribution, and quantitative characterization is not always simple. In many cases the best method is to use polished sections with lineal or area analysis. This is an effective method for glazes, enamels, porcelains, refractories, and abrasives and probably should be more widely used than it has been in the past. The main difficulties with this technique have arisen from (1) relatively soft specimens that are difficult to polish and (2) samples in which grains tend to pull out during polishing so that misleading high values result. Polishing soft specimens can be done satisfactorily by impregnating the sample with a resin. Pullout of individual particles is mainly caused by differences in constituent hardness or by microfissures or microstresses already present in the sample. Hardness differences cause high relief that encourages pullouts; this can be corrected by using a suitably hard abrasive for polishing (diamond powder, for example) and a hard, flat polishing surface. Microstresses or microfissures are flat cracks along grain boundaries that allow grains to pop out with very small added stresses. Pullouts that occur in spite of careful polishing technique are one of the best indications that microstresses and microfissures are present.

Density. The size, shape, distribution, and amount of the total porosity can be determined from the microstructure. The total porosity can also be measured by determining the bulk density ρ_b of a sample (total weight/total volume, including pores) and comparing this with the true density ρ_t (total weight/volume of solids). Then

$$f_p = \frac{\rho_t - \rho_b}{\rho_t} = 1 - \frac{\rho_b}{\rho_t} \tag{11.19}$$

Sometimes it is convenient to measure bulk density as the fraction of theoretical density achieved, $\rho_b/\rho_t = 1 - f_p$.

The true density can be determined readily for a single-phase material but not so easily for a polyphase material. For a crystalline solid the density can be calculated from the crystal structure and lattice constant, since the atomic weight for each constituent is known. This calculation

has been illustrated in Chapter 4. True density can also be determined by comparing porefree samples with a liquid having a known density. For glasses and single crystals this can be done by weighing the material in air and then suspended in a liquid, determining the volume by Archimedes' method; it can be done more precisely by adjusting the composition or temperature of a liquid column just to balance the density of the solid so that it neither sinks nor rises but remains suspended in the liquid. For complex mixtures and porous solids the sample must be pulverized until there are no residual closed pores, and the density is then determined by the pycnometer method. The sample is put in a known-volume pycnometer bottle and weighed; then liquid is added to give a known volume of liquid plus solid and another weight is taken. To ensure penetration of the solid among all particles, the sample and liquid should be boiled or heated under vacuum. The differences in weights obtained give the liquid volume; this is subtracted from the total pycnometer volume to give the solid sample volume from which the density can be calculated.

The bulk density of porous bodies requires determination of the total volume of solid plus pores. For samples such as bricks this can be done by measuring the sample dimensions and calculating the volume. For smaller samples bulk density can be determined by measuring the weight of mercury (or of any other nonwetting liquid that does not penetrate the pores) displaced by the sample with a mercury volumeter, or the force required to submerge the sample (Archimedes' method). For small samples bulk density can also be determined by coating the sample with an impermeable film such as paraffin. The weight of the film is measured by difference so that the film volume is known. Then the volume of the sample plus film can be determined by Archimedes' method and the sample volume measured by difference. The total porosity can be determined at the same time the open-pore volume is measured by first weighing a sample in air W_a and then heating in boiling water for 2 hr to fill the open pores completely with water. After cooling, the weight of the saturated piece is determined (1) suspended in water W_{sus} and (2) in air W_{sat}. The difference between these last two values gives the sample volume and allows calculation of the bulk density. The difference between saturated and dry weights gives the open-pore volume.

Open Porosity. Various methods have been devised for characterizing the open pores by regarding them as capillaries and determining their equivalent diameter from the rate of fluid flow through them or the extent to which liquid mercury can be forced into them. In the mercury method, for example, the sample is placed in a container and evacuated, and then mercury is admitted and pressure applied. The pressure necessary to force mercury into a capillary depends on the contact angle and surface

tension (discussed in Chapter 7) and, according to L. Lecrivain* is given by

$$P = \frac{4\gamma \cos\theta}{d} \simeq \frac{14}{d} \qquad (11.20)$$

where P is the pressure (kg/cm^2), d is the pore diameter (micron), γ is the surface tension of mercury, and θ is the contact angle (140° for most oxides). As the pressure is increased, smaller-size pores are permeated. Their amount is measured by the decrease of the apparent volume of mercury plus sample. The result attained is a distribution of open-pore sizes characteristic of a particular material. Average pore sizes for open porosity vary from less than a micron for clay and other fine-grained bodies to the millimeter range for some coarse-textured refractories.

11.3 Triaxial Whiteware Compositions

A wide range of traditional ceramic compositions, the basis for much of the whiteware industry, is mixtures of clay, feldspar, and flint. These compositions include hard porcelain for artware, tableware, vitreous sanitary ware, electrical porcelain, semivitreous tableware, hotel china, dental porcelain, and others (Table 11.2). A typical composition could be considered equal parts of china clay, ball clay, feldspar, and flint. In these

Table 11.2. Composition of Triaxial Whiteware Compositions

Type Body	China Clay	Ball Clay	Feld-spar	Flint	Other
Cone 16 hard porcelain	40	10	25	25	–
Cone 14 electrical insulation ware	27	14	26	33	–
Cone 12 vitreous sanitary ware	30	20	34	18	–
Cone 12 electrical insulation	23	25	34	18	–
Cone 10 vitreous tile	26	30	32	12	–
Cone 9 semivitreous whiteware	23	30	25	21	–
Cone 10 bone china	25	–	15	22	38 bone ash
Cone 10 hotel china	31	10	22	35	2 $CaCO_3$
Cone 10 dental porcelain	5	–	95	–	–
Cone 9 electrical insulation	28	10	35	25	2 talc

*Trans. Brit. Ceram. Soc., 57, 687 (1958).

compositions the clays serve a dual purpose of (1) providing fine particle sizes and good plasticity for forming, as discussed in Chapter 1, and (2) forming fine pores and a more or less viscous liquid essential to the firing process, as discussed in Chapter 10. The feldspar acts as a flux, forming a viscous liquid at the firing temperature, and aids in vitrification. The flint is mainly an inexpensive filler material which during firing remains unreactive at low temperature and at high temperature forms a high-viscosity liquid.

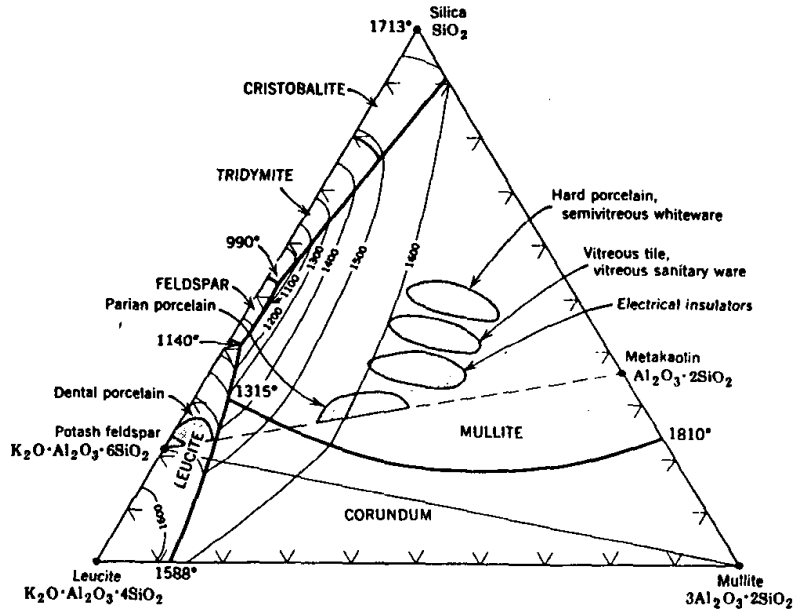

Fig. 11.9. Areas of triaxial whiteware compositions shown on the silica-leucite-mullite phase-equilibrium diagram.

Typical Compositions. Typical composition ranges for different types of bodies are illustrated in the silica-leucite-mullite phase diagram in Fig. 11.9 (these compositions can be readily visualized as flint-clay-feldspar mixtures by drawing in the feldspar-metakaolin join on the diagram). On this diagram the clays have all been lumped together. The main differences among compositions are in the relative amounts and kinds of feldspar and clay used. As an increasing amount of feldspar is added, the amount of liquid formed at the eutectic temperature increases, vitrifica-

tion proceeds at a lower temperature, there is more liquid present, and greater vitrification and higher translucency are obtained. As feldspar is replaced by clay, higher temperatures are required for vitrification, and the firing process becomes more difficult and expensive. However, the forming processes become easier, and the mechanical and electrical properties of the resulting body are improved. The amount and kinds of clay used are determined for the most part by requirements with regard to forming; as more difficult forming techniques are used, a larger clay content is required.

Considering the different compositions illustrated in Table 11.2 and Fig. 11.9, dental porcelains require higher translucency and are formed in small simple shapes so that high-feldspar–low-clay compositions are clearly indicated. In contrast, hard porcelain artware and tableware must be formed into complicated thin-wall shapes by hand throwing, jiggering, and slip casting. For successful forming it must have a substantial clay content. China clay has relatively large particles (medium plasticity, drying shrinkage, and dry strength) and is white-burning; ball clay has fine particles (high plasticity, drying shrinkage, dry strength) and contains larger amounts of impurities which make it less translucent and usually not white-burning. A balance is struck by using as much china clay as will permit successful forming. For automatic forming machines, such as those used for American hotel china and semivitreous ware, larger amounts of ball clay are used. Compositions such as low-tension electrical porcelain are not critical as regards either forming or firing operations. A balance is desired which leads to the most economical ware. Since the largest individual manufacturing cost is labor, a body is used which is easy to form but at the same time can be fired without difficulty. Firing is not carried to complete vitrification, thus avoiding problems of high firing temperature, high firing shrinkage, and warping.

Changes during Firing. The changes that occur in the structure of a triaxial porcelain during firing depend to a great extent on the particular composition and conditions of firing. As shown in Figs. 11.9 and 7.24, the ternary eutectic temperature in the system feldspar-clay-flint is at 990°C, whereas the temperature at which feldspar grains themselves form a liquid phase is 1140°C. At higher temperatures an increasing amount of liquid is formed which at equilibrium would be associated with mullite as a solid phase. In actual practice equilibrium is not reached during normal firing because diffusion rates are low and the free-energy differences are small between the various phases present. The general equilibrium conditions do not change at temperatures above about 1200°C (see Fig. 7.26) so that long firing times at this temperature give results that are very similar to shorter times at higher temperatures (the relative times required

can be determined from the temperature dependence of diffusion and viscosity, as discussed in Chapter 9). Also fine grinding to reduce diffusion paths gives equivalent results in shorter firing times or at lower temperatures.

The initial mix is composed of relatively large quartz and feldspar grains in a fine-grained clay matrix. During firing the feldspar grains melt at about 1140°C, but because of their high viscosity there is no change in shape until above 1200°C. Around 1250°C feldspar grains smaller than about 10 microns have disappeared by reaction with the surrounding clay, and the larger grains have interacted with the clay (alkali diffuses out of the feldspar, and mullite crystals form in a glass). The clay phase initially shrinks and frequently fissures appear. As illustrated in Fig. 7.29, fine mullite needles appear at about 1000°C but cannot be resolved with an optical microscope until temperatures of at least 1250° are reached. With further increases of temperature mullite crystals continue to grow. After firing at temperatures above 1400°C, mullite is present as prismatic crystals up to about 0.01 mm in length. No change is observed in the quartz phase until temperatures of about 1250°C are reached; then rounding of the edges can be noticed in small particles. The solution rim of high-silica glass around each quartz grain increases in amount at higher temperatures. By 1350°C grains smaller than 20 microns are completely dissolved; above 1400°C little quartz remains, and the porcelain consists almost entirely of mullite and glass.

The heterogeneous nature of the product is illustrated in Fig. 11.10, in which quartz grains surrounded by a solution rim of high-silica glass, the outlines of glass-mullite areas corresponding to the original feldspar grains, and the unresolved matrix corresponding to the original clay can be clearly distinguished. Pores are also seen to be present. Although mullite is the crystalline phase in both the original feldspar grains and in the clay matrix, the crystal size and development are quite different (Fig. 11.11). Large mullite needles grow into the feldspar relicts from the surface as the composition changes by alkali diffusion. A quartz grain and the surrounding solution rim of silica-rich glass is shown in Fig. 11.12. Mullite needles extend into the outer edge of the solution rim, and a typical microstress crack is seen; the crack is caused by the greater contraction of the quartz grain compared with that of the surrounding matrix. Usually the quartz forms only glass, but for some compositions fired at high temperatures there is a transformation into cristobalite which starts at the outer surface of the quartz grain (Fig. 11.13). The overall structure of quartz grains, microfissures, solution rims, feldspar relicts of glass and mullite, and fine mullite-glass matrices is shown with great clarity in Fig. 11.14.

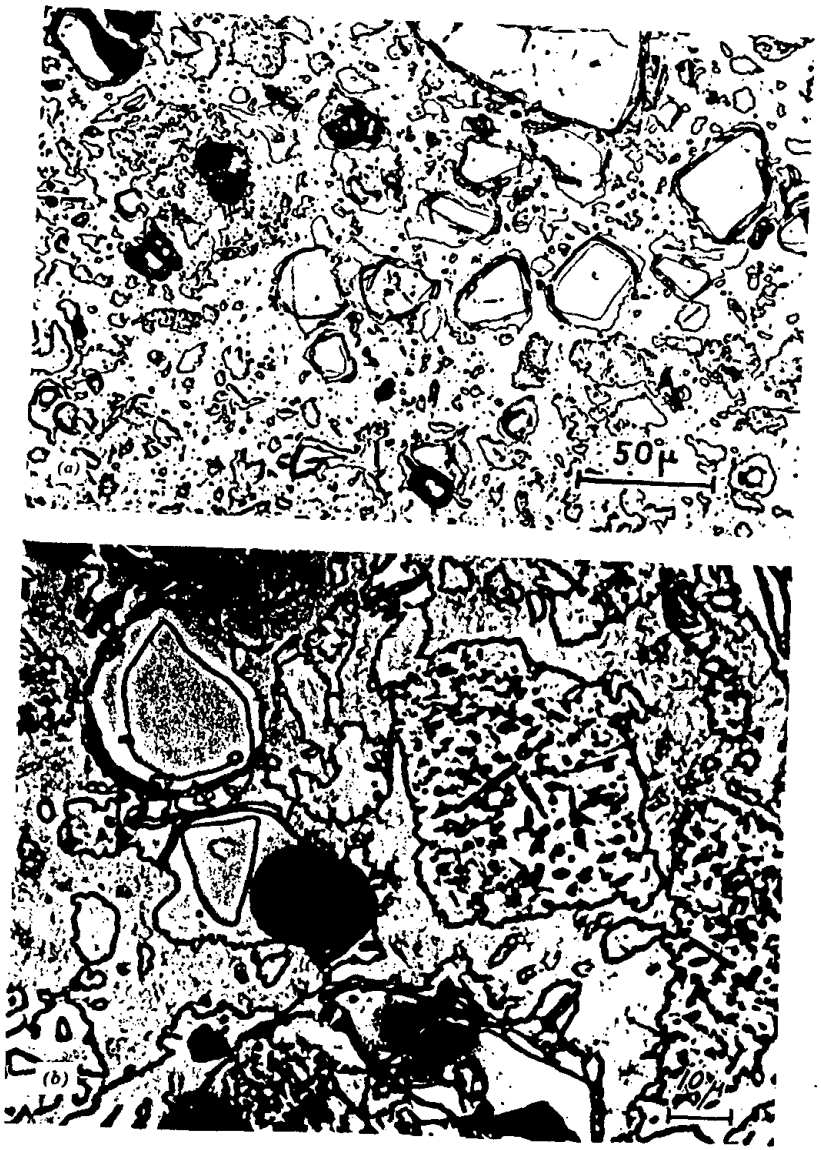

Fig. 11.10. Photomicrographs of electrical insulator porcelain (etched 10 sec, 0°C, 4% HF) showing liquid quartz grains with solution rim, feldspar relicts with indistinct mullite, unresolved clay matrix, and dark pores. Courtesy S. T. Lundin.

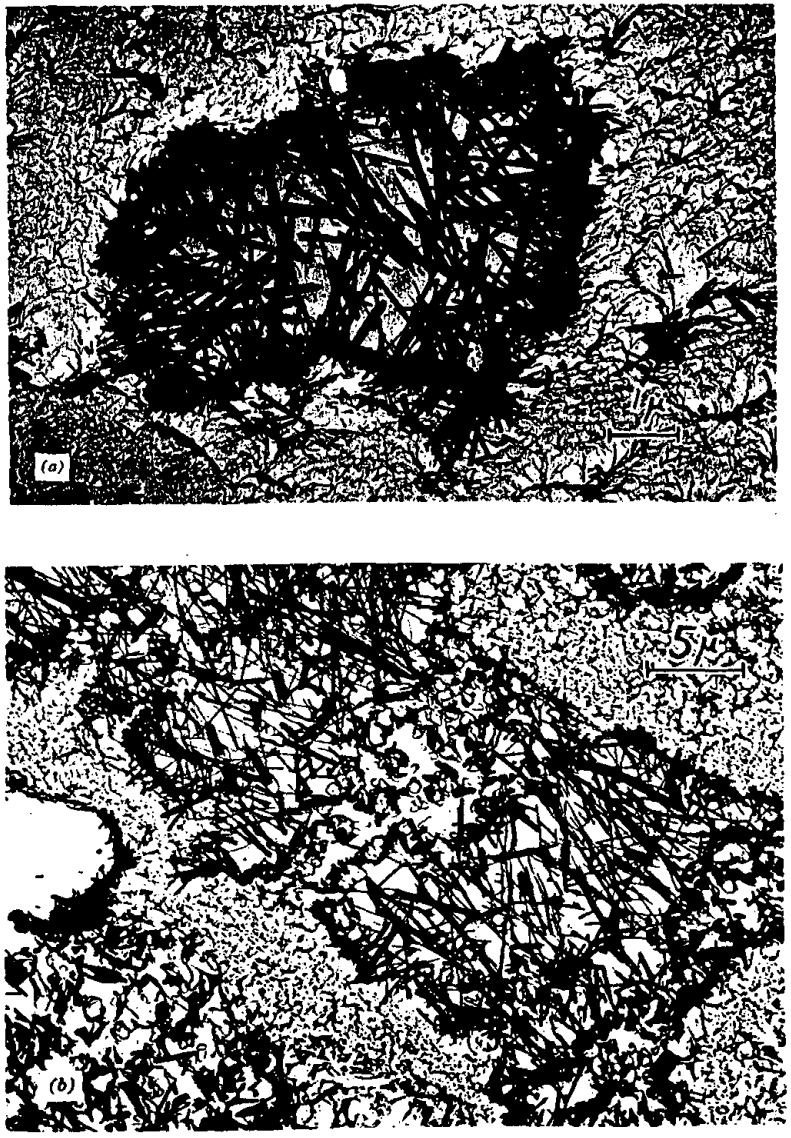

Fig. 11.11. Mullite needles growing into a feldspar relict (etched 10 sec, 0°C, 40% HF). Courtesy S. T. Lundin.

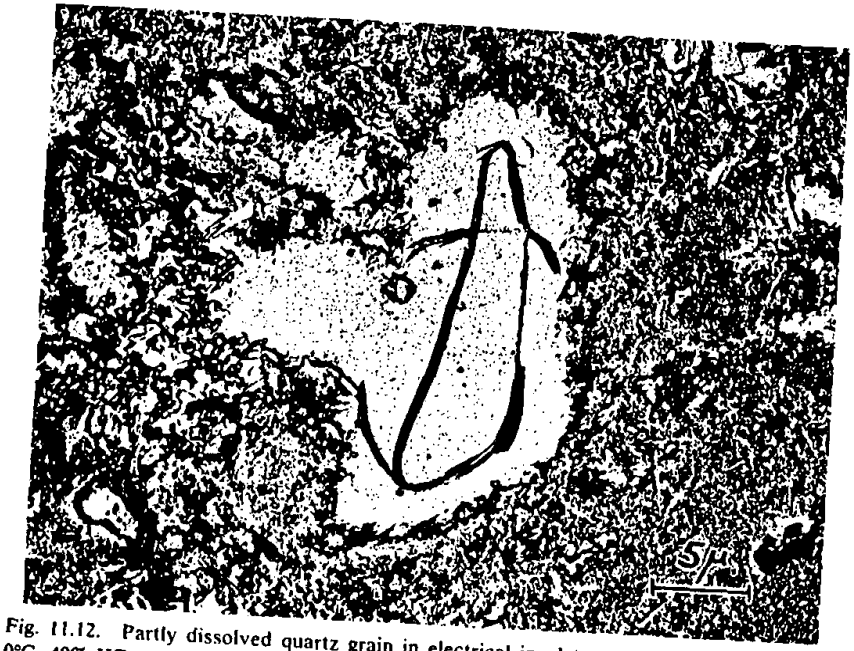

Fig. 11.12. Partly dissolved quartz grain in electrical insulator porcelain (etched 10 sec, 0°C, 40% HF, aluminum replica, 2750×. Courtesy S. T. Lundin.

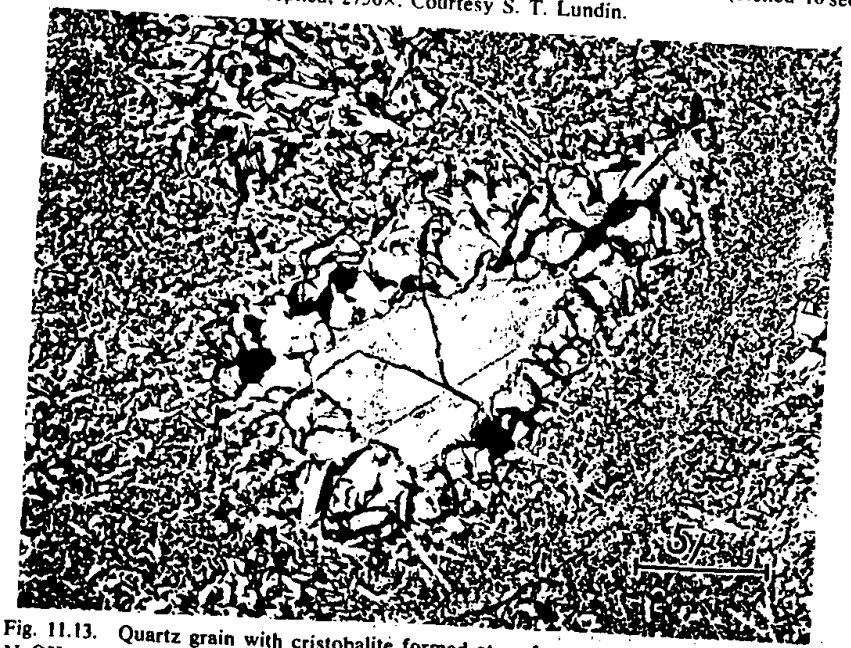

Fig. 11.13. Quartz grain with cristobalite formed at surface (etched 20 min, 100°C, 50% NaOH, silica replica. Courtesy S. T. Lundin.

Fig. 11.14. Electron micrograph of electrical insulator porcelain (etched 10 sec, 0°C, 40% HF, silica replica. Courtesy S. T. Lundin.

The changes taking place during firing occur at a rate depending on time, temperature, and particle size. The slowest process is the quartz solution. Under normal firing conditions equilibrium at the firing temperature is only achieved at temperatures above 1400°C, and the structure consists of a mixture of siliceous liquid and mullite. In all cases the liquid at the firing temperature cools to form a glass so that the resulting phases present at room temperature are normally glass, mullite, and quartz in amounts depending on the initial composition and conditions of firing treatment. Compositions with a larger feldspar content form larger amounts of siliceous liquid at lower temperatures and correspondingly vitrify at lower temperatures than the compositions with larger clay contents.

Advantages of Triaxial Porcelains. One of the great advantages of quartz-clay-feldspar bodies is the fact that they are not sensitive to minor changes in composition, fabrication techniques, and firing temperature. This adaptability results from the interaction of the phases present to increase continuously the viscosity of the fluid phase as more of it is formed at higher temperatures. If we consider the phase-equilibrium diagram in Fig. 11.9, the eutectic liquid is increased in amount but also in viscosity (silica content) as the feldspar relict interacts with the clay. At 1300°C, equilibrium is reached between the clay and feldspar to give mullite in a glassy matrix (Fig. 11.15). Further interaction with the quartz grains forms more liquid, but it is of continuously increasing silica content and is consequently more viscous. As a result of these reactions, the body has an unusually long firing range and low sensitivity to compositional variations.

11.4 Refractories

Refractory materials cover a wide range of compositions and structures and are difficult to characterize easily, particularly since the structure is

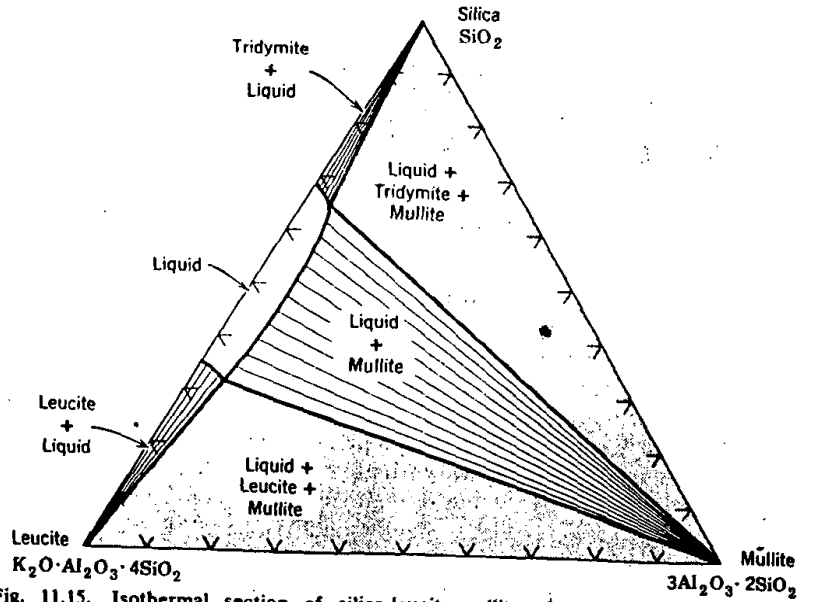

Fig. 11.15. Isothermal section of silica-leucite-mullite phase-equilibrium diagram at 1300°C.

frequently affected by service conditions and changes during the lifetime of the refractory. Generally, refractories are composed of large grog or refractory-grain particles held together with a fine-grained bond. Both the bond material and the refractory grains have a fine structure, and both are often multiphase. Many variations occur among bricks made from different raw materials and by different manufacturers. Some typical compositions are given in Table 11.3.

Fire-Clay Refractories. The largest group of fire-clay refractories is based on mixtures of plastic fire clay, flint clay, and fire-clay grog. Large numbers of brick are also made with increased alumina content by adding sillimanite, kyanite, topaz, diaspore, or bauxite. All these materials tend to form mullite on heating. In addition, quartz is often present as an impurity in the plastic fire clay and is sometimes added to reduce firing and drying shrinkage. The fine structure in the grog (prefired clay) or flint-clay particles and in the plastic fire-clay bond is difficult to resolve with an optical microscope but consists of fine mullite crystals in a siliceous matrix (Fig. 7.29). Alkali, alkaline earth, iron, and similar impurities that are present largely combine with the siliceous material to form a low-melting glass and decrease the refractoriness of the brick.

The brick texture—relation of grog or flint-clay particles to bond clay and porosity—is important to developing good properties. Large amounts of plastic clay, which is less refractory, decrease the refractoriness of the brick. In general, the coarse grog particles form an interlocking mass of bonded particles with numerous cracks and pores also present. These pores tend to prevent the extension of cracks or fissures and contribute resistance to spalling (breaking off of pieces of the brick caused by thermal or mechanical stresses), even though surface checks and cracks may form more readily than in a denser structure.

As discussed in Chapter 1, the volume fraction porosity in a graded series of particle sizes to give dense packing is about 25 to 30%. This is the space available for bond clay during the forming process. During firing the plastic fire-clay bond has a higher shrinkage than the grog or flint clay; if it just fits in between the particles, it contributes little to the overall firing shrinkage; if more than this amount is used, the shrinkage of the body increases. However, if the grog particles are in contact before firing, the shrinkage of the bond clay frequently causes fissures to open up during firing, contributing to stresses and reduced property values. Similarly, if the grog particles have larger contractions during firing than the plastic bond clay, boundary stresses are set up, as discussed in Chapter 5, and cracks tend to form (Fig. 11.16). These result in lower strength and poorer resistance to thermal stresses.

Silica Refractories. Silica brick have a high load-bearing capacity at

Table 11.3. Composition of Some Typical Refractory Brick

Type	Composition								Apparent Porosity (%)	Main Phases in Order of Amount Normally Present
	Al_2O_3	SiO_2	MgO	Cr_2O_3	Fe_2O_3	CaO	TiO_2	Total		
Chrome ore	30.0	5.3	19.0	30.5	13.5	0.7	...	99.0	22	$(MgFe)(AlCr)_2O_4$, R_2O_3 solid solution, $MgFe_2O_4$
Chrome ore–periclase	19.0	6.0	40.0	22.0	11.0	1.2	...	99.2	25	$(MgFe)(AlCr)_2O_4$, MgO, $MgFe_2O_4$, Mg_2SiO_4
Periclase–chrome ore	9.0	5.0	73.0	8.2	2.0	2.2	...	99.4	21	MgO, $(MgFe)(AlCr)_2O_4$, $MgFe_2O_4$, $MgCaSiO_4$
Periclase	1.0	3.0	90.0	0.3	3.0	2.5	...	99.8	22	MgO, $MgFe_2O_4$, $MgCaSiO_4$, $MgSiO_4$
Pitch-bonded low-flux dolomite	0.3	0.4	40.0	0.3	0.3	56.0	...	97.3	20	MgO, CaO, $MgCaSiO_4$, 2.7% residual carbon
Forsterite	1.0	33.3	54.5	0.7	9.1	1.0	...	99.6	23	Mg_2SiO_4, $MgFe_2O_4$, MgO, $MgAl_2O_4$
Silica	0.2	96.3	0.6	...	...	2.2	...	99.3	25	Tridymite, cristobalite
Fire clay	25–45	70–50	0–1	...	0–1	0–1	1–2	...	10–25	Mullite, siliceous phase, quartz
High-alumina fire clay	90–50	10–45	0–1	...	0–1	0–1	1–4	...	18–25	Mullite, siliceous phase

Fig. 11.16. Fissures in test fire-clay brick (50 grain, 50 bond) caused by (*a*) shattering of grains because they shrink more than matrix does and (*b*) cracking of matrix and separation from form because of greater shrinkage of matrix (8×). Courtesy C. Burton Clark.

elevated temperatures and consequently have been widely used for sprung arches as roofs for open-hearth furnaces, glass tanks, kilns, and coke ovens. Bricks are manufactured from ground ganister rock (quartzite) containing about 98% SiO_2 to which is added some 2% CaO as milk of lime. The added lime serves as a mineralizer during firing. Fired brick consist of shattered quartz grains that have been almost completely transformed into cristobalite (starting at the edges of the grain, as illustrated in Fig. 11.13) in a matrix of fine tridymite, cristobalite, and glass. Small amounts of unconverted quartz (about 10%) normally remain with nearly equal amounts of cristobalite and tridymite formed. Excessive quartz, (frequently present in brick at one time) is deleterious because of the large volume change accompanying the α to β transformation at 573°C.

Long firing times normally tend to favor tridymite development during firing. The quartz initially present transforms into cristobalite, starting at the grain edges. This dissolves in the calcium silicate liquid phase and precipitates as tridymite. During firing the amount of quartz present continually decreases, the amount of cristobalite initially increases and then later decreases, and the amount of tridymite continuously increases.

Basic Refractories. In the class of basic refractories are included brick

manufactured from chrome ore [$(MgFe)(AlCr)_2O_4$], periclase (MgO), calcined dolomite (CaO, MgO), olivine [$(MgFe)_2SiO_4$], and mixtures of these materials.

Chrome ore contains serpentine and other silicates as impurities which are low-melting and deleterious. If sufficient magnesia is added, it reacts with this material to form forsterite, which is refractory, thus improving the properties of the brick. Brick consist of large chromite grains which usually contain a precipitate of $(Fe, Al, Cr)_2O_3$ resulting from iron oxidation during firing; the bond phase consists of fine chrome ore, magnesioferrite, and forsterite. A typical structure is illustrated in Fig. 11.17. When more than a small amount of magnesite is added, we enter a range of chrome-ore–periclase compositions in which there are usually large grains of chromite in a matrix of fine MgO, $MgFe_2O_4$, and Mg_2SiO_4.

Periclase brick are formed mainly from magnesite ore or seawater magnesia and contain large MgO grains in a bond phase of fine MgO together with some Mg_2SiO_4 and $MgAl_2O_4$. The large magnesia grains are normally made up of smaller crystals separated by thin films of iron- and silica-rich boundary material. On heating in air, the FeO present is oxidized to form a precipitate of magnesioferrite in the periclase crystals (see Fig. 9.44). The morphology of the precipitate depends on its mode of formation. Chrome ore is sometimes added as a bond phase in periclase–chrome-ore brick. The bond is a complex mixture of MgO, $(MgFe)(AlCr)_2O_4$, and Mg_2SiO_4.

A minor class of basic brick are those manufactured from olivine, $(MgFe)_2SiO_4$. The major phase present is forsterite.

Recent years have seen better control of raw-material composition, firing procedures, and methods of production to control microstructure and improve properties as well as a wider range of products available for special purposes. As a result, the compositions and structures of basic brick cover a wide range. A matrix of pure chrome ore usually contains high percentages of metasilicate materials, principally $MgSiO_3$ and $CaMg(SiO_3)_2$, which are low-melting and cause low load-bearing capacity at high temperatures. Additions of magnesia, as in chrome-ore–magnesite brick, remedy this and improve the load-bearing capacity at high temperature. Chemically bonded brick, unfired before service, have this reaction take place during use. Low-silica chrome ore has a high iron oxide content, which results in friability under the cyclic oxidation-reduction atmosphere in open-hearth use and is therefore unsuited for chemically bonded brick. However, the low-silica ore gives an improved product when it is first fired with magnesia to a high enough temperature to form a stable spinel structure and has given a much improved product. Sufficiently high temperatures to form a diffusion bond between phases and

Fig. 11.17. Basic brick. (*a*) Chrome ore–magnesite brick at low magnification. Light grains are chrome ore, gray phase is periclase, and dark gray areas are porosity (5½×). Courtesy F. Trojer. (*b*) Different chrome ore–magnesite brick at higher magnification. Angular chrome ore grain and magnesite grain (rounded periclase particles in silicate matrix) in fine-grained bond (150×). Courtesy G. R. Eusner. (*c*) Higher magnification of chromite grain showing lamellar $(CrFe)_2O_3$ precipitate parallel to the (111) plane in spinel (1380×). Courtesy F. Trojer.

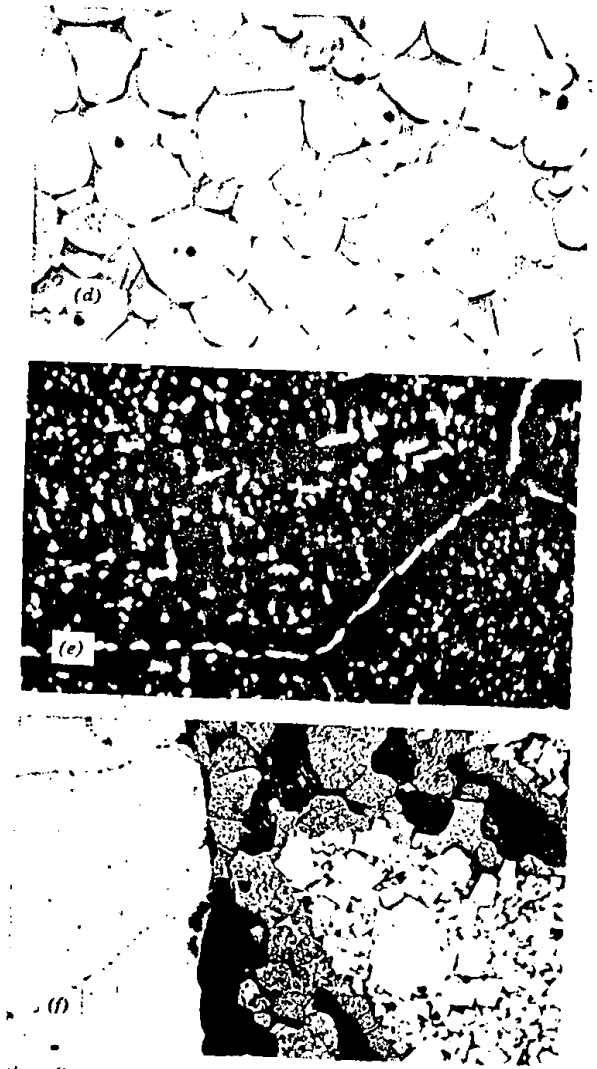

Fig. 11.17 (*Continued*). (*d*) Structure of magnesite grain showing rounded periclase crystals in silicate matrix of forsterite (Mg_2SiO_4) and monticellite ($MgCaSiO_4$) (275×). Courtesy F. Trojer. (*e*) Interior of oxidized periclase crystal showing precipitate of magnesioferrite ($MgFe_2O_4$), the light phase, dicalcium silicate, the dark triangular grains (1180×). Courtesy F. Trojer. (*f*) Complex structure of chromemagnesite brick showing large chromite grains on left, angular spinel grains, rounded periclase with magnesioferrite precipitate, and gray forsterite-monticellite matrix; dark gray is porosity (106×). Courtesy F. Trojer.

formation of large magnesia grains without penetration of the silicate liquid between grains improve performance, and much of the chrome-ore–magnesite brick used for severe service is now either fusion-cast as brick or formed from fused grain or fired at temperatures above the anticipated service temperature to give *direct-bonded* brick, in which the controlled microstructure leads to superior properties.

In pure periclase brick formed from seawater magnesia, the matrix tends to include relatively low-melting calcium-magnesium orthosilicates such as montecellite, $CaMgSiO_4$, and merwinite, $Ca_3Mg(SiO_4)_2$, which give rise to low load-bearing capacity at high temperatures. Not only the total amount of impurities but also the CaO to SiO_2 ratio is significant; when the weight ratio of calcia to silica is greater than 1.86, dicalcium silicate becomes the second phase rather than merwinite and montecellite, and the melting temperature is much increased. At the same time, the wetting behavior of the matrix phase is lessened such that there is enhanced bonding between the periclase grains. Higher firing temperatures to give greater grain growth and an increased CaO to SiO_2 ratio to decrease wetting result in a microstructure that markedly improves properties.

Dolomite ($MgCO_3$–$CaCO_3$) is a raw material of high refractoriness, low cost, and wide availability. Calcined dolomite consists of a mixture of CaO and MgO solid solutions, as shown in Fig. 7.16, plus a minor amount of silicate phase. For use as large blocks in basic open-hearth furnaces and to improve hydration resistance, these brick are formed by warm pressing with 5 to 8% pitch, which dissociates on first use, leaving a residual 2 to 3% carbon. As with other refractory brick, microstructure control is critical. It is found that by tempering the formed brick at 200 to 500°C, the pitch phase distributes itself uniformly in the interstices between grains and leads to greatly improved performance. Until recently, dolomites with up to 10% $Fe_2O_3 + Al_2O_3 + SiO_2$ were used; however, it has been found that low-flux raw materials containing less than 1% $Fe_2O_3 + Al_2O_3 + SiO_2$ with a smaller amount of silicate phase have greatly improved performance. Use of the low-flux material was made possible by developing a two-stage calcination process in which lightly calcined material is pressed to high-density briquettes and subsequently fired to a high temperature sufficient to give a large enough grain size and low enough grain porosity to provide adequate resistance to hydration without the protective silicate or ferrite phase previously thought necessary.

In almost all refractory brick, control of the porosity present is an important aspect of microstructure control. Lower porosity improves strength, load-bearing capacity, and corrosion resistance, but it also leads to catastrophic failure from thermal shock, since the pores present act as

crack stoppers in a more porous brick. As a result, control of porosity is a compromise for which the optimum depends on specific service conditions. Users of refractory brick, particularly steelmakers, are very conscious of the refractory cost per ton of product. As a result, first cost of the brick is carefully weighed against useful life and replacement cost.

Special Refractories. Many special refractory compositions are used that are more expensive than either fire clay or basic brick; these are used only where required. For exceptional resistance to corrosion by liquid slag and glasses, porefree fusion-cast refractories of various compositions are used. Fused alumina brick of 99.5% Al_2O_3 plus Na_2O consists of nearly close-packed crystals of β-Al_2O_3 with almost no bond phase present. Other compositions consist of α-alumina crystals, fusion-cast mullite, fusion-cast basic brick, and a special glass tank block containing 45 to 50Al_2O_3, 30 to 40ZrO_2, 12 to 13SiO_2, 2Fe_2O_3, and 2Na_2O for use in glass-melting furnaces. The principal phases present are corundum and baddeleyite, ZrO_2, together with a glassy phase. In all these compositions the porosity is small and the crystallite size large.

Silicon carbide refractories are used where high-temperature load-bearing capacity and high thermal conductivity are desirable, such as in tiles for muffles, kiln furniture, and heat exchanges. The major difficulty is a tendency toward oxidation at high temperatures. For refractory purposes dense packing of the silicon carbide grains is required. Each silicon carbide grain normally develops a thin siliceous coating during firing, and the individual particles are bonded together with a glassy phase or with a mixture of glass and crystals.

A special class of materials are the thermal-insulating refractories, which have a variety of structures, depending on the particular composition and use. For relatively low-temperature brick, porosity is obtained from plaster of paris mixtures that include extremely fine pores which remain after firing. Also for relatively low-temperature use, diatomaceous earth brick are prepared in which the porosity is derived from the extremely high and fine-grained residual porosity in the siliceous skeletons of diatoms; this provides particularly effective thermal insulation. For higher-temperature insulating firebrick the porosity is normally induced by incorporating combustible materials such as sawdust in the mix; these burn out during firing and form a large fraction of interconnected pores with a firebrick matrix material, similar to other firebrick compositions, as the solid phase. To obtain stability at the higher temperatures, the pore size is increased, and the amount of porosity is subsequently reduced. This means that the effective conductivity is higher for higher-temperature brick, and they should only be used when temperature conditions require it.

11.5 Structural Clay Products

Structural clay products include materials such as building brick, sewer pipe, drainpipe, and various kinds of tile; their manufacture is characterized by inexpensive raw materials, efficient material handling methods, and a low cost for the resultant product, necessary if structural clay products are to compete with other construction materials. The main raw materials are locally available clays having a variety of compositions and structures, depending on the particular locality. The high cost of transportation requires that local clays be used; similarly, the distribution radius for products is usually not large. The clays used are commonly glacial clays, shale or alluvial clays that contain considerable amounts of impurities. The clay minerals present are normally mixed with quartz, feldspar, mica, and other impurities. Secondary impurities include dolomite, rutile, and ferruginous materials.

During regular firing the larger-grain quartz and other accessory minerals are normally not affected. The clay used contains sufficient impurities for a glassy phase to form readily. The resulting structure normally consists of large grains of secondary constituents embedded in a matrix of fine-grained mullite and glass. The fine grain size of the matrix material makes its resolution in normal microscopic observation difficult. A typical structure observed for a stoneware is shown in Fig. 11.18. A glaze body interface for a similar composition has been illustrated in Fig. 5.25.

The details of the resultant structure depend on the particular composition of clays and the firing procedure used, but a structure similar to that in Fig. 11.18 is normally reached. In material that is underfired the clay phase contains many small pores, leading to low strength, poor resistance to frost and freezing, and generally unsatisfactory properties. Material that has been fired to an excessively high temperature is mostly a glass. The lack of porosity gives high strength but leads to failure of the entire brick when mechanical and thermal stresses are applied and prevents obtaining a satisfactory bond when used with mortars. The coloring constituents are mainly iron and TiO_2; these give products varying from yellow to salmon to buff to dark gray or black, depending on the particular impurities present.

11.6 Glazes and Enamels

As discussed in Chapter 8, glazes for ceramic ware and porcelain enamels for iron, aluminum, and jewelry metals are usually silicate glasses that may or may not include dispersed crystals or bubbles. As a

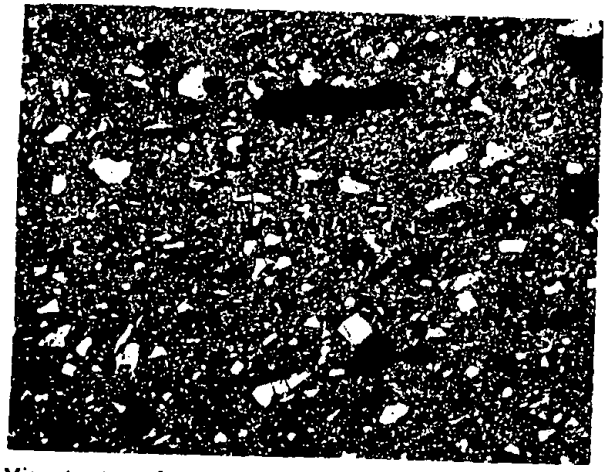

Fig. 11.18. Microstructure of stoneware. Ion-bombardment-etched (100×).

glaze is fired, the structure changes continuously. The materials initially present decompose and fuse, bubbles are formed and rise to the surface, and reaction takes place with the body under the glaze. The interface between the glaze and body is rough (Fig. 5.25) because of differences in solubility in the body constituents. Mullite crystals develop at the interface of porcelain bodies fired at high temperatures.

In a clear, glossy glaze the glass phase has no dispersed particles or porosity, and the surface is ideally perfectly smooth. Gloss is most commonly lost because bubbles rise and burst at the surface, forming small craters. Although the bubble content is initially high, the larger bubbles are rapidly eliminated during firing; the smaller bubbles are only slowly removed unless fluid glazes, which tend to run, are used. In mat glazes the surface texture and low gloss result from the extensive development of fine crystals (Fig. 11.19). For different glazes the composition of these crystals is variable, but anorthite, $CaO \cdot Al_2O_3 \cdot 2SiO_2$, is most common; mullite and wollastonite are also frequently observed. Large crystals in the glaze are sometimes desired for art products, as discussed in Chapter 8.

Perhaps the most common glaze defect is crazing; this occurs when the contraction of the glaze during cooling is greater than that of the underlying body so that tensile stresses develop in the glaze. Fissures appear, as illustrated in Fig. 12.22. In order to eliminate crazing, the composition of the glaze must be adjusted to decrease its thermal expansion coefficient, discussed in Chapter 12.

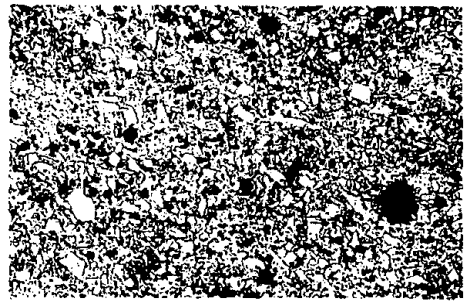

Fig. 11.19. Fine crystals dispersed in a mat glaze (polished section, H_3PO_4 etch, 78×).

Porcelain enamels on metal are similar to glazes in that they are basically a silicate glass coating. However, they are normally fired for shorter periods and at lower temperatures, and a wide range of defects is common. During firing, a ground coat containing nickel or cobalt oxide or a nickel dip (of the metal in a nickel sulfate solution) is frequently used to improve adherence. The main effect is to cause galvanic corrosion of the base metal; certain grains corrode more rapidly than others, providing a rough interface and improved adherence. This interface is similar to the rough interface obtained in glaze-porcelain structures as a result of variable solubility. A typical cross section of an interface boundary is illustrated in Fig. 11.20.

For good results with porcelain enamels it is found that the *bubble structure* is particularly important. Clays containing some organic impurities form fine bubbles adjacent to the metal surface. These provide reservoirs for hydrogen evolved from the metal on cooling and prevent *fish scaling*, the breaking out of pieces of the coating on cooling. Overfiring that eliminates the bubble structure is deleterious. A typical satisfactory bubble structure is illustrated in Fig. 11.20. Many defects in porcelain enamels result from defects in the metal used. Laminations in sheet iron for enameling give off gas during firing and cause blisters, as do surface inclusions such as slag or oxide. Large bubbles formed at the firing temperature may expose the metal underneath and allow rapid oxidation to occur, with the formation of Fe_2O_3 spots called copper heads.

Cover-coat enamels and opaque enamels are prepared with TiO_2, SnO_2, or other additives as opacifiers. These materials form a fine-grained second-phase dispersion, as discussed in Chapter 8. In most glazes and porcelain enamels colors can be obtained by using either colorants in solution to form a colored single-phase glass or pigments which remain

(a)

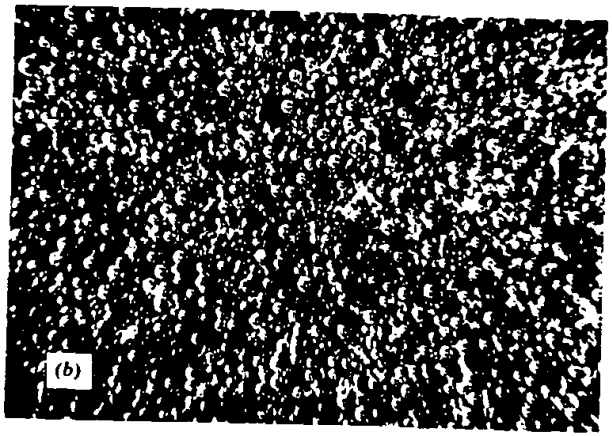

Fig. 11.20. Microstructure of porcelain enamel. (*a*) Cross section of enamel-metal interface showing rough boundary (525×). (*b*) Top view of bubble structure at metal-enamel interface provides space for gas evolution from metal on cooling (38×).

undissolved as a second phase. Optical properties of both glazes and enamels are discussed in Chapter 13.

11.7 Glasses

As discussed in Chapter 3, liquid-liquid immiscibility is widespread in glass-forming systems, and many glasses which appear optically homogeneous may be phase-separated on a scale of 30 to 50 Å up to a few

(c)

(d)

Fig. 11.20 (*Continued*). (*c*) Cross section of ground coat (192×). (*d*) Cross section of ground coat and cover coat (96×). Courtesy G. H. Spencer-Strong.

hundred angstroms. The characteristic forms of structure on this scale have been illustrated in Chapters 3 and 8. The sensitivity of these structural features to thermal history has been discussed in Chapter 8. Interconnected structures may form by spinodal decomposition or by the growth and coalescence of discrete particles, and such structures coarsen with time, retaining a high degree of connectivity in some cases and necking off and spheroidizing in others. Such two-phase submicrostruc-

tures may be developed to a sufficiently coarse scale so that they scatter light strongly, and such scattering can result in opalescence or opacity. Even single-phase glasses are characterized by fluctuations in density and composition. These fluctuations, which vary significantly with composition and with the melting conditions used, have become important in a number of applications in which low levels of scattering are of concern, as in the fabrication of optical wave guides.

On the scale of microns to millimeters and larger, a number of types of defects are found in glasses.

1. Seed. These are small gaseous bubbles which were not removed during the melting operation. The process by which such gaseous inclusions are removed from the molten glass is termed *fining*, and the time required for fining represents the rate-limiting part of many glass-melting operations. The large bubbles are eliminated from the melt by rising under the influence of gravity to the free surface; the small bubbles are removed by dissolving into the molten glass. To facilitate this dissolution, small concentrations, in the range of 0.1 to 0.3%, of fining agents such as Sb_2O_3 or As_2O_3 are added to the batch.

2. Stone. These are small crystalline imperfections found in the glass. These usually result from melting for periods of time which are too short to permit complete dissolution in the molten glass. The refractory linings of the glass tanks are a frequent source of such crystalline fragments, and refractory oxides such as ZrO_2 are often found as stone constituents, as illustrated in Fig. 11.21*a*.

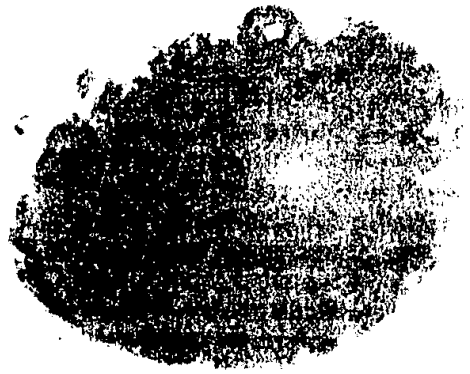

(*a*)

Fig. 11.21. (*a*) Refractory stone.

3. Cord and Striae. Cord are attenuated amorphous inclusions in the glass which have properties, in particular an index of refraction, different from those of the surrounding glass (Fig. 11.21*b*). These result from incomplete homogenization of the melt (inadequate mixing). Striae are cord of low intensity, which are of greatest concern in the preparation of optical glasses. To minimize the occurrence of cord and striae, a stirring step, generally carried out with platinum paddles, is often introduced after fining and before forming these glasses.

(*b*)

Fig. 11.21 (*Continued*). (*b*) Cord in soda-lime-silica glass.

Among commercial glasses, the occurrence of microstructural features such as seed, stone, and cord is most frequent in operations based on high throughput (output of a tank relative to its capacity) such as the production of glass containers, particularly near the end of the campaign (service life) of the refractories. These features occur with smallest frequency in optical glasses, which are melted with relatively high-purity-batch raw materials, often in platinum-lined tanks or pots, at relatively small throughputs.

11.8 Glass-Ceramics

As discussed in Chapter 8, the formation of glass-ceramic bodies often occurs with phase separation into two amorphous phases as the first step, which is followed by crystallization of the minor nucleant-rich phase,

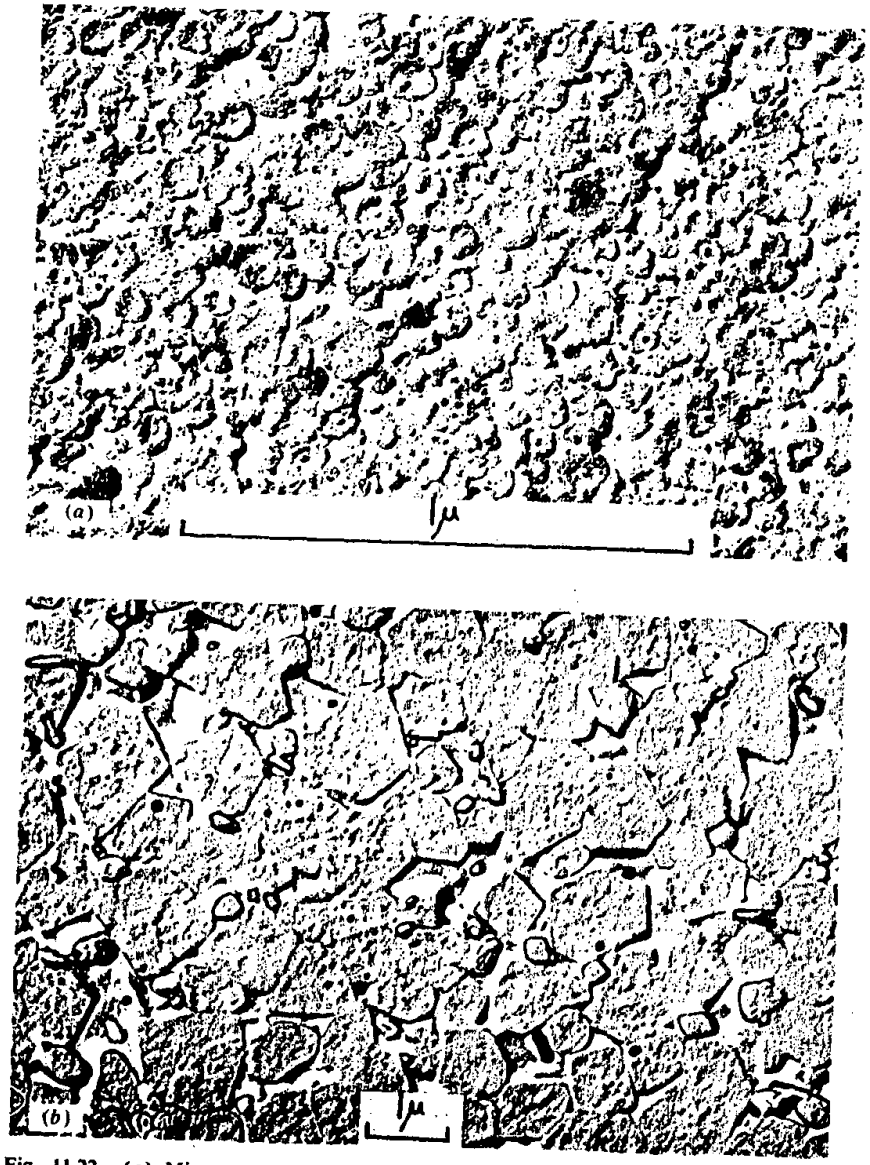

Fig. 11.22. (*a*) Microstructure of transparent, low-expansion Li_2O–Al_2O_3–SiO_2 glass-ceramic body; (*b*) microstructure of highly crystalline glass-ceramic body. From R. H. Redwine and M. A. Conrad in R. M. Fulrath and J. A. Pask, Eds., *Ceramic Microstructures*, John Wiley & Sons, Inc., New York, 1968, pp. 900–922.

which serves as precursor for the formation of the major crystalline phase or phases. The amount and characteristics of the final-phase assemblage depend both on the composition and on the heat treatment. An example of differences resulting from heat treatment of the same composition has been shown in Fig. 8.32. By controlled heat treatment $Li_2O{\cdot}Al_2O_3{\cdot}SiO_2$ glass-ceramics can be prepared in a highly crystalline form with a particle size as small as 0.05 micron (Fig. 11.22*a*). Since this particle size is less than a tenth of the wavelength of light and the phases have similar indices of refraction, this material is transparent. Modifying the heat treatment of the same material gives particle sizes in the micron range (Fig. 11.22*b*), and this product is opaque. As discussed in Chapter 8, heat treatment at relatively low temperatures at which the ratio of nucleation rate to growth rate is greater leads to a smaller-particle product. The crystalline content of the sample illustrated in Fig. 11.22 is about 85 vol% for the fine-particle product and about 95 vol% for the larger-particle material.

Many glass-ceramic bodies are composed of more than one phase. Figure 11.23 shows a Li_2O–Al_2O_3–SiO_2 glass-ceramic nucleated with TiO_2, in which small rutile crystals, several hundred angstroms in diameter, are observed with the β-spodumene grains. Figure 11.24*a* shows a MgO–Al_2O_3–SiO_2 glass-ceramic nucleated with ZrO_2, in which ZrO_2 crystals are observed in the boundary regions between the β-quartz grains. In this case, the ZrO_2 crystals were rejected at the advancing crystal-melt interface during crystallization of the major phase. Prolonged heat treatment of this same composition results in a solid-state transformation in which spinel forms at the expense of the quartz grains (Fig. 11.24*b*). Such solid-state transformations are often encountered in systems used for glass-ceramic applications in which a metastable phase first crystallizes or in which initial crystallization at a low temperature is followed by a higher-temperature heat treatment.

Compositional variations in the crystalline phase are characteristic of many glass-ceramic microstructures. As discussed in Chapter 2, eucryptite, $LiAlSiO_4$, is a *stuffed derivative* of β-quartz, and these phases are ones commonly occurring in glass-ceramics. Variations in the amount of aluminum and other ion substitution in the silica structure with accompanying changes in the alkali ion content are common.

Special properties of glass-ceramics can be developed when sheet silicates, primarily those of the fluorine mica family, are precipitated as the major phase in the glass-ceramic body. Such glass-ceramics containing more than 65 to 70 vol% mica can be machined to close tolerances if the aspect ratios of the crystals are large enough to cause contact between them. The desirable machinability is associated with basal cleavage of the mica crystals, because of relatively weak bonding between the layers, and

Fig. 11.23. Submicrostructure of Li_2O–Al_2O_3–SiO_2 glass-ceramic nucleated with TiO_2, approximately 80% crystalline. Small rutile crystals shown in larger crystals of β-spodumene. From P. E. Doherty in R. M. Fulrath and J. A. Pask, Eds., *Ceramic Microstructures*, John Wiley & Sons, Inc., New York, 1968, pp. 161–185.

with the difficulty of fracture propagation across the basal planes. Fractures therefore follow the crystal boundaries, causing detachment of individual crystals or small groups of crystals. Figure 11.25 shows mica crystals having low and high aspect ratios in glass-ceramic bodies. The microstructure of high aspect ratio, referred to as an interlocking *house of cards* structure, has the more desirable properties.

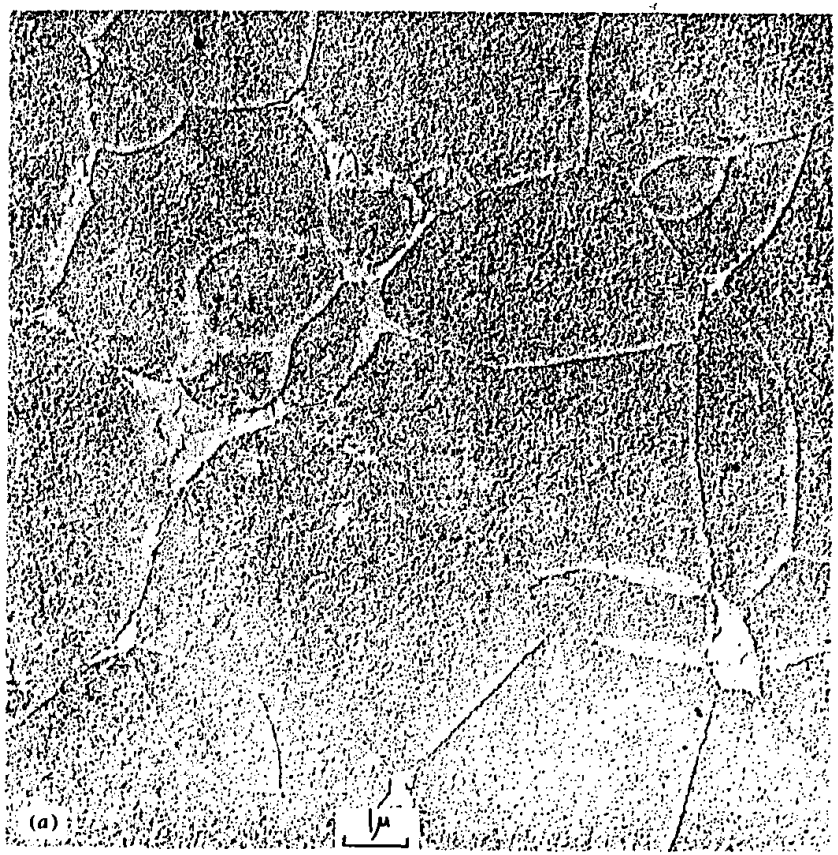

Fig. 11.24. (*a*) Submicrostructure of $MgO \cdot Al_2O_3 \cdot 3SiO_2$ glass-ceramic nucleated with ZrO_2. Small zirconia crystals at grain boundaries between high-quartz crystals.

Finally, the process of ion-exchange strengthening, discussed in Chapter 8, when applied to glass-ceramic bodies can result in phase transformations in the near-surface regions which have been ion-exchanged. Such transformations can have a pronounced effect on mechanical strength. An example of the microstructures which result from ion-exchange treatments of this type is shown in Fig. 11.26. A glass-ceramic body in the MgO–Al_2O_3–SiO_2 system containing cordierite and cristobalite as the stable crystalline phase assembly has been ion-exchanged in a Li_2SO_4 bath at 1000°C. In the $2Li^+ \rightleftharpoons Mg^{2+}$ exchange, the phase assemblage in the near-surface region transforms successively to a β-quartz solid solution and then to a β-spodumene solid solution as the Li^+ concentration increases.

Fig. 11.24 (*Continued*). (*b*) Same composition held at 977°C for 20 hr. Spinel forms at the expense of previously crystallized high-quartz phase. From R. H. Redwine and M. A. Conrad in R. M. Fulrath and J. A. Pask, Eds., *Ceramic Microstructures*, John Wiley & Sons, Inc., New York, 1968, pp. 900–922.

11.9 Electrical and Magnetic Ceramics

The general category of electrical and magnetic ceramics is one that includes a wide range of compositions and structures. Most ceramic materials can be used as electrical insulators or for other electrical purposes. The composition that is most widely used for low-tension insulators are triaxial porcelains, already discussed in Section 11.3. Glasses are also widely used for electrical-insulation purposes. For low-loss and high-frequency applications steatite, forsterite, and alumina ceramics are

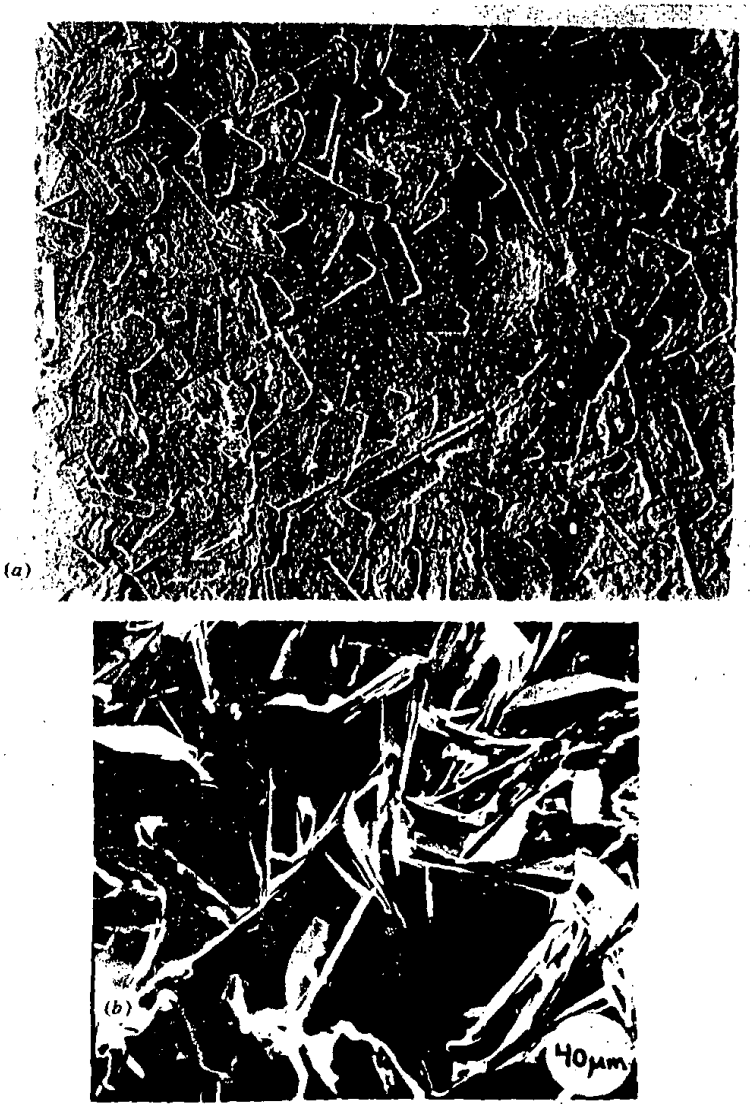

Fig. 11.25. (*a*) Saturated phlogopite mica solid-solution crystals of low-aspect ratio in highly siliceous residual glass; (*b*) Potassia-deficient phlogopite mica solid-solution crystals of high-aspect ratio showing interlocking house-of-cards microstructure. From G. H. Beall in L. L. Hench and S. W. Freiman, Eds., *Advances in Nucleation and Crystallization in Glasses*, American Ceramic Society, 1972, pp. 251–261.

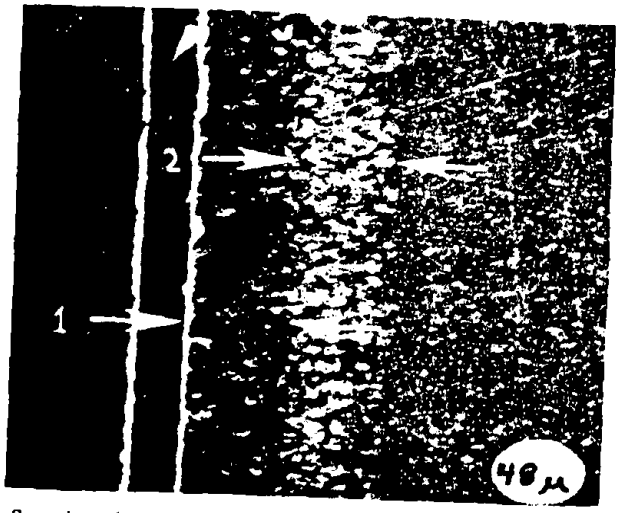

Fig. 11.26. Scanning electron micrograph of $2Li^+ \rightleftharpoons Mg^{2+}$ ion exchanged cordierite + cristobalite glass-ceramic body showing quartz and spodumene solid solutions developed in the near-surface region. After G. H. Beall in L. L. Hench and S. W. Freiman, Eds., *Advances in Nucleation and Crystallization in Glasses*, American Ceramic Society, 1972, pp. 251–261.

generally used. Reactions occurring during firing and the phase composition of these materials have been discussed in Chapter 7.

Steatite compositions are a general class of dielectrics which contain steatite, or talc, as a major constituent. They are extensively used for high-frequency insulators because of their good strength, relatively high dielectric constant, and low dielectric losses. Two main phases are present in the fired body (Fig. 11.27). The crystalline phase is enstatite, which appears as small discrete prismatic crystallites in a glassy matrix. The high-temperature equilibrium form is protoenstatite, which converts to clinoenstatite on cooling. The conversion is inhibited by the glassy phase, which isolates the individual crystals, and large crystals are converted more rapidly than small ones. The presence of large crystals is harmful to properties, since they tend to crack, owing to differences in expansion coefficient between the crystals and glassy matrix, illustrated in Fig. 10.44.

Electrical properties of steatite ceramics are largely determined by the amount and composition of the glassy phase. Triaxial porcelains contain considerable amounts of alkalies derived from the feldspar used as a flux. This leads to high electrical conductivity and high dielectric loss. Steatite porcelains that have feldspar added as an aid in firing also have high

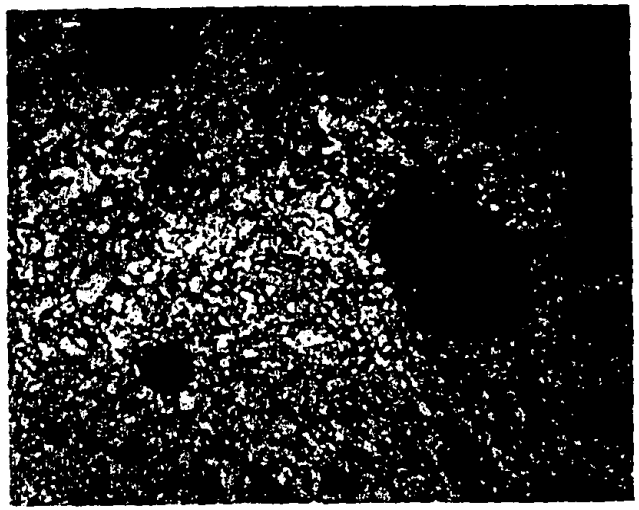

Fig. 11.27. Microstructure of steatite porcelain (500×).

dielectric loss. The low-loss compositions are nearly alkalifree, using alkaline earth oxides as fluxing constituents.

Forsterite ceramics have this material, Mg_2SiO_4, as the major crystalline phase bonded with a glassy matrix. The crystals are prismatic and usually larger in size than the enstatite crystals present in steatite. A typical structure has been illustrated in Fig. 7.33. Differences among various compositions depend for the most part on the amount of glassy phase present. Forsterite ceramics are particularly useful as low-loss dielectrics in designs in which the thermal expansion coefficient must be suitable for metal-ceramic bonding.

Alumina ceramics have Al_2O_3 as the crystalline phase bonded with a glassy matrix. In some bodies the alumina has a prismatic habit, whereas in others particles are nearly spheroidal. The factors controlling crystal habit are not completely understood; a typical microstructure is illustrated in Fig. 11.28. The properties obtained depend in large part on the amount and properties of the glassy phase, which is usually alkalifree, being compounded from mixtures of clay, talc, and alkaline earth fluxes. The firing temperature of alumina ceramics is relatively high. The body must be carefully compounded for satisfactory results. The main imperfection is excessive porosity; the pore size is usually larger than that of the individual grains of raw materials used and results from poor forming or firing techniques. The main advantages of alumina ceramics usually given are

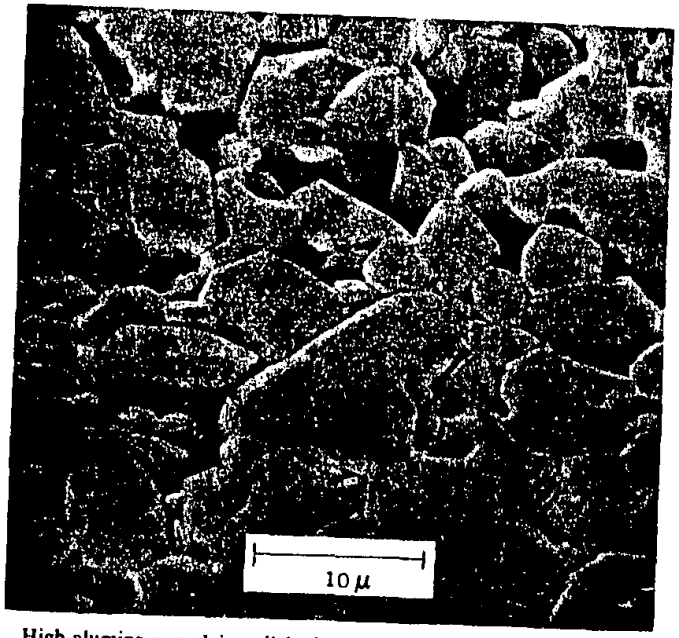

Fig. 11.28. High-alumina porcelain polished and heavily etched to remove silicate bonding phase (2300×).

relatively high dielectric constant and low dielectric losses. Its main usefulness in fact arises mostly from its high strength and resistance to thermal stresses. These properties allow it to be used in automatic forming machinery without excessive breakage or special handling. Alumina is widely used as a substrate for electronic-device applications in which surface resistivity and dielectric losses dictate use of a material containing 99% or more Al_2O_3. Surface smoothness depends in large part on grain size and a small-grain material such as illustrated in Fig. 11.29 is much preferred.

Cordierite ceramics, as discussed in Chapter 7, are useful because of their very low thermal expansion and consequent high resistance to thermal shock. Bodies are manufactured with a variety of fluxes; the cordierite phase develops as prismatic-habit crystals and is associated with a glassy phase, often together with some mullite, corundum, spinel, forsterite, or enstatite.

For ultralow-loss applications, particularly where large energy transfer through a ceramic is required, as in windows for high-powered electronic tubes, it is desirable to eliminate the glassy phase entirely. This can be done

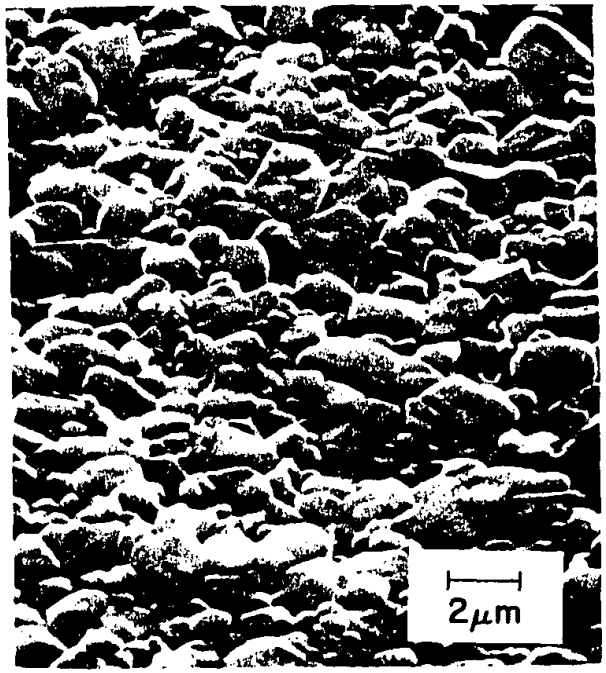

Fig. 11.29. Surface replica of an as-fired fine-grained 99% Al_2O_3 substrate surface. Courtesy R. Mistler.

with alumina by sintering pure fine-grained materials in the solid state at high temperatures. Structures obtained are ideally fine-grained with little porosity (Fig. 10.27*e*). Frequently, secondary crystallization occurs at the high firing temperatures used so that structures such as those illustrated in Fig. 10.13 are obtained. The main effect of increased grain size is to reduce the strength; it has little effect on electrical properties.

For applications in which very high dielectric constants are required, titania (dielectric constant about 100) or barium titanite (dielectric constant about 1500) ceramics are used. In titania ceramics TiO_2 is the major crystalline phase with small amounts of fluxes such as zinc oxide added to form a liquid phase at the firing temperatures. The resulting structure is similar to that of Fig. 7.11. Barium titanite bodies normally consist entirely of crystalline $BaTiO_3$. The individual crystals in a polycrystalline sample contain multiple domains of different ferroelectric orientations (see Chapter 18) which are clearly distinguished on etching (Fig. 11.30). Frequently, some secondary crystallization occurs during firing (Fig. 10.12).

Fig. 11.30. Microstructure of barium titanate ceramic. Different ferroelectric domain orientations are brought out by etching (500×). Courtesy R. C. DeVries.

Magnetic ceramics are ideally composed of a single crystalline phase having a composition determined by the magnetic properties desired ($FeNiFeO_4$, $BaFe_{12}O_{19}$, $FeMnFeO_4$, and so forth; see Chapter 19) and usually with as high density and fine grain size as can be obtained. A typical structure is illustrated in Fig. 11.31. As with other materials formed by solid-phase sintering, secondary recrystallization may occur (illustrated in Fig. 10.15).

As shown for the Fe–O system in Fig. 7.9, the desired single phase of magnetite, Fe_3O_4, occurs only over a limited range of oxygen content corresponding to a limited range of oxygen pressure. This is also true of other magnetic ferrite phases, and in production all manufacturers control the oxygen pressure during firing to ensure obtaining the desired magnetic properties normal to a particular composition of the single-phase ferrite. Where this is not done and two phases occur, the result is frequently similar to that found by R. E. Carter for $NiFe_2O_4$ in which an (MgFe)O phase forms (Fig. 11.32). Differences in the expansion coefficient of the two phases lead to cracking of the ferrite and have an adverse effect on the magnetic properties obtained.

11.10 Abrasives

Abrasive products have as their essential constituent a hard phase that provides many individual particles with sharp cutting edges; a bonding

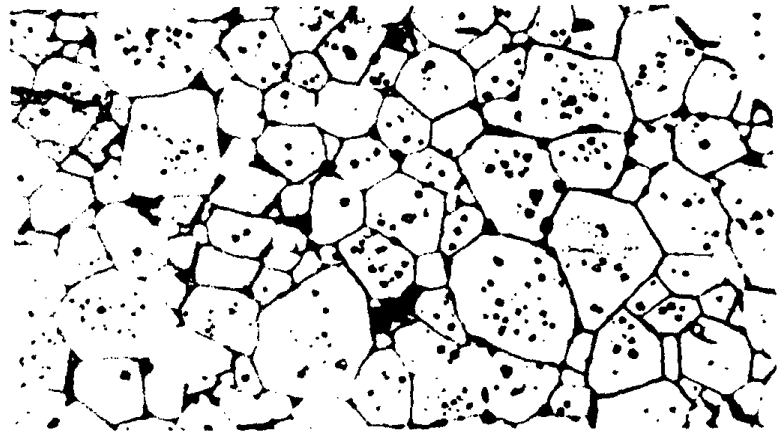

Fig. 11.31. Microstructure of nickel ferrite. Etch pits visible in grains result from sulfuric acid–oxalic acid etchant (638×). Courtesy S. L. Blum.

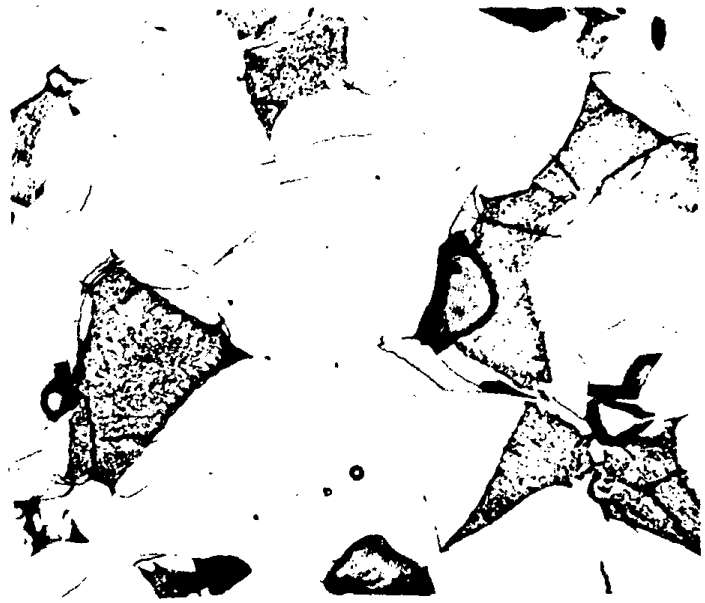

Fig. 11.32. Microstructure of two-phase ferrite ceramic. Light phase is $MgFe_2O_4$, dark phase (MgFe)O. Cracks due to microstresses are evident (500×). Courtesy R. E. Carter.

Fig. 11.33. Abrasive products. (*a*) Section of silicon carbide wheel, unetched (50×); (*b*) aluminum oxide wheel, unetched (100×). In both light area is grain, gray area bond, and dark area porosity. Courtesy A. Sidhwa.

phase holds these particles in a more or less tight grip, and a certain amount of porosity provides channels for air or liquid flow through the structure. For the hard abrasive grain either aluminum oxide or silicon carbide is usually used. Aluminum oxide grains are tougher than silicon carbide grains and wear more slowly, but they are not quite so hard. Silicon carbide grains are harder and more satisfactory for grinding hard materials but tend to fracture in use so that the life of the abrasive is shorter. In either abrasive individual grains are bonded to a wheel or paper or cloth with a strength depending on their proposed use. It is desirable that grains break out of the bond material once they become dull. Bond materials include fired ceramic bonds and a variety of organic resins and rubbers. Fired ceramic bonds are relatively hard, provide for a long life, can be used at high speeds satisfactorily, and account for the major part of grinding-wheel production.

No matter what hard grain and bond material are used, the overall structure is similar to those illustrated in Fig. 11.33 in which a section of a silicon carbide wheel and an aluminum oxide wheel are shown. In both the abrasive grains are held together with a glassy bond which determines the relative hardness of the individual wheel. The alumina product illustrated in Fig. 11.33*b* has a greater strength and hardness than the silicon carbide wheel, which has a larger proportion of abrasive grain to bond. In both the structure of the wheel is open with a large void fraction to provide for efficient cooling, either by air currents or liquid coolants during the grinding operation. This also allows grains to fracture and break off as they become worn.

11.11 Cement and Concrete

A wide variety of cementitious materials are used for different purposes. The structures of the products resulting from most of these have not been studied in much detail. The one that is of most economic importance and is most widely used is portland cement; high-alumina cement, *ciment fondu*, is used for refractory purposes. Portland cement is manufactured in rotary kilns, using various raw materials to give an overall composition in which the major resulting constituents are tricalcium silicate, $3CaO{\cdot}SiO_2$, and dicalcium silicate, $2CaO{\cdot}SiO_2$. The product is made in a rotary furnace and sintered under such conditions that a fraction of the charge becomes a liquid phase. The transformation occurring in the dicalcium silicate on rapid cooling causes a sufficient volume change to give rise to *dusting*, that is, to break up the particles. Polished sections of portland cement clinker are shown in Fig. 11.34. In addition to the major dicalcium silicate and tricalcium silicate phases, which are the basic materials present, there are frequently smaller amounts of tricalcium aluminate, $3CaO{\cdot}Al_2O_3$, brownmillerite (approximately $4CaO{\cdot}Al_2O_3{\cdot}Fe_2O_3$), some CaO, some MgO, and glass. The amounts, composition, and morphology of the minor phases present depend a great deal on the raw materials used and conditions for sintering. Aluminous cement has a much higher alumina content (approximately $40Al_2O_3$, 40CaO, $7SiO_2$, $7Fe_2O_3$, 5FeO, and five other oxides) and

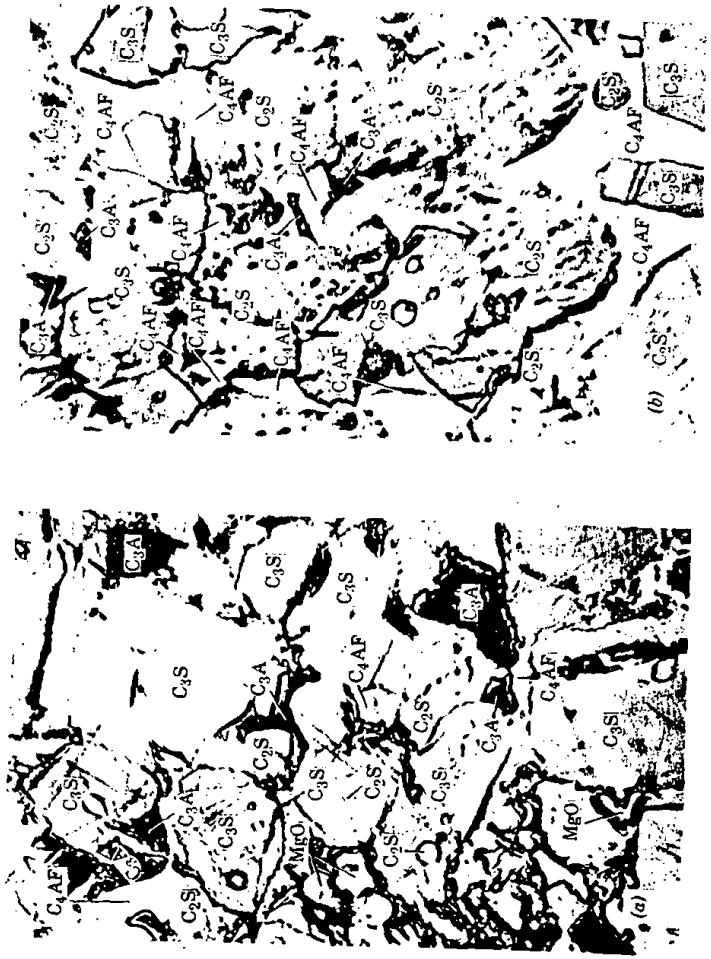

Fig. 11.34. Micrographs of portland cement clinker (835×). (*a*) Type I, high in $3CaO \cdot SiO_2$ (major gray phase is C_3S, dark gray phase C_3A, light gray phase C_2S, white phase mainly C_4AF); (*b*) type II, containing nearly equal parts of $3CaO \cdot SiO_2$ and $2CaO \cdot SiO_2$ (gray C_3S, light gray C_2S, black C_3A, white C_4AF). Courtesy Portland Cement Association.

during the firing process forms a much more fluid liquid phase which gives rise to the name *melted* cement. The main constituents in the clinker are *unstable* $5CaO \cdot 3Al_2O_3$, monocalcium aluminate, $CaO \cdot Al_2O_3$, and calcium dialuminate, $CaO \cdot 2Al_2O_3$. The unstable $5CaO \cdot 3Al_2O_3$ probably has the approximate composition $6CaO \cdot 4Al_2O_3 \cdot FeO \cdot SiO_2$.

On reaction with water the clinker forms a complex hydrated product which is a cementitious material. The main cementitious product that forms is a noncrystalline calcium silicate gel resulting from the tricalcium silicate and dicalcium silicate present in the clinker material. Along with the calcium silicate hydrate, calcium hydroxide is formed as a by-product and occurs as small hexagonal plates. The calcium hydroxide reacts with carbon dioxide in the air or water available to form calcium carbonate. The resulting structure of the gel as formed after reaction is illustrated in simplified form in Fig. 11.35. In the gel phase itself there are pore spaces between the individual gel particles; in addition, there are large residual capillary pores remaining from the excess water content required to form the cement and place it satisfactorily. This excess capillary porosity should be kept as low as possible if the optimum mechanical properties from the

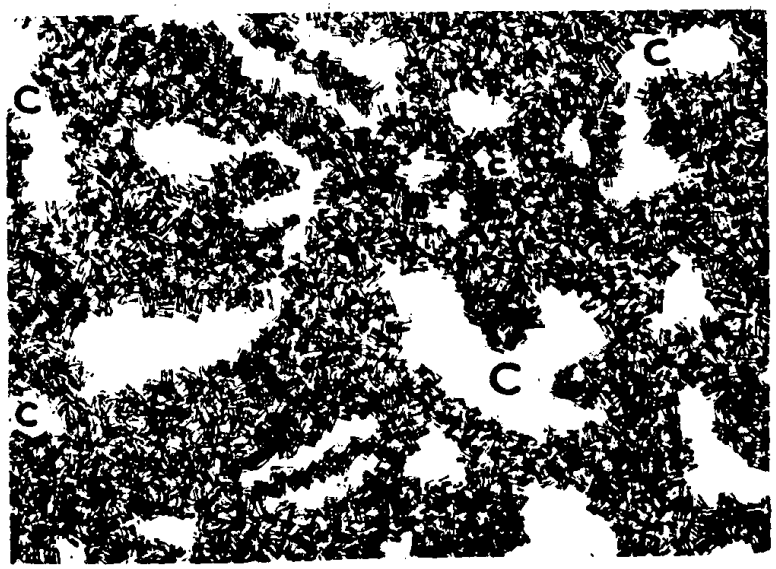

Fig. 11.35. Simplified model of portland cement paste structure showing needle or platelet gel particles and capillary cavities C. From T. C. Powers, *J. Am. Ceram. Soc.*, 41, 1 (1958).

cement are to be obtained. In addition to the cement gel, there is present in concrete an aggregate of crushed stone that acts as a filler material. The portland cement paste serves to bond together the aggregate particles in much the same way as a bond material present in a refractory brick or an abrasive wheel. The properties of the concrete formed depend on the amount of porosity present, particularly as capillary pores, the strength of the aggregate material, and the properties of the cement paste gel.

In contrast to portland cement, which forms a noncrystalline cement paste having good adhesive properties to bond together the aggregate materials when completely set, plaster of paris, which is widely used as a cementing and mold material in ceramics, has little strength and poor adhesive properties. The structure of set plaster is a highly crystalline reaction product, as shown in Fig. 11.36. Plaster is formed by calcining gypsum and then is used by rehydration:

Calcination: $$CaSO_4 \cdot 2H_2O = CaSO_4 \cdot \tfrac{1}{2}H_2O + \tfrac{3}{2}H_2O$$

Rehydration: $$CaSO_4 \cdot \tfrac{1}{2}H_2O + \tfrac{3}{2}H_2O = CaSO_4 \cdot 2H_2O$$

The individual crystals present are in the form of fine needles so that the resulting structure corresponds to a feltlike arrangement in which there are very fine pores, and the interlocking of the crystal needles provides sufficient strength. The amount of residual porosity depends on the amount

Fig. 11.36. Interlocking crystallite network in pottery plaster, $CaSO_4 \cdot 2H_2O$. Courtesy W. Gourdin.

of water present in the original mix. As the water content is increased, the volume fraction porosity after drying is also increased; the absorption capacity of the mold is raised, but at the same time its strength and durability are reduced.

A variety of other cementitious materials are used for various applications of ceramics. These range from tars and sugar solutions to reactions that form oxychlorides or acid phosphates and include the use of fine-grained clay materials as bonding agents. In all cases the resultant structure obtained is similar to that illustrated in Fig. 11.33, in which the bonding material is distributed at the contact points between grains, holding them together. More or less bonding material may be required, depending on the strength desired and the properties of the particular bond used. The general characteristic that all these materials have is a tendency to form noncrystalline products. In many cases this corresponds to the opportunity for extensive development of hydrogen bonds, which provide a mechanism for adherence. However, for many applications great strengths are not particularly required, and as long as a liquid phase distributes itself in positions between solid grains and then is solidified, there is sufficient adherence developed for satisfactory results. The major concern with regard to adhesion is first wetting and then the possibility of deleterious side effects such as gas evolution, volume changes, and adsorption of impurities at the interface; as long as these effects are absent, sufficient adherence is obtained.

11.12 Some Special Compositions

In addition to the classes of materials discussed thus far, in which the great majority of all ceramic production can be included, there are many materials that are difficult to introduce into any of these specific product groups. Although they do not contribute much to the overall volume of the ceramics industry, they frequently supply critical needs or provide properties that cannot be obtained elsewhere; consequently, they are particularly important from the point of view of developing new materials and the understanding of material properties.

Cermets. A group of materials that come under the general classification of refractories are the combinations of metals and ceramic materials called cermets. The compositions of most significance for their practical or potential application are carbides having high-temperature strength (Ni–TiC) and, in particular, great hardness. Also, oxide-base cermets have some valuable properties as high-temperature, high-strength materials that are reasonably stable in air; the most extensively investigated and only commercially available ones are mixtures primarily composed of

aluminum oxide and chromium suitably alloyed to give useful high-temperature properties. The carbide-metal compacts consist of either spheroidal or prismatic carbide grains completely enclosed by the metal phase. The bond phase is usually liquid at the firing temperature and completely wets and flows between the carbide particles, forming thin films of metal. These compositions have excellent high-temperature strength and also satisfactory toughness. The carbides used are hard so that they can be used in cutting tools. In the aluminum oxide–chromium system, in contrast, there is a continuous phase of both the oxide and chromium. This gives rise to high-temperature strength and resistance to thermal stresses. During cooling to room temperature there is a tendency for boundary stresses to develop, and the strength and other properties are less favorable at room temperature than at higher temperatures. Microstructures of these compositions are illustrated in Fig. 11.37.

Coatings. The only kinds of coating that have been discussed thus far are glazes and enamels based primarily on forming a glassy liquid which flows over and covers the surface. A variety of compositions has been used as enamel or glass coatings, in much the same way. In addition, however, coating of nonmetals can be applied by reactions from the vapor phase which deposit a coating on the surface, by flame-spraying oxide material through a high-intensity heat source so that it fuses in the flame and solidifies when it strikes the relatively cool surface, or by spraying a suspension on a hot surface so that a fine-particle dispersion is formed on hitting the surface to develop a suitable coating. The microstructures of these different types of coating vary substantially, depending on the particular method of application. Flame-sprayed coatings normally have a porosity of 7 to 10% and frequently show evidences of some layered structure during the buildup, although this depends on the particular techniques used. Layers formed by the evaporation of a solvent have very small crystals in the resultant coating. In contrast, coatings developed from the vapor phase by reaction frequently show large crystals, owing to the nucleation of new crystals in the surface and then subsequent growth in the coating phase. Very often the structure of the coating is parallel to the underlying structure, in that new crystals are nucleated and grow on sites of crystals of the underlying material. Graphite coolings, for example, can be formed by passing hot CH_4, a gas, over a hot surface. In this process the new *pyrolytic* graphite crystals form a deposit with their *c* axis normal to the underlying surface, in parallel bundles consisting of individual crystallites of nearly the same orientation (Fig. 11.38).

Sintered Oxides. Another kind of material which we have mentioned is the pure sintered single-phase oxide for uses requiring high strength, high-temperature capabilities, good electrical properties, or great hard-

Fig. 11.37. Metal-ceramic compositions. (*a*) 96WC–6Co (1500×). Courtesy M. Humenik. (*b*) 70TiC–30Ni (1580×). Courtesy M. Humenik. (*c*) 30Al_2O_3–70Cr (545×). Courtesy F. R. Charvat.

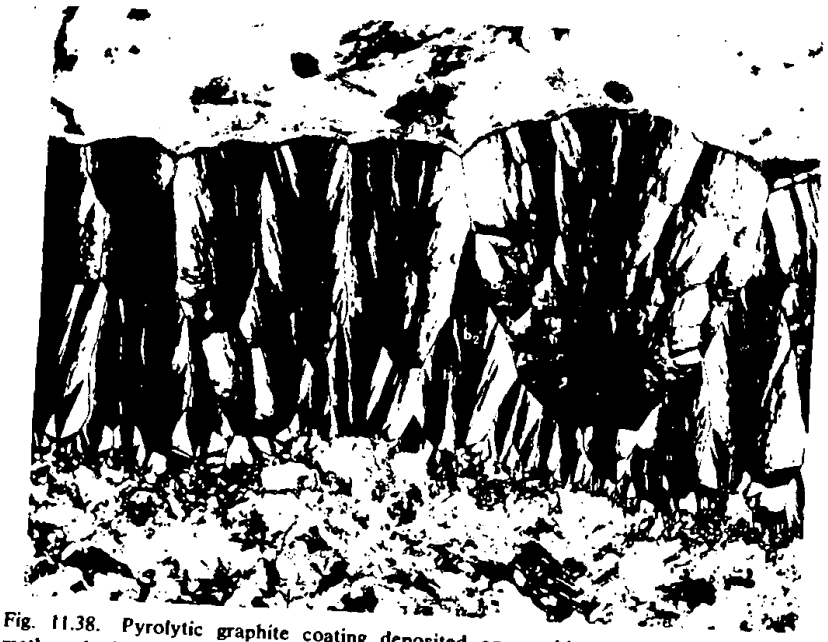

Fig. 11.38. Pyrolytic graphite coating deposited on graphite rod at bottom from a methane-hydrogen atmosphere (164×). Courtesy Avco Research and Advanced Development Division.

ness. For example, Al_2O_3 has been used as a tool material, its great hardness and low friction with metal combined with its high strength and its high-temperature capability making it particularly effective. Resulting structures in these ceramic compounds have been discussed in connection with solid-state sintering in Chapter 10, and some structures have been illustrated there. One of the interesting recent applications for this class of material is the use of uranium oxide as a nuclear-reactor-fuel material. It is particularly useful in that a large fraction of the uranium atoms can be fissioned without degradation of the structure. Other oxides which have been used for special or refractory applications include BeO, MgO, ThO_2, ZrO_2, and $MgAl_2O_4$.

Single Crystals. For many special applications, single crystals of oxide and other ceramic materials have been used. Single crystals of Al_2O_3 have been used as windows for heat resistance and good infrared transmission, as high-intensity light-bulb enclosures, and as electronic-device substrates. They have also been used in the form of rods and other special shapes as

high-temperature refractory materials. Single crystals of rutile (TiO_2), spinel ($MgAl_2O_4$), strontium titanate ($SrTiO_4$), ruby (Al_2O_3 with some Cr_2O_3 in solid solution), and others have been used as synthetic jewel materials. Lithium niobate ($LiNbO_3$) is used as a laser host and as a substrate. The optical properties of single crystals of magnesium oxide have been of potential interest; the use of alkali and alkaline earth halide crystals for prisms and windows in optical equipment has been widespread for many years. Single crystals of calcium fluoride, lithium fluoride, sodium chloride, and many others are commercially available.

Whiskers. An area of interest from a research point of view has been the structure and properties of whiskers of ceramic materials in which extremely high-strength values have been observed. Under certain conditions of growth, crystals form in which the growth is rapid in one direction, developing filamentary crystals that are presumably free from gross imperfection and have strengths up to several million pounds per square inch. Whiskers of this type of aluminum oxide, several sulfides, several alkali halides, graphite, and others have been grown in the laboratory.

Graphite. A ceramic material that has been widely used but not extensively described from a structural point of view is graphite. Graphite is normally made from mixtures of coke and pitch which are formed and heat-treated to develop a graphite crystal structure. The graphite crystals formed are highly anisometric, forming platelets, as would be expected from the crystal structure. The general microstructure of graphite consists of grains of highly graphitized material in a matrix of very fine-grained material which is more or less graphitized and more or less strongly crystallized, depending on the particular heat treatment. A microstructure of one sample is illustrated in Fig. 11.39. Details of the structure depend a great deal on the structure of the original coke, which again depends on the original petroleum, coal, or tar used for its formation, together with its distribution and heat treatment during graphitization. The properties of the resulting graphite are strongly dependent on the details of the structure; this is indicated by the fact that the properties of graphite products are strongly directional and depend on details of forming techniques. However, exact relationships between structure and properties have not been worked out for any detailed system.

High-Porosity Structures. Another group of materials, mentioned earlier but not discussed in much detail, is highly porous compositions for various insulating purposes. These include fibrous products such as glass wool, powdered insulated grain, and strong insulating firebrick. The common characteristic of all these materials is high porosity. In general,

Fig. 11.39. Microstructure of graphite (104×). Courtesy A. Tarpinian.

as the pore size decreases and the amount of porosity increases, materials become more effective as thermal insulators. However, for use at high temperatures, the minimum pore size that can be present without inducing sintering and instability of volume is limited. Consequently, materials used in brick form for high-temperature insulation have a much larger pore size than materials used at temperatures below the sintering range. This is the main reason why powdered carbon has been useful as an extremely high-temperature insulation; the mobility of carbon atoms is very low, as discussed in Chapter 8, so that sintering does not take place, and a very fine particle size material can be used satisfactorily.

Suggested Reading

1. E. E. Underwood, *Quantitative Stereology*, Addison-Wesley Publishing Company, Inc., Reading, Mass., 1970.
2. R. M. Fulrath and J. A. Pask, Eds., *Ceramic Microstructures*, John Wiley & Sons, Inc., New York, 1968.
3. H. Insley and V. D. Fiechette, *Microscopy of Ceramics and Cements*, Academic Press, Inc., New York, 1955.
4. American Society Testing Materials, *Symposium on Light Microscopy, A.S.T.M. Spec. Publ.* 143, 1952.
5. G. R. Rigby, *Thin Section Mineralogy of Ceramic Materials*, 2d ed., British Ceramic Resin Association, Stoke-on-Trent, England, 1953.
6. A. A. Klein, "Constitution and Microstructure of Porcelain," *Natl. Bur. Std., Tech. Pap.* 80, 1916–1917.
7. C. S. Smith, "The Shape of Things," *Sci. Am.*, **190**, 58 (January, 1954).
8. S. T. Lundin, "Electron Microscopy of Whiteware Bodies," *Transactions of the IVth International Ceramic Congress*, Florence, Italy, 1954.

Problems

11.1. A typical porcelain body has the composition 50 clay–25 feldspar–25 quartz. Sketch an expected microstructure of such a body, indicating scale, when (*a*) fired to achieve phase equilibrium (1450°C for 6 hr) and (*b*) fired to 1300°C for 1 hr. Explain how and why these two different firings would affect mechanical, optical, thermal, and electrical properties.

11.2. Suppose that the 10% porosity existing in a sintered alumina ceramic is due to a uniform distribution of pores trapped at the interstices of particles during the sintering process (grain boundary or bulk diffusion). Considering the initial powder compact to be an ideal packing of spheres 1 micron in radius with sixfold coordination for pores as well as spheres, that is, one pore per particle, what is the average size of pore in microns viewed in the microsection? How many pores per square centimeter in a microsection? Consider the theoretical density to be 4.00 g/cc and the atomic weight 102.

11.3. In a triaxial porcelain fired at 1200°C, feldspar grains ($K_2O \cdot Al_2O_3 \cdot 6SiO_2$) melt at the firing temperature to form a blob of viscous liquid surrounded by the product formed by heating clay ($Al_2O_3 \cdot 2SiO_2 \cdot 2H_2O$). In a microstructure of a fired porcelain, needlelike crystals of mullite ($3Al_2O_3 \cdot 2SiO_2$) are observed to extend into the feldspar *pseudomorphs*. Discuss the kinetics of the mullite crystal growth including (*a*) your choice of the most probable rate-limiting step, (*b*) your reasons for that choice, and (*c*) how you would experimentally or analytically confirm or negate that choice.

11.4. List the following in order of importance for control of microstructure during sintering of a typical oxide (like UO_2). Justify the order with suitable numerical

approximations for the range of value for each variable over which control can be exercised:

Surface energy
Temperature
Atmosphere
Distribution of particle size
Heating rate
Bulk density (prior to firing)
Inhomogeneity in bulk density
Time

11.5. How would you go about making a large-grain *controlled-orientation* (i.e., all or most crystals oriented parallel to one another) polycrystalline ceramic? Explain the principle on which you base your proposed procedure.

11.6. Draw clear sketches of the microstructure, showing pores, solid phases, and grain boundaries, paying particular care to clearly illustrate the relationship among pores, different phases present, and grain boundaries, for:
(*a*) A triaxial porcelain sintered to maximum density in an atmosphere in which the gas would not diffuse at an appreciable rate in the solid.
(*b*) A single-phase crystalline refractory material such as MgO of large initial particle size (10 microns) sintered at a low temperature (1500°C).
(*c*) A single-phase crystalline material of small initial particle size (0.5 micron) sintered to a high temperature in high vacuum:
(1) In which discontinuous grain growth has occurred.
(2) In which the firing time is much longer than that required for discontinuous grain growth.
(3) In which discontinuous grain growth has been inhibited.

11.7. Describe how you would experimentally determine the fractional porosity, fractional glass content, and fractional crystal content in a steatite porcelain containing three phases (pores, glass, and $MgSiO_3$ crystals).

11.8. From a lineal analysis, estimate the fraction of porosity present in the porcelain in Fig. 11.3. What is the true pore radius?

11.9. How would you determine the surface profile of a fired ceramic? What governs the surface profile at equilibrium?

11.10. On examining a polished section, what characteristics of the microstructure enable one to decide whether it is single-phase or polyphase?

11.12. You are placed in charge of the production control of a ferrite processing line which has been recently set up without quality control. (What you are producing is a soft ferrite for a transformer yoke at intermediate frequencies.) The process involves the use of copper oxide as an addition to the batch which facilitates sintering because of the formation of a liquid phase at elevated temperatures. Draw the microstructure that you would expect to result; then list several microstructural features which you expect to significantly affect magnetic properties, and indicate which properties are most strongly affected by each. For quality control, what microstructural measurements would you have set up. Give the relations between those measurements and the microstructural features of interest. Also indicate what magnetic and other characteristics you would have measured for quality control.

part IV

PROPERTIES OF CERAMICS

The aim of a ceramist in selecting or modifying a particular composition, fabrication method, firing process, or heat treatment is to obtain a product having certain useful properties. This requires a good understanding of material properties per se, which is of course a very broad subject. In this book we concentrate on the ceramic aspects of material properties—how properties can be usefully controlled or improved by the proper selection of composition, forming methods, firing techniques, and application. To do this, and at the same time avoid an excessively long book, we do not give quantitative derivations of different parameters used to describe properties. We do not attempt to present complete tabulations of material properties.

The properties to be considered and the methods of presentation are in large measure arbitrary; no attempt has been made to be exhaustive or completely consistent. In general, we consider the properties of crystals, the properties of glasses, and the properties of mixtures of these phases. The topics presented are based on either their general importance, the state of current development, or their particular significance in illustrating the ceramic parameters involved.

10

Grain Growth, Sintering, and Vitrification

We have previously discussed phase changes, polymorphic transformations, and other processes independent of, or subsequent to, the fabrication of ceramic bodies. Phenomena that are of great importance are the processes taking place during heat treatment before use; these are the subject of this chapter.

During the usual processing of ceramics, crystalline or noncrystalline powders are compacted and then fired at a temperature sufficient to develop useful properties. During the firing process changes may occur initially because of decomposition or phase transformations in some of the phases present. On further heating of the fine-grained, porous compact, three major changes commonly occur. There is an increase in grain size; there is a change in pore shape; there is change in pore size and number, usually to give a decreased porosity. In many ceramics there may be solid-state reactions forming new phases, polymorphic transformations, decompositions of crystalline compounds to form new phases or gases, and a variety of other changes which are frequently of great importance in particular cases but are not essential to the main stream of events.

We shall be mainly concerned with developing an understanding of the major processes taking place. There are so many things which can happen, and so many variables that are occasionally important, that no mere cataloging of phenomena can provide a sound basis for further study. In general, we shall be concerned first with recrystallization and grain-growth phenomena, second with the densification of single-phase systems, and finally with more complex multiphase processes. There are many important practical applications for each of these cases.

10.1 Recrystallization and Grain Growth

The terms recrystallization and grain growth have had a very broad and indefinite usage in much of the ceramic literature; they have sometimes been used to include phase changes, sintering, precipitation, exsolution, and other phenomena which produce changes in the microstructure. We are mainly concerned with three quite distinct processes. *Primary recrystallization* is the process by which nucleation and growth of a new generation of strainfree grains occurs in a matrix which has been plastically deformed. *Grain growth* is the process by which the average grain size of strainfree or nearly strainfree material increases continuously during heat treatment without change in the grain-size distribution. *Secondary recrystallization*, sometimes called abnormal or discontinuous grain growth, is the process by which a few large grains are nucleated and grow at the expense of a fine-grained, but essentially strain-free, matrix. Although all these processes occur in ceramic materials, grain growth and secondary recrystallization are the ones of major interest.

Primary Recrystallization. This process has as its driving force the increased energy of a matrix which has been plastically deformed. The energy stored in the deformed matrix is of the order of 0.5 to 1 cal/g. Although this is small compared with the heat of fusion, for example (which is a 1000 or more times this value), it provides a sufficient energy change to effect grain-boundary movement and changes in grain size.

If the isothermal change in grain size of strainfree crystals in a deformed matrix is measured after an initial induction period, there is a constant rate of grain growth for the new strainfree grains. If the grain size is d,

$$d = U(t - t_0) \tag{10.1}$$

where U is the growth rate (cm/sec), t is the time, and t_0 is the induction period. This is illustrated in Fig. 10.1 for recrystallization of a sodium chloride crystal which had been deformed at 400°C and then annealed at 470°C. The induction period corresponds to the time required for a nucleation process, so that the overall rate of recrystallization is determined by the product of a nucleation rate and a growth rate.

The nucleation process is similar to those discussed in Chapter 8. For a nucleus to be stable, its size must be larger than some critical diameter at which the lowered free energy of the new grain is equal to the increased surface free energy. The induction period corresponds to the time required for unstable embryos present to grow to the size of a stable nucleus. If an unlimited number of sites is available, the rate of nucleation increases to some constant rate after an initial induction period. In

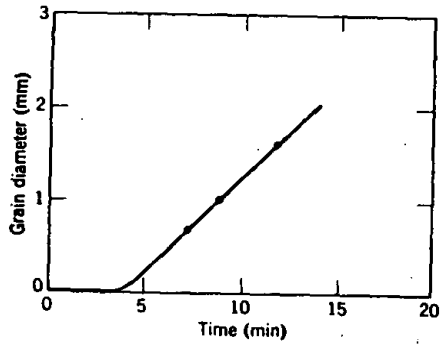

Fig. 10.1. Recrystallization of NaCl deformed at 400°C (stress = 4000 g/mm²) and recrystallized at 470°C. From H. G. Muller, *Z. Phys.*, **96**, 279 (1935).

practice the number of favorable sites available is limited, and the rate of nucleation passes through a maximum as they are used up. H. G. Müller* observed that nuclei in sodium chloride tended to form first at grain corners, for example. As the temperature is increased, the rate of nucleation increases exponentially:

$$\frac{N}{dt} = N_0 \exp\left(-\frac{\Delta G_N}{RT}\right) \tag{10.2}$$

where N is the number of nuclei and ΔG_N is the experimental free energy for nucleation. Consequently, the induction period, $t_0 \sim 1/(dN/dt)$, decreases rapidly as the temperature level is raised.

As indicated in Eq. 10.1, the growth rate remains constant until the grains begin to impinge on one another. The constant in growth rate results from the constant driving force (equal to the difference in energy between the strained matrix and strainfree crystals). The final grain size is determined by the number of nuclei formed, that is, the number of grains present when they finally impinge on one another. The atomistic process necessary for grain growth is the jumping of an atom from one side of a boundary to the other and is similar to a diffusional jump in the boundary. Consequently the temperature dependence is similar to that of diffusion:

$$U = U_0 \exp\left(-\frac{E_U}{RT}\right) \tag{10.3}$$

where the activation energy E_U is normally intermediate between that for boundary and lattice diffusion. The growth-rate-temperature curve for

*Z. Phys., 96, 279 (1935).

recrystallization of sodium chloride has a knee similar to that observed for diffusion and conductivity data, as discussed in Chapter 6.

Since both the nucleation rate and the growth rate are strongly temperature-dependent, the overall rate of recrystallization changes rapidly with temperature. For a fixed holding time, experiments at different temperatures tend to a show either little or nearly complete recrystallization. Consequently, it is common to plot data as the amount of cold work or the final grain size as a function of the *recrystallization temperature.* Since the final grain size is limited by impingement of the grains on one another, it is determined by the relative rates of nucleation and growth. As the temperature is raised, the final grain size is larger, since the growth rate increases more rapidly than the rate of nucleation. However, at higher temperatures recrystallization is completed more rapidly, so that the larger grain size observed in constant-time experiments (Fig. 10.2) may be partly due to the greater time available for grain growth following recrystallization. The growth rate increases with increasing amounts of plastic deformation (increased driving force), whereas the final grain size decreases with increasing deformation.

In general, it is observed that (1) some minimum deformation is required for recrystallization, (2) with a small degree of deformation a higher temperature is required for recrystallization to occur, (3) an increased annealing time lowers the temperature of recrystallization, and

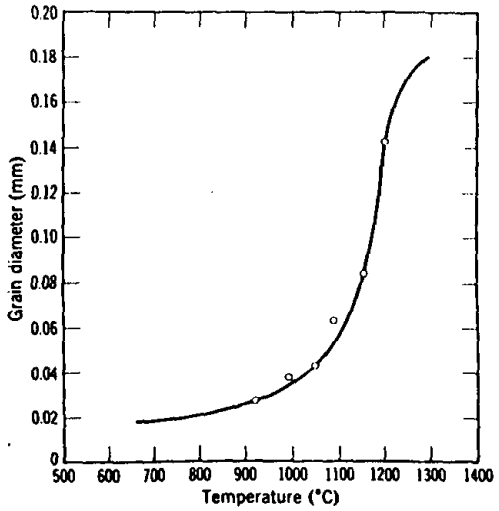

Fig. 10.2. Effect of annealing temperature on grain size of CaF_2 following compression at 80,000 psi and 10 hr at temperature. From M. J. Buerger, *Am. Mineral.*, 32, 296 (1947).

(4) the final grain size depends on the degree of deformation, the initial grain size, and the temperature of recrystallization. In addition, continued heat after recrystallization is completed leads to the continuation of grain growth.

Primary recrystallization is particularly common in metals which are extensively deformed in normal processing techniques. Ceramic materials are seldom plastically deformed during processing, so that primary recrystallization is not commonly observed. For relatively soft materials, such as sodium chloride or calcium fluoride, deformation and primary recrystallization do occur. It has also been observed directly in magnesium oxide; also, the polygonization process described in Chapter 4 (see Fig. 4.24) for aluminum oxide has many points of similarity.

Grain Growth. Whether or not primary recrystallization occurs, an aggregate of fine-grained crystals increases in average grain size when heated at elevated temperatures. As the average grain size increases, it is obvious that some grains must shrink and disappear. An equivalent way of looking at grain growth is as the rate of disappearance of grains. Then the driving force for the process is the difference in energy between the fine-grained material and the larger-grain-size product resulting from the decrease in grain-boundary area and the total boundary energy. This energy change corresponds to about 0.1 to 0.5 cal/g for the change from a 1-micron to a 1-cm grain size.

As discussed in Chapter 5, an interface energy is associated with the boundary between individual grains. In addition, there is a free-energy difference across a curved grain boundary which is given by

$$\Delta G = \gamma \bar{V}\left(\frac{1}{r_1}+\frac{1}{r_2}\right) \tag{10.4}$$

where ΔG is the change in free energy on going across the curved interface, γ is the boundary energy, $\bar{V}$ is the molar volume, and r_1 and r_2 are the principal radii of curvature. (This relationship has been derived and discussed in Chapter 5. That part of Chapter 5 should be reviewed if its meaning is not clear.) This difference in the free energy of material on the two sides of a grain boundary is the driving force that makes the boundary move toward its center of curvature. The rate at which a boundary moves is proportional to its curvature and to the rate at which atoms can jump across the boundary.

Grain growth provides an opportunity to apply the absolute-reaction-rate theory already discussed in Chapter 6. If we consider the structure of a boundary (Fig. 10.3), the rate of the overall process is fixed by the rate at which atoms jump across the interface. The change in energy with an atom's position is shown in Fig. 10.3*b*, and the frequency of atomic jumps

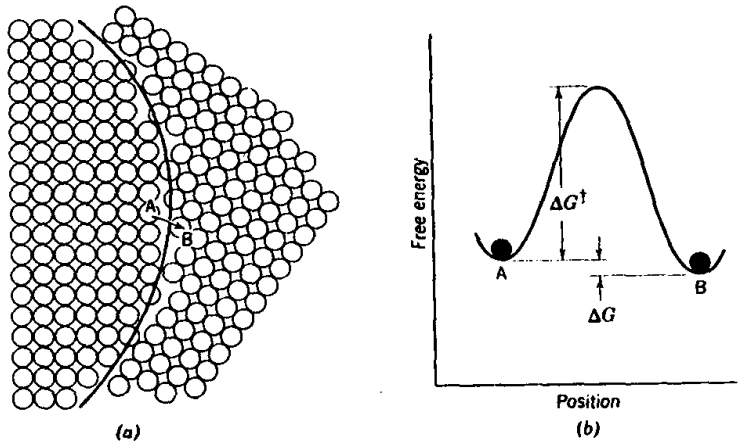

Fig. 10.3. (*a*) Structure of boundary and (*b*) energy change for atom jump.

in the forward direction is given by

$$f_{AB} = \frac{RT}{Nh}\exp\left(-\frac{\Delta G'}{RT}\right) \tag{10.5}$$

and the frequency of reverse jumps is given by

$$f_{BA} = \frac{RT}{Nh}\exp\left(-\frac{\Delta G' + \Delta G}{RT}\right) \tag{10.6}$$

so that the net growth process, $U = \lambda f$, where λ is the distance of each jump is given by

$$U = \lambda f = \lambda(f_{AB} - f_{BA}) = \frac{RT}{Nh}(\lambda)\exp\left(-\frac{\Delta G'}{RT}\right)\left(1-\exp\frac{\Delta G}{RT}\right) \tag{10.7}$$

and since $1-\exp\frac{\Delta G}{RT} \cong \frac{\Delta G}{RT}$, where $\Delta G = \gamma\bar{V}\left(\frac{1}{r_1}+\frac{1}{r_2}\right)$ and $\Delta G' = \Delta H' - T\,\Delta S'$,

$$U = \left(\frac{RT}{Nh}\right)(\lambda)\left[\frac{\gamma\bar{V}}{RT}\left(\frac{1}{r_1}+\frac{1}{r_2}\right)\right]\exp\frac{\Delta S'}{R}\exp\left(-\frac{\Delta H'}{RT}\right) \tag{10.8}$$

which is equivalent in form to Eq. 10.3 given previously. That is, the rate of growth increases exponentially with temperature. The unit step involved is the jump of an atom across the boundary, so that the activation energy should correspond approximately to the activation energy for boundary diffusion.

If all the grain boundaries are equal in energy, they meet to form angles of 120°. If we consider a two-dimensional example for illustrative purposes, angles of 120° between grains with straight sides can occur only for six-sided grains. Grains with fewer sides have boundaries that are concave when observed from the center of the grain. Shapes of grains having different numbers of sides are illustrated in Fig. 10.4; a sample with uniform grain size is shown in Fig. 10.5. Since grain boundaries migrate toward their center of curvature, grains with less than six sides tend to grow smaller, and grains with more than six sides tend to grow larger. For any one grain, the radius of curvature of a side is directly proportional to the grain diameter, so that the driving force, and therefore the rate of grain growth, is inversely proportional to grain size:

$$\dot{d} = \frac{d(d)}{dt} = \frac{k}{d} \tag{10.9}$$

and integrating,

$$d - d_o = (2k)^{1/2} t^{1/2} \tag{10.10}$$

where d_o is the grain diameter at time zero. Experimentally it is found that when log d is plotted versus log t, a straight line is obtained (Fig. 10.6). Frequently the slope of curves plotted in this way is smaller than one-half,

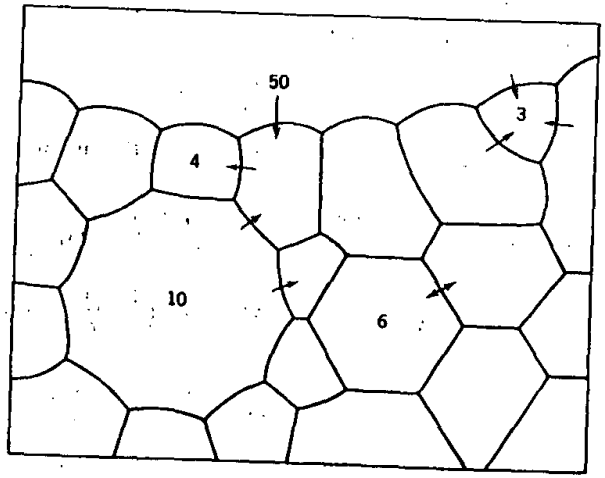

Fig. 10.4. Schematic drawing of polycrystalline specimen. The sign of curvature of the boundaries changes as the number of sides increases from less than six to more than six, and the radius of curvature is less, the more the number of sides differs from six. Arrows indicate the directions in which boundaries migrate. From J. E. Burke.

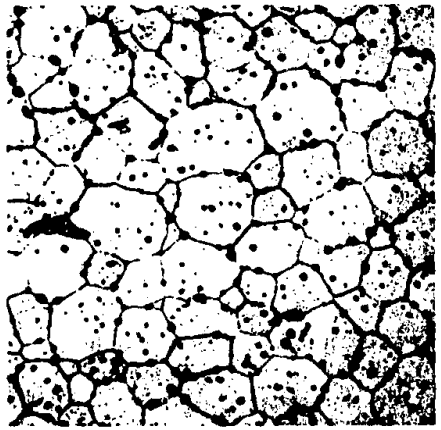

Fig. 10.5. Polycrystalline CaF_2 illustrating normal grain growth. Average angle at grain junctures is 120°.

usually falling between 0.1 and 0.5. This may occur for several reasons, one being that d_o is not a large amount smaller than d; another common reason is that inclusions or solute segregation or sample size inhibits grain growth.

A somewhat different approach is to define a grain-boundary mobility B_i such that the boundary velocity v is proportional to the applied driving force F_i resulting from boundary curvature:

$$v = B_i F_i \tag{10.11a}$$

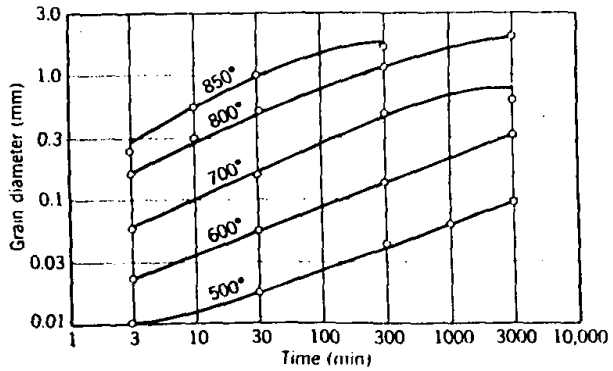

Fig. 10.6. Log grain diameter versus log time for grain growth in pure α-brass. From J. E. Burke.

For the atomic-jump mechanism illustrated in Fig. 10.3, the boundary mobility is given by the atomic mobility divided by the number of atoms involved, n_a:

$$B_i = \frac{B_a}{n_a} = \left(\frac{D_b}{kT}\right)\left(\frac{\Omega}{Sw}\right) \qquad (10.11b)$$

where D_b is the grain-boundary diffusion coefficient, Ω is the atomic volume, S is the boundary area, and w is the boundary width. Since the average boundary velocity is equal to v and the driving force is inversely proportional to grain size, a grain-growth law of the form of Eqs. 10.9 and 10.10 results. However, as discussed in Chapter 5, the actual structure of a ceramic grain boundary is not quite so simple as pictured in deriving Eqs. 10.8 and 10.11*b*. Even for a completely pure material there is a space-charge atmosphere of lattice defects associated with the boundary and usually solute segregation as well, as shown in Figs. 5.11, 5.12, 5.17, and 5.18. The effect of this lattice defect and impurity atmosphere is to sharply reduce the grain-boundary velocity at low driving forces, as shown in Fig. 10.7 and analysed by J. Cahn* and K. Lücke and H. D. Stuwe.† The influence of this atmosphere becomes stronger as the grain

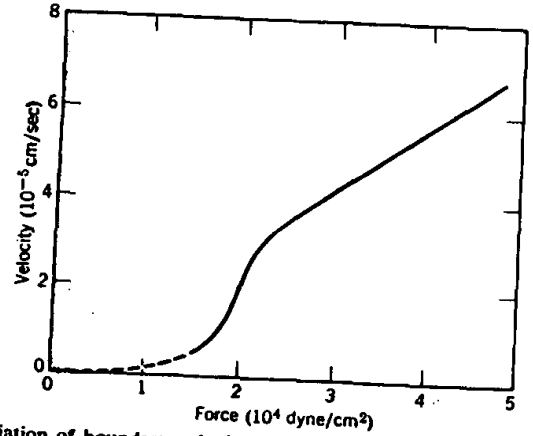

Fig. 10.7. Variation of boundary velocity v with driving force F at 750°C for a 20° tilt boundary in NaCl. From R. C. Sun and C. L. Bauer, *Acta Met.*, 18, 639 (1970).

size increases, the solute segregate concentration increases, and the average boundary curvature decreases. Additions of MgO to Al_2O_3, $CaCl_2$

*Acta Met., 10, 789 (1962).
†Acta Met., 19, 1087 (1971).

to KCl and of ThO_2 to Y_2O_3 in amounts below the solubility limit have proved effective as grain-growth inhibitors.

When grains grow to such a size that they are nearly equal to the specimen size, grain growth is stopped. In a rod sample, for example, when the grain size is equal to the rod diameter, the grain boundaries tend to form flat surfaces normal to the axis so that the driving force for boundary migration is eliminated and little subsequent grain growth occurs. Similarly, inclusions increase the energy necessary for the movement of a grain boundary and inhibit grain growth. If we consider a boundary such as the one illustrated in Fig. 10.8, the boundary energy is decreased when it reaches an inclusion proportional to the cross-sectional area of the inclusion. The boundary energy must be increased again to pull it away from the inclusion. Consequently, when a number of inclusions are present on a grain boundary, its normal curvature becomes insufficient for continued grain growth after some limiting size is reached. It has been found that this size is given by

$$d_l \approx \frac{d_i}{f_{d_i}} \qquad (10.12)$$

where d_l is the limiting grain size, d_i is the particle size of the inclusion, and f_{d_i} is the volume fraction of inclusions. Although this relationship is only approximate, it indicates that the effectiveness of inclusions increases as their particle size is lowered and the volume fraction increases.

For the process illustrated in Fig. 10.8, the boundary approaches, is attached to, and subsequently breaks away from a second-phase particle. Another possibility is that the grain boundary drags along the particle

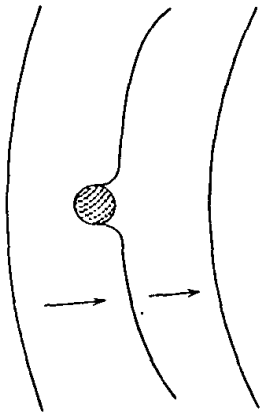

Fig. 10.8. Changing configuration of a boundary w... passing an inclusion.

which remains attached to the boundary as it moves. This requires material transport across the particle, which may occur by interface or surface or volume diffusion, by viscous flow, or by solution (precipitation in a liquid or glass inclusion), or by evaporation (condensation in a gas inclusion). We can define an inclusion particle mobility B_p relating the driving force and particle velocity $v_p = B_p F_p$ in the same way as has been done for the boundary (Eq. 10.11*b*) and for atomic diffusion in Chapter 6. When the inclusion is dragged by the boundary, their velocities are identical; in the case in which $B_p \ll B_b$ we can neglect the intrinsic boundary mobility, and the resulting grain-boundary velocity is controlled by the driving force on the boundary together with the mobility and number of inclusions per grain boundary, p:

$$v_b = \frac{B_p F_b}{p} \tag{10.13}$$

The inclusion particle moves along with the boundary, gradually becoming concentrated at boundary intersections and agglomerating into larger particles as grain growth proceeds. This is illustrated for the special case of pore agglomeration in Figs. 10.9 and 10.10.

Thus, second-phase inclusions can either (1) move along with boundaries, offering little impedance; (2) move along with boundaries, with the inclusion mobility controlling the boundary velocity; or (3) be so immobile that the boundary pulls away from the inclusion, depending on the relative values of the boundary driving force (inversely proportional to grain size), the boundary mobility (Fig. 10.7), and the inclusion particle mobility, which, depending on the assumed mechanism and particle shape, may be proportional to r_p^{-2}, r_p^{-3}, or r_p^{-4}.* As grain growth proceeds, the driving force diminishes, and any inclusions dragged along by the boundary increase in size so that their mobility decreases. As a result, the exact way in which second-phase inclusions inhibit grain growth not only depends on the properties of the particular system but also can easily change during the grain-growth process. Sorting out these effects requires a careful evaluation of the microstructure evolution in combination with the kinetics of grain growth and a detailed knowledge of system properties. Inhibition of grain growth by solid second-phase inclusions has been observed for MgO additions to Al_2O_3, for CaO additions to ThO_2, and in other systems.

A second phase that is always present during ceramic sintering and in almost all ceramic products prepared by sintering is residual porosity

*P. G. Shewmon, *Trans. A.I.M.E.*, 230, 1134 (1964); M. F. Ashby and R. M. A. Centamore, *Acta Met.*, 16, 1081 (1968).

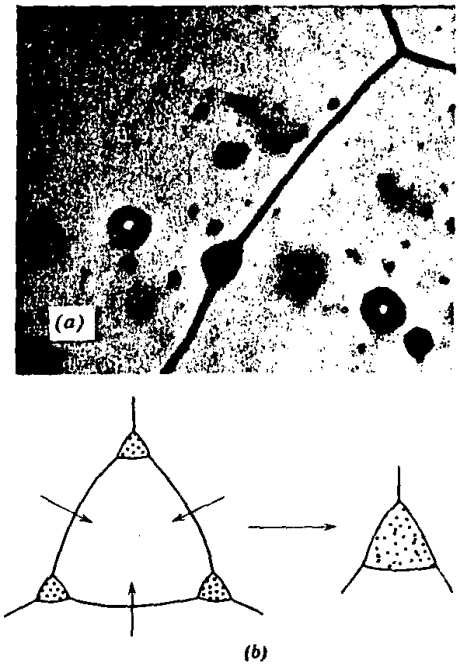

Fig. 10.9. (*a*) Pore shape distorted from spherical by moving boundary and (*b*) pore agglomeration during grain growth.

remaining from the interparticle space present in the initial powder compact. This porosity is apparent both on the grain boundaries (intergranular) and within the grains (intragranular) in the sintered CaF_2 sample shown in Fig. 10.5. It is present almost entirely at the grain corners (intergranular) in the sintered UO_2 samples shown in Fig. 10.10. As with particulate inclusions, pores on the grain boundaries may be left behind by the moving boundary or migrate with the boundary, gradually agglomerating at grain corners, as illustrated in Figs. 10.9 and 10.10. In the early stages of sintering, when the boundary curvature and the driving force for boundary migration are high, pores are often left behind, and a cluster of small pores in the center of a grain is a commonly observed result (see Fig. 10.5). In the later stages of sintering, when the grain size is larger and the driving force for boundary migration is lower, it is more usual for pores to be dragged along by the boundary, slowing grain growth.

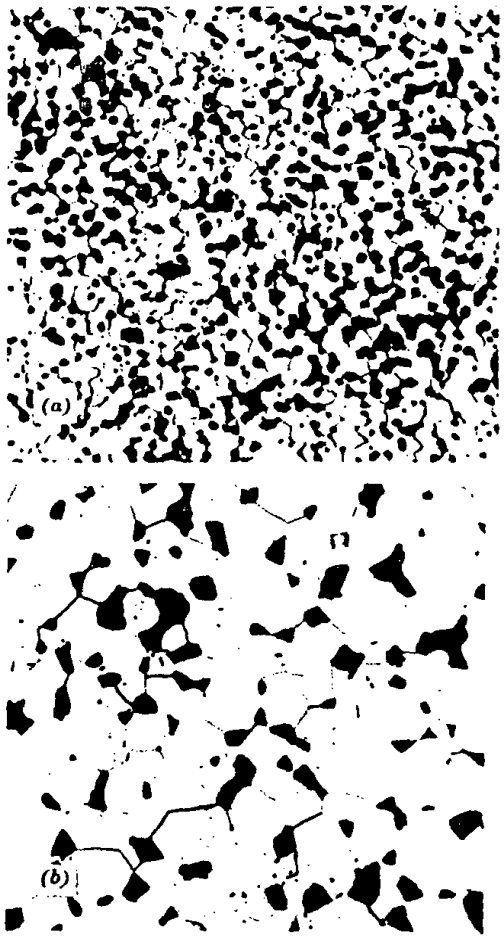

Fig. 10.10. Grain growth and pore growth in sample of UO_2 after (*a*) 2 min, 91.5% dense, and (*b*) 5 hr, 91.9% dense, at 1600°C (400×). From Francois and Kingery.

Another factor that may restrain grain growth is the presence of a liquid phase. If a small amount of a boundary liquid is formed, it tends to slow grain growth, since the driving force is reduced and the diffusion path is increased. There are now two solid-liquid interfaces, and the driving force is the difference between them, that is, $(1/r_1 + 1/r_2)_A - (1/r_1 + 1/r_2)_B$, which

is smaller than either alone; in addition, if the liquid wets the boundary, the interface energy must be lower than the pure-grain-boundary energy. Also, the process of solution, diffusion through a liquid film, and precipitation is usually slower than the jump across a boundary. However, this case is more complex in that grain growth may be enhanced by the presence of a reactive liquid phase during the densification process, as discussed in Section 10.4. In addition, a very small amount of liquid may enhance secondary recrystallization, as discussed later, whereas larger amounts of liquid phase may give rise to the grain-growth process described in Chapter 9. In practice, it is found that addition of a moderate amount of silicate liquid phase to aluminum oxide prevents the extensive grain growth which frequently occurs with purer materials.

Secondary Recrystallization. The process of secondary recrystallization, sometimes called discontinuous or exaggerated grain growth, occurs when some small fraction of the grains grow to a large size, consuming the uniform-grain-size matrix. Once a single grain grows to such a size that it has many more sides than the neighboring grains (such as the grain with fifty sides illustrated in Fig. 10.4), the curvature of each side increases, and it grows more rapidly than the smaller grains with fewer sides. The increased curvature on the edge of a large grain is particularly evident in Fig. 10.11, which shows a large alumina crystal growing at the expense of a uniform-particle-size matrix.

Secondary crystallization is particularly likely to occur when continuous grain growth is inhibited by the presence of impurities or pores. Under these conditions the only boundaries able to move are those with a curvature much larger than the average; that is, the exaggerated grains with highly curved boundaries are able to grow, whereas the matrix material remains uniform in grain size. The rate of growth of the large grains is initially dependent on the number of sides. However, after growth has reached the point at which the exaggerated grain diameter is much larger than the matrix diameter, $d_e \gg d_m$, the curvature is determined by the matrix grain size and is proportional to $1/d_m$. That is, there is an induction period corresponding to the increased growth rate and the formation of a grain large enough to grow at the expense of the constant-grain-size matrix. Therefore, the growth rate is constant as long as the grain size of the matrix remains unchanged. Consequently, the kinetics of secondary recrystallization is similar to that of primary recrystallization, even though the nature of the nucleation and driving force is different.

Secondary recrystallization is common for oxide, titanate, and ferrite ceramics in which grain growth is frequently inhibited by minor amounts of second phases or by porosity during the sintering process. A typical resultant structure is illustrated for barium titanate in Fig. 10.12, and the

Fig. 10.11. Growth of a large Al_2O_3 crystal into a matrix of uniformly sized grains (495×). Compare with Fig. 10.4. Courtesy R. L. Coble.

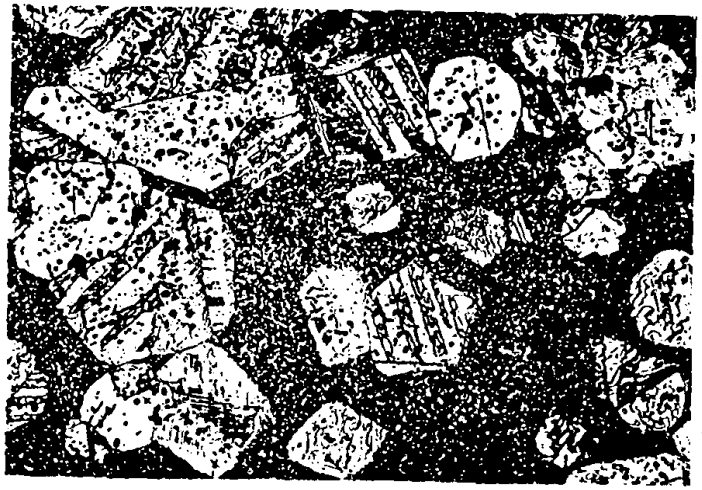

Fig. 10.12. Large grains of barium titanate growing by secondary recrystallization from a fine-grained matrix (250×). Courtesy R. C. DeVries.

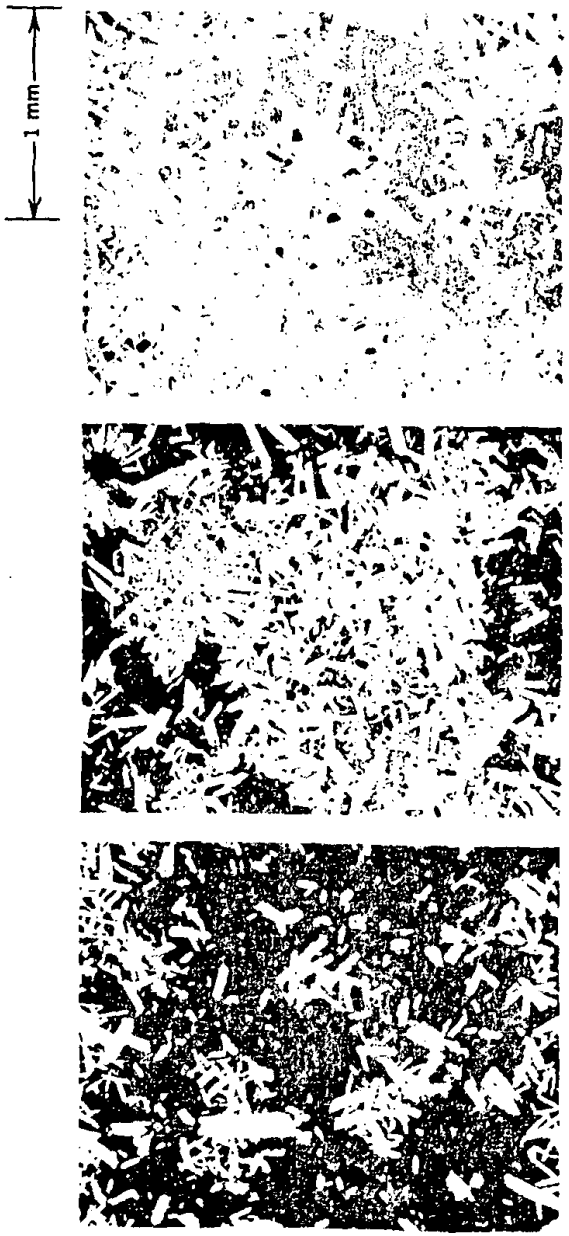

Fig. 10.13. Large grains of Al_2O_3 growing by secondary recrystallization from a fine-grained matrix. Courtesy I. B. Cutler, in reference 5.

progressive growth of aluminum oxide crystals during secondary recrystallization is illustrated in Fig. 10.13.

When polycrystalline bodies are made from fine powder, the extent of secondary recrystallization depends on the particle size of the starting material. Coarse starting material gives a much smaller relative grain growth, as illustrated in Fig. 10.14 for beryllia. This is caused by both the rate of nucleation and the rate of growth. There are almost always present in the fine-grained matrix a few particles of substantially larger particle size than the average; these can act as embryos for secondary recrystallization, since already $d_s > d_m$, and growth proceeds to a rate proportional to $1/d_m$. In contrast, as the starting particle size increases, the chances of grains being present which are much larger in particle size than the average are much decreased, and consequently the nucleation of secondary recrystallization is much more difficult; the growth rate, proportional to $1/d_m$, is also smaller. In the data shown in Fig. 10.14, material having a starting particle size of 2 microns grows to a final particle size of about 50 microns, whereas material with an initial particle size of 10 microns shows a final grain size of only about 25 microns. This result of a much larger final grain size for a smaller initial particle size would be very puzzling if the process of secondary recrystallization was not known to occur.

Secondary recrystallization has been observed to occur with the boundaries of the large grains apparently perfectly straight (Fig. 10.15). Here the previous discussion of the surface tension and curvature of the phase boundary does not apply directly. That is, the boundary energy is

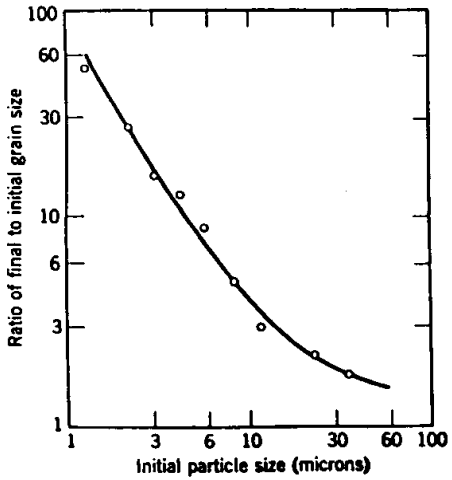

Fig. 10.14. Relative grain growth during secondary recrystallization of BeO heated 2½ hr at 2000°C. From P. Duwez, F. Odell, and J. L. Taylor, *J. Am. Ceram. Soc.*, 32, 1 (1949).

not independent of crystal directions, and the growth planes are those of low surface energy. These structures all seem to occur in systems having a small concentration of impurity which gives rise to a small amount of a boundary phase. The driving force for secondary recrystallization is the lower surface energy of the large grain compared with the high-surface-energy faces or small radius of curvature of adjacent grains. Transfer of material under these conditions can only occur when there is an intermediate boundary phase separating the surfaces of the small and large grains. The amount of second phase present tends to increase at the boundaries of the large crystals compared with that at other boundaries in the system, and a large grain continues to grow once it is initiated. If the amount of boundary phase is increased, however, normal grain growth and this kind of secondary recrystallization are both inhibited, as discussed previously.

Secondary recrystallization affects both the sintering of ceramics and resultant properties. Excessive grain growth is frequently harmful to mechanical properties (see Sections 5.5 and 15.5). For some electrical and magnetic properties either a large or a small grain size may contribute to improved properties. Occasionally grain growth has been discussed in the literature as if it were an integral part of the densification process. That this is not true can best be seen from Fig. 10.16. A sample of aluminum oxide with an initial fine pore distribution was heated to a high temperature so that secondary recrystallization occurred. The recrystallization has left almost the same amount of porosity as was present in the initial

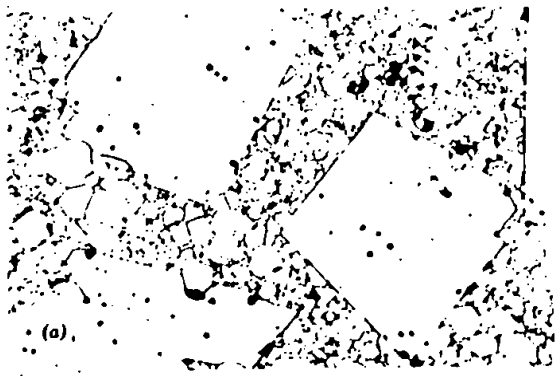

Fig. 10.15. (*a*) Idiomorphic grains in a polycrystalline spinel. The large grain edges appear straight, whereas the shape of the small grains is controlled by surface tension (350×). Courtesy R. L. Coble.

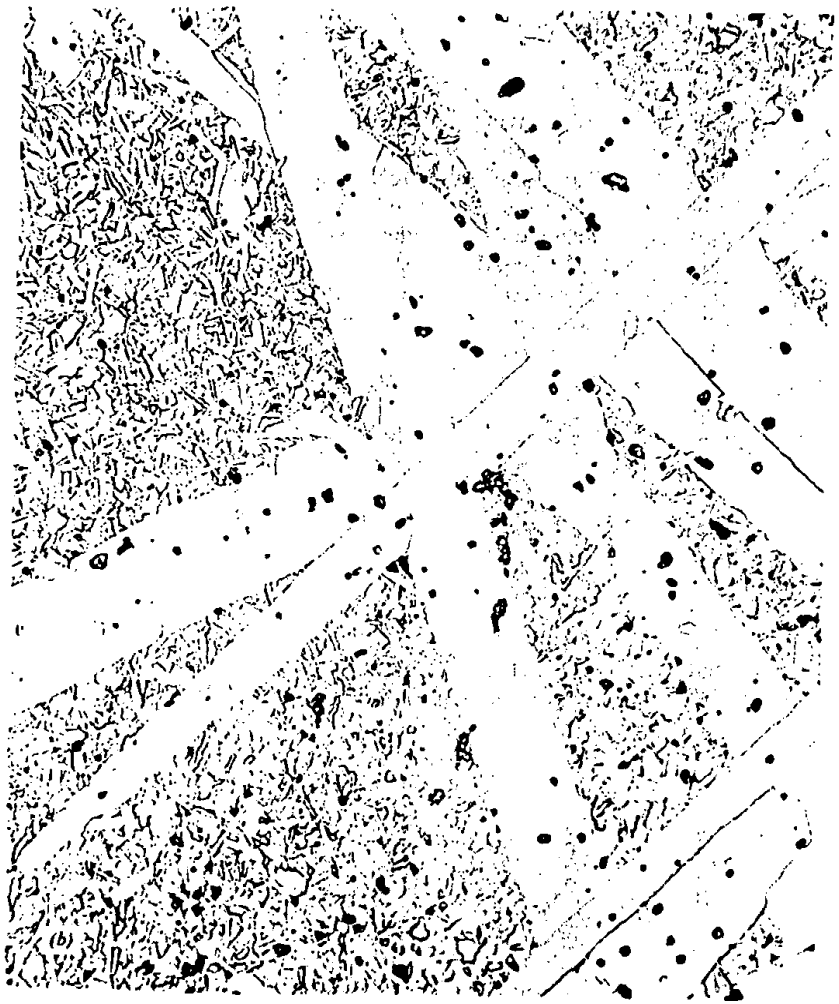

Fig. 10.15 (*Continued*). (*b*) Idiomorphic grains of α-6H SiC in a β-SiC matrix (1000×).

compact. Elimination of porosity is a related but separate subject and is considered in following sections. An application in which secondary recrystallization has been useful is in the development of preferred orientation on firing of the magnetically hard ferrite, $BaFe_{12}O_{19}$.* For this

*A. L. Stuijts, *Trans. Brit. Ceram. Soc.*, *55*, 57 (1956).

Fig. 10.15 (*Continued*). (*c*) Detail of boundary (75,000×). Courtesy S. Prochazka.

magnetic material it is desirable to obtain a high density as well as a high degree of preferred orientation in the sintered product. Particles of the powdered material can be oriented to a considerable extent by subjecting them to a high magnetic field while forming. On sintering there was a 57% alignment after heating at 1250°C. On further heating at 1340°C the

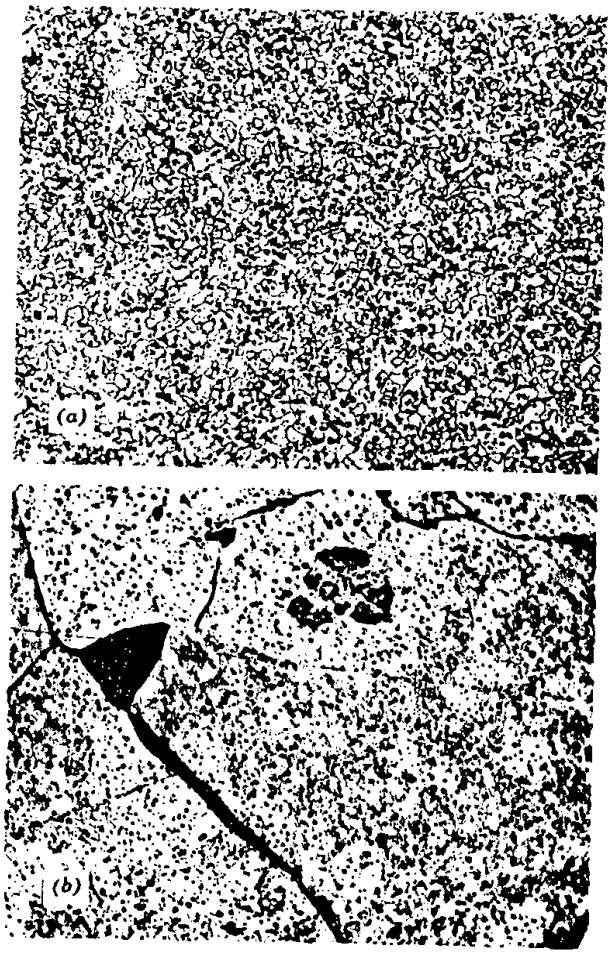

Fig. 10.16. A specimen of alumina (*a*) sintered 1 hr at 1800°C and (*b*) heated 1 hr at 1900°C to give secondary recrystallization. Note that the pore spacing has not changed. Courtesy J. E. Burke.

preferred orientation increased to 93% alignment, corresponding to the structural change brought about by secondary recrystallization. It seems apparent that the few large grains in the starting material are more uniformly aligned than the fine surrounding material. These grains serve as nuclei for the secondary recrystallization process and give rise to a highly oriented final product.

10.2 Solid-State Sintering

Changes that occur during the firing process are related to (1) changes in grain size and shape, (2) changes in pore shape, and (3) changes in pore size. In Section 10.1 we concentrated on changes in grain size; in this and the following section we are mainly concerned with changes in porosity, that is, the changes taking place during the transformation of an originally porous compact to a strong, dense ceramic. As formed, a powder compact, before it has been fired, is composed of individual grains separated by between 25 and 60 vol% porosity, depending on the particular material used and the processing method. For maximizing properties such as strength, translucency, and thermal conductivity, it is desirable to eliminate as much of this porosity as possible. For some other applications it may be desirable to increase this strength without decreasing the gas permeability. These results are obtained during firing by the transfer of material from one part of the structure to the other. The kind of changes that may occur are illustrated in Fig. 10.17. The pores initially present can change shape, becoming channels or isolated spheres, without necessarily changing in size. More commonly, however, both the size and shape of the pores present change during the firing process, the pores becoming more spherical in shape and smaller in size as firing continues.

Driving Force for Densification. The free-energy change that gives rise to densification is the decrease in surface area and lowering of the surface free energy by the elimination of solid-vapor interfaces. This usually takes place with the coincidental formation of new but lower-energy

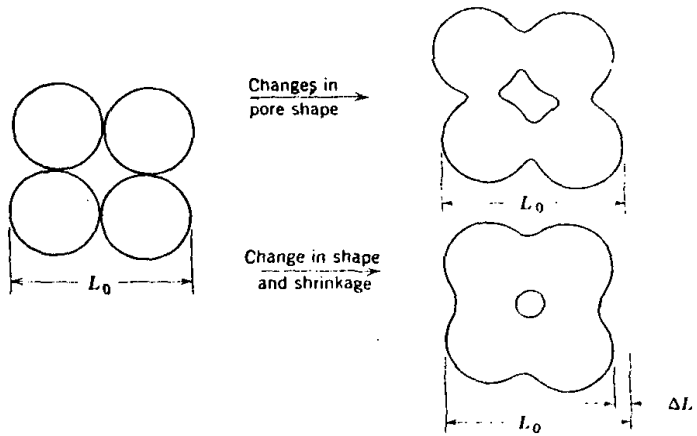

Fig. 10.17. Changes in pore shape do not necessarily require shrinkage.

solid-solid interfaces. The net decrease in free energy occurring on sintering a 1-micron particle size material corresponds to an energy decrease of about 1 cal/g. On a microscopic scale, material transfer is affected by the pressure difference and changes in free energy across a curved surface. These changes are due to the surface energy and have been discussed in Chapter 5 and referred to in Section 10.1. If the particle size, and consequently the radius of curvature, is small, these effects may be of a substantial magnitude. As indicated in Chapter 5, they become large when the radius of curvature is less than a few microns. This is one of the major reasons why much ceramic technology is based on and depends on the use of fine-particle materials.

Most of the insight into the effect of different variables on the sintering process has come from considering simple systems and comparing experimental data with simple models. Since our major aim is to be sure we understand the importance of different variables in traditional or new systems, we use this method here. Since the driving force is the same (surface energy) in all systems, considerable differences in behavior in various types of systems must be related to different mechanisms of material transfer. Several can be imagined—evaporation and condensation, viscous flow, surface diffusion, grain-boundary or lattice diffusion, and plastic deformation are among those that occur to us. Of these, diffusion and viscous flow are important in the largest number of systems; evaporation-condensation is perhaps the easiest to visualize.

Evaporation-Condensation. During the sintering process there is a tendency for material transfer because of the differences in surface curvature and consequently the differences in vapor pressure at various parts of the system. Material transfer brought about in this way is only important in a few systems; however, it is the simplest sintering process to treat quantitatively. We derive the sintering rate in some detail, since it provides a sound basis for understanding more complex processes.

Let us consider the initial stages of the process when the powder compact is just beginning to sinter and concentrate on the interaction between two adjacent particles (Fig. 10.18). At the surface of the particle there is a positive radius of curvature so that the vapor pressure is somewhat larger than would be observed for a flat surface. However, just at the junction between particles there is a neck with a small negative radius of curvature and a vapor pressure an order of magnitude lower than that for the particle itself. The vapor-pressure difference between the neck area and the particle surface tends to transfer material into the neck area.

We can calculate the rate at which the bonding area between particles increases by equating the rate of material transfer to the surface of the

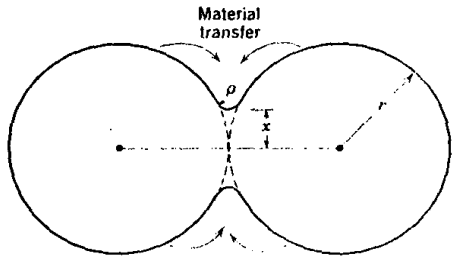

Fig. 10.18. Initial stages of sintering by evaporization-condensation.

lens between the spheres with the increase in its volume. The vapor pressure over the small negative radius of curvature is decreased because of the surface energy in accordance with the Thomson-Freundlich (Kelvin) equation discussed in Chapter 5:

$$\ln \frac{p_i}{p_0} = \frac{\gamma M}{dRT}\left(\frac{1}{\rho} + \frac{1}{x}\right) \tag{10.14}$$

where p_i is the vapor pressure over the small radius of curvature, M is the molecular weight of the vapor, and d is the density. In this case the neck radius is much larger than the radius of curvature at the surface, ρ, and the pressure difference $p_0 - p_i$ is small. Consequently, to a good approximation, $\ln p_i/p_0$ equals $\Delta p/p_0$, and we can write

$$\Delta p = \frac{\gamma M p_0}{d\rho RT} \tag{10.15}$$

where Δp is the difference between the vapor pressure of the small negative radius of curvature and the saturated vapor in equilibrium with the nearly flat particle surfaces. The rate of condensation is proportional to the difference in equilibrium and atmospheric vapor pressure and is given by the Langmuir equation to a good approximation as

$$m = \alpha\, \Delta p \left(\frac{M}{2\pi RT}\right)^{1/2} \quad \text{g/cm}^2\text{/sec} \tag{10.16}$$

where α is an accommodation coefficient which is nearly unity. Then the rate of condensation should be equal to the volume increase. That is,

$$\frac{mA}{d} = \frac{dv}{dt} \quad \text{cm}^3\text{/sec} \tag{10.17}$$

From the geometry of the two spheres in contact, the radius of curvature at the contact points is approximately equal to $x^2/2r$ for x/r less than 0.3;

the area of the surface of the lens between spheres is approximately equal to $\pi^2 x^3/r$; the volume contained in the lenticular area is approximately $\pi x^4/2r$. That is,

$$\rho = \frac{x^2}{2r}; \qquad A = \frac{\pi^2 x^3}{r}; \qquad v = \frac{\pi x^4}{2r} \tag{10.18}$$

Substituting values for m in Eq. 10.16, A and v in Eq. 10.18 into Eq. 10.17 and integrating, we obtain a relationship for the rate of growth of the bond area between particles:

$$\frac{x}{r} = \left(\frac{3\sqrt{\pi}\gamma M^{3/2} p_o}{\sqrt{2} R^{3/2} T^{3/2} d^2}\right)^{1/3} r^{-2/3} t^{1/3} \tag{10.19}$$

This equation gives the relationship between the diameter of the contact area between particles and the variables influencing its rate of growth.

The important factor from the point of view of strength and other material properties is the bond area in relation to the individual particle size, which gives the fraction of the projected particle area which is bonded together—the main factor in fixing strength, conductivity, and related properties. As seen from Eq. 10.19, the rate at which the area between particles forms varies as the two-thirds power of time. Plotted on a linear scale, this decreasing rate curve has led to characterizations of *end point* conditions corresponding to a certain sintering time. This concept of an end point is useful, since periods of time for sintering are not widely changed; however, the same rate law is observed for the entire process (Fig. 10.19*b*).

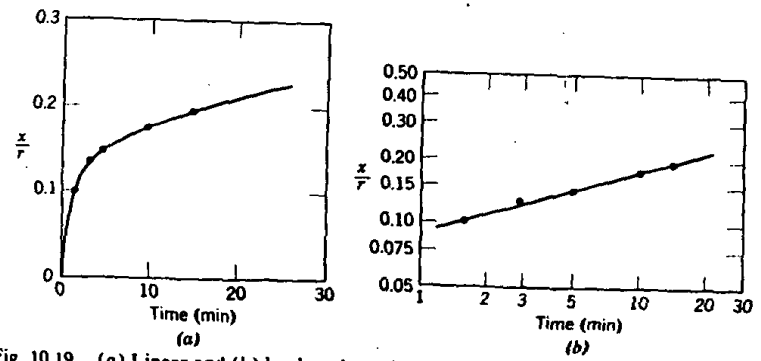

Fig. 10.19. (*a*) Linear and (*b*) log-log plots of neck growth between spherical particles of sodium chloride at 725°C.

If we consider the changes in structure that take place during a process such as this, it is clear that the distance between centers of spherical particles (Fig. 10.18) is not affected by the transfer of material from the particle surface to the interparticle neck. This means that the total shrinkage of a row of particles, or of a compact of particles, is unaffected by vapor-phase-material transfer and that only the shape of pores is changed. This changing shape of pores can have an appreciable effect on properties but does not affect density.

The principal variables in addition to time that affect the rate of pore-shape change through this process are the initial particle radius (rate proportional to $1/r^{2/3}$) and the vapor pressure (rate proportional to $p_o^{1/3}$). Since the vapor pressure increases exponentially with temperature, the process of vapor-phase sintering is strongly temperature-dependent. From a processing point of view, the two main variables over which control can be exercised for any given material are the initial particle size and the temperature (which fixes the vapor pressure). Other variables are generally not easy to control, nor are they strongly dependent on conditions of use.

The negligible shrinkage corresponding to vapor-phase-material transfer is perhaps best illustrated in Fig. 10.20, which shows the shape changes that occur on heating a row of initially spherical sodium chloride particles. After long heating the interface contact area has increased; the

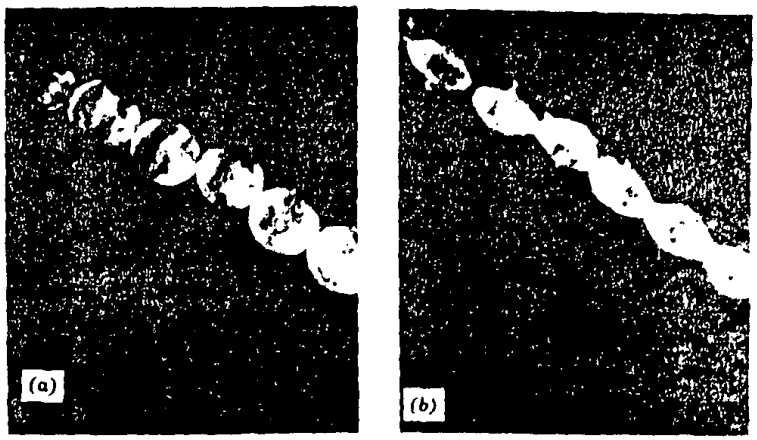

Fig. 10.20. Photomicrographs of sintering sodium chloride at 750°C: (*a*) 1 min; (*b*) 90 min.

particle diameter has been substantially decreased, but the distance between particle centers, that is, the shrinkage, has not been affected.

Vapor-phase-material transfer requires that materials be heated to a temperature sufficiently high for the vapor pressure to be appreciable. For micron-range particle sizes this requires vapor pressures in the order of 10^{-4} to 10^{-5} atm, a pressure higher than those usually encountered during sintering of oxide and similar phases. Vapor-phase transfer plays an important part in the changes occurring during treatment of halides such as sodium chloride and is important for the changes in configuration observed in snow and ice technology.

Solid-State Processes. The difference in free energy or chemical potential between the neck area and the surface of the particle provides a driving force which causes the transfer of material by the fastest means available. If the vapor pressure is low, material transfer may occur more readily by solid-state processes, several of which can be imagined. As shown in Fig. 10.21 and Table 10.1, in addition to vapor transport (process 3), matter can move from the particle surface, from the particle bulk, or from the grain boundary between particles by surface, lattice, or grain-boundary diffusion. Which one or more of these processes actually contributes significantly to the sintering process in a particular system depends on their relative rates, since each is a parallel method of lowering the free energy of the system (parallel reaction paths have been discussed in Chapter 9). There is a most significant difference between these paths for matter transport: the transfer of material from the surface to the neck by surface or lattice diffusion, like vapor transport, does not lead to any decrease in the distance between particle centers. That is, these processes do not result in shrinkage of the compact and a decrease in porosity. Only

Table 10.1. Alternate Paths for Matter Transport During the Initial Stages of Sintering[a]

Mechanism Number	Transport Path	Source of Matter	Sink of Matter
1	Surface diffusion	Surface	Neck
2	Lattice diffusion	Surface	Neck
3	Vapor transport	Surface	Neck
4	Boundary diffusion	Grain boundary	Neck
5	Lattice diffusion	Grain boundary	Neck
6	Lattice diffusion	Dislocations	Neck

[a] See Fig. 10.21.

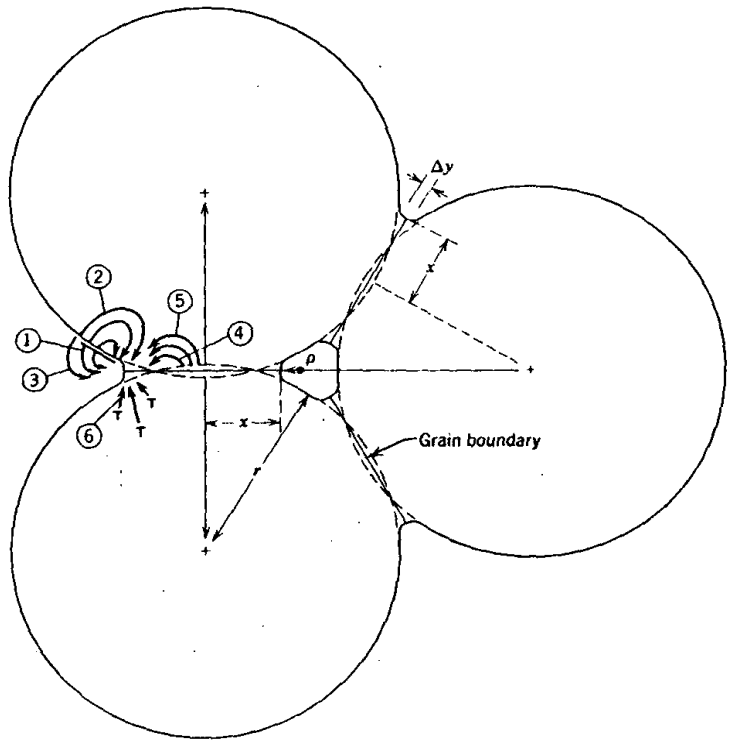

Fig. 10.21. Alternate paths for matter transport during the initial stages of sintering. Courtesy M. A. Ashby. (See Table 10.1.)

transfer of matter from the particle volume or from the grain boundary between particles causes shrinkage and pore elimination.

Let us consider mechanism 5, matter transport from the grain boundary to the neck by lattice diffusion. Calculation of the kinetics of this process is exactly analogous to determination of the rate of sintering by a vapor-phase process. The rate at which material is discharged at the surface area is equated to the increase in volume of material transferred. The geometry is slightly different:

$$\rho = \frac{x^2}{4r}; \qquad A = \frac{\pi^2 x^3}{2r}; \qquad V = \frac{\pi x^4}{4r} \tag{10.20}$$

The process can be visualized most easily by considering the rate of

migration of vacancies. In the same way that there are differences in vapor pressure between the surface of high negative curvature and the nearly flat surfaces, there is a difference in vacancy concentration. If c is the concentration of vacancies and Δc is the excess concentration over the concentration on a plane surface c_o, then, equivalent to Eq. 10.15,

$$\Delta c = \frac{\gamma a^3 c_0}{kT\rho} \tag{10.21}$$

where a^3 is the atomic volume of the diffusing vacancy and k is the Boltzmann constant. The flux of vacancies diffusing away from the neck area per second per centimeter of circumferential length under this concentration gradient can be determined graphically and is given by

$$J = 4D_V \Delta c \tag{10.22}$$

Where D_V is the diffusion coefficient for vacancies, D_V equals D^*/a^3c_0 if D^* is the self-diffusion coefficient. Combining Eqs. 10.22 and 10.21 with the continuity equation similar to Eq. 10.17, we obtain the result

$$\frac{x}{r} = \left(\frac{40\gamma a^3 D^*}{kT}\right)^{1/5} r^{-3/5} t^{1/5} \tag{10.23}$$

With diffusion, in addition to the increase in contact area between particles, there is an approach of particles centers. The rate of this approach is given by $d(x^2/2r)/dt$. Substituting from Eq. 10.23, we obtain

$$\frac{\Delta V}{V_0} = \frac{3\,\Delta L}{L_0} = 3\left(\frac{20\gamma a^3 D^*}{\sqrt{2}kT}\right)^{2/5} r^{-6/5} t^{2/5} \tag{10.24}$$

These results indicate that the growth of bond formation between particles increases as a one-fifth power of time (a result which has been experimentally observed for a number of metal and ceramic systems) and that the shrinkage of a compact densified by this process should be proportional to the two-fifths power of time. The decrease in densification rate with time gives rise to an apparent end-point density if experiments are carried out for similar time periods. However, when plotted on a log-log basis, the change in properties is seen to occur as expected from Eq. 10.24. Experimental data for sodium fluoride and aluminum oxide are shown in Fig. 10.22.

The relationships derived in Eqs. 10.23 and 10.24 and similar relationships for the alternate matter transport processes, which we shall not derive, are important mainly for the insight that they provide on the variables which must be controlled in order to obtain reproducible processing and densification. It is seen that the sintering rate steadily decreases with time, so that merely sintering for longer periods to obtain

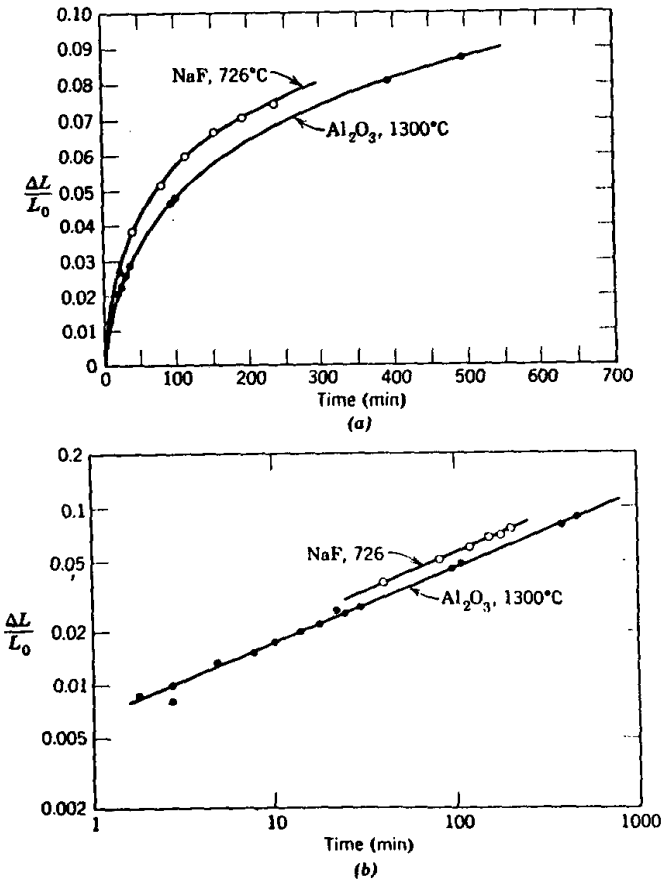

Fig. 10.22. (*a*) Linear and (*b*) log-log plots of shrinkage of sodium fluoride and aluminum oxide compacts. From J. E. Burke and R. L. Coble.

improved properties is impracticable. Therefore, time is not a major or critical variable for process control.

Control of particle size is very important, since the sintering rate is roughly proportional to the inverse of the particle size. The interface diameter achieved after sintering for a period of 100 hr at 1600°C is illustrated in Fig. 10.23 as a function of particle size. For large particles even these long periods do not cause extensive sintering; as the particle size is decreased, the rate of sintering is raised.

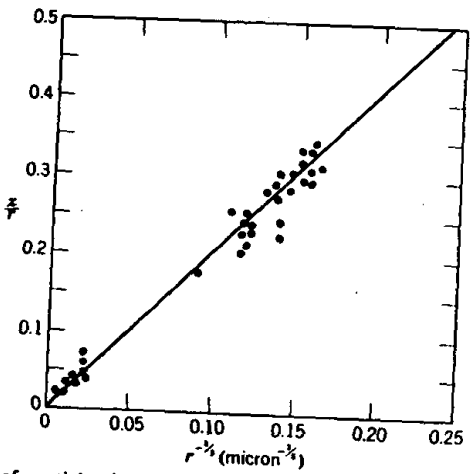

Fig. 10.23. Effect of particle size on the contact area growth in Al_2O_3 heated 100 hr at 1600°C. From R. L. Coble.

The other variable appearing in Eqs. 10.22 and 10.24 that is subject to analysis and some control is the diffusion coefficient; it is affected by composition and by temperature; the relative effectiveness of surfaces, boundaries, and volume as diffusion paths is affected by the microstructure. A number of relationships similar to Eqs. 10.23 and 10.24 have been derived, and it has been shown that surface diffusion is most important during early stages of sintering (these affect the neck diameter between particles but not the shrinkage or porosity); grain-boundary diffusion and volume diffusion subsequently become more important. In ionic ceramics, as discussed in Chapter 9, both the anion and the cation diffusion coefficients must be considered. In Al_2O_3, the best studied material, oxygen diffuses rapidly along the grain boundaries, and the more slowly moving aluminum ion at the boundary or in the bulk controls the overall sintering rate. As discussed in Chapter 5, the grain-boundary structure, composition, and electrostatic charge are influenced strongly by temperature and by impurity solutes; as discussed in Chapter 6, the exact mechanism of grain-boundary diffusion remains controversial. Estimates of the grain-boundary-diffusion width from sintering data range from 50 to 600 Å. These complications require us to be careful not to overanalyze data in terms of specific numerical results, since the time or temperature dependence of sintering may be in accordance with several plausible models. In general the presence of solutes which enhance either

boundary or volume diffusion coefficients enhance the rate of solid-state sintering. As discussed in Chapter 6, both boundary and volume diffusion coefficients are strongly temperature-dependent, which means that the sintering rate is strongly dependent on the temperature level.

In order to effectively control sintering processes which take place by solid-state processes, it is essential to maintain close control of the initial particle size and particle-size distribution of the material, the sintering temperature, the composition and frequently the sintering atmosphere.

As an example of the influence of solutes, Fig. 10.24 illustrates the effect of titania additions on the sintering rate of a relatively pure alumina in a region of volume diffusion. (Both volume and boundary diffusion processes are enhanced.) It is believed that Ti enters Al_2O_3 substitutionally as Ti^{+3} and Ti^{+4} (Ti_{Al} and $Ti_{Al}^{\cdot}$). At equilibrium

$$3Ti_{Al} + \frac{3}{4}O_2(g) = 3Ti_{Al}^{\cdot} + V_{Al}''' + \frac{3}{2}O_0 \qquad (10.25)$$

from which

$$K_1 = \frac{[Ti_{Al}^{\cdot}]^3[V_{Al}''']}{[Ti_{Al}]^3[P_{O_2}]^{3/4}} \qquad (10.26)$$

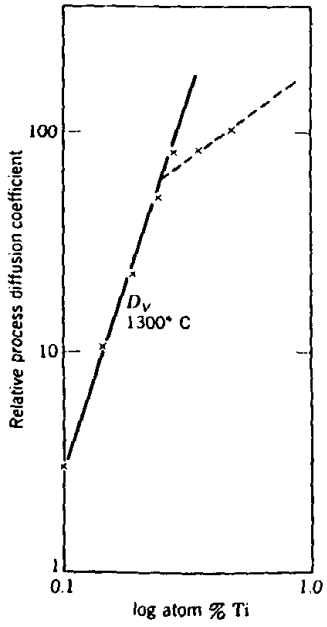

Fig. 10.24. Data for the relative sintering process diffusion coefficient with Ti additions to Al_2O_3. $D_V[Ti]^1$. From R. D. Bagley, I. B. Cutler, and D. L. Johnson, *J. Am. Ceram. Soc.*, 53, 136 (1970); R. J. Brook, *J. Am. Ceram. Soc.*, 55, 114 (1972).

In the powders used, divalent impurities such as magnesium exceed in concentrations the intrinsic defect levels, so that overall charge neutrality at moderate titania levels is achieved by

$$[\mathrm{Ti}_{\mathrm{Al}}^{\cdot}] = [\mathrm{Mg}_{\mathrm{Al}}^{\prime}] \tag{10.27}$$

and at constant impurity and oxygen pressure levels, combining Eqs. 10.26 and 10.27 gives

$$[V_{\mathrm{Al}}^{\prime\prime\prime}] = K_2[\mathrm{Ti}_{\mathrm{Al}}]^3 \tag{10.28}$$

Since the total Ti addition ($\mathrm{Ti}_{\mathrm{Al}} + \mathrm{Ti}_{\mathrm{Al}}^{\cdot}$) is much greater than the impurity levels, $[\mathrm{Ti}]_{\mathrm{Total}} \approx [\mathrm{Ti}_{\mathrm{Al}}^{\cdot}]$ and $[V_{\mathrm{Al}}^{\prime\prime\prime}] \approx K_2[\mathrm{Ti}]_{\mathrm{Total}}^3$. The dependence of lattice defect concentrations on titania concentration is shown in Fig. 10.25 for the proposed model. As discussed in Chapter 6, the diffusion coefficient is proportional to the vacancy concentration; as a result the effect of this model is to anticipate an increase in the sintering rate proportional to the third power of titania concentration as experimentally observed (Fig. 10.24). At higher concentrations the dependence on titania concentration should become less steep, which is suggested by the sintering data.

Thus far our discussion of the variables influencing the sintering process has been based on the initial stages of the process, in which models are based on solid particles in contact. As the process continues, an intermediate microstructure forms in which the pores and solid are both continuous, followed by a later stage in which isolated pores are separated from one another. A number of analytical expressions have

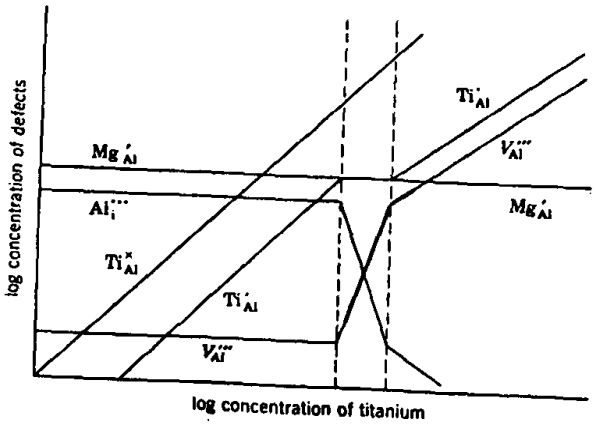

Fig. 10.25. Model for the dependence of defect concentrations on the Ti concentration in Al_2O_3. From R. J. Brook, *J. Am. Ceram. Soc.*, **55**, 114 (1972).

been derived from specific microstructural models for the transport processes listed in Table 10.1. In the later stages of the process only two mechanisms are important: boundary diffusion from sources on the boundary and lattice diffusion from sources on the boundary. For a nearly spherical pore the flux of material to a pore can be approximated as

$$J = 4\pi D_v \, \Delta c \left(\frac{rR}{R-r}\right) \tag{10.29}$$

where D_v is the volume diffusion coefficient, Δc is the excess vacancy concentration (Eq. 10.21), r is the pore radius, and R is the effective-material-source radius. The importance of microstructure in applying this sort of analysis to specific systems is illustrated in Fig. 10.26. For a sample

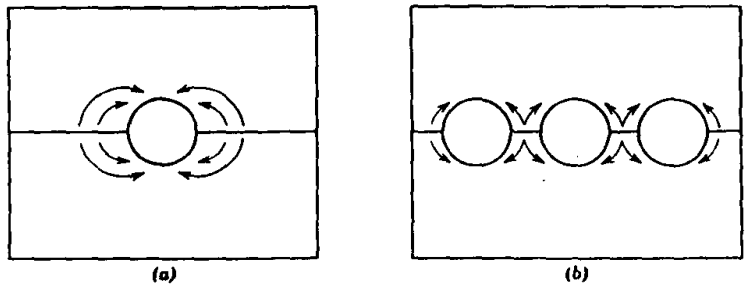

Fig. 10.26. The mean diffusion distance for material transport is smaller when there are more of the same size of pores in a boundary.

with a larger number of pores, all the same size, on a boundary the mean diffusion distance is smaller when there are more pores, and pore elimination is accomplished more quickly for the sample with the higher porosity. Thus, although the terms which influence the rate of sintering—volume or boundary diffusion coefficient (and therefore temperature and solute concentration) surface energy and pore size—are well established, the geometrical relationship of grain boundaries to the pores may have a variety of forms and is critical in determining what actually occurs.

With fine-grained materials such as oxides, it is usual to observe an increase in both grain size and pore size during the early stages of heat treatment, as illustrated for Lucalox alumina in Fig. 10.27. This partially results from the presence of agglomerates of the fine particles which sinter rapidly, leaving interagglomerate pores, and is partly due to the rapid grain growth during which pores are agglomerated by moving with the boundaries, as illustrated in Fig. 10.9. In cases in which agglomeration

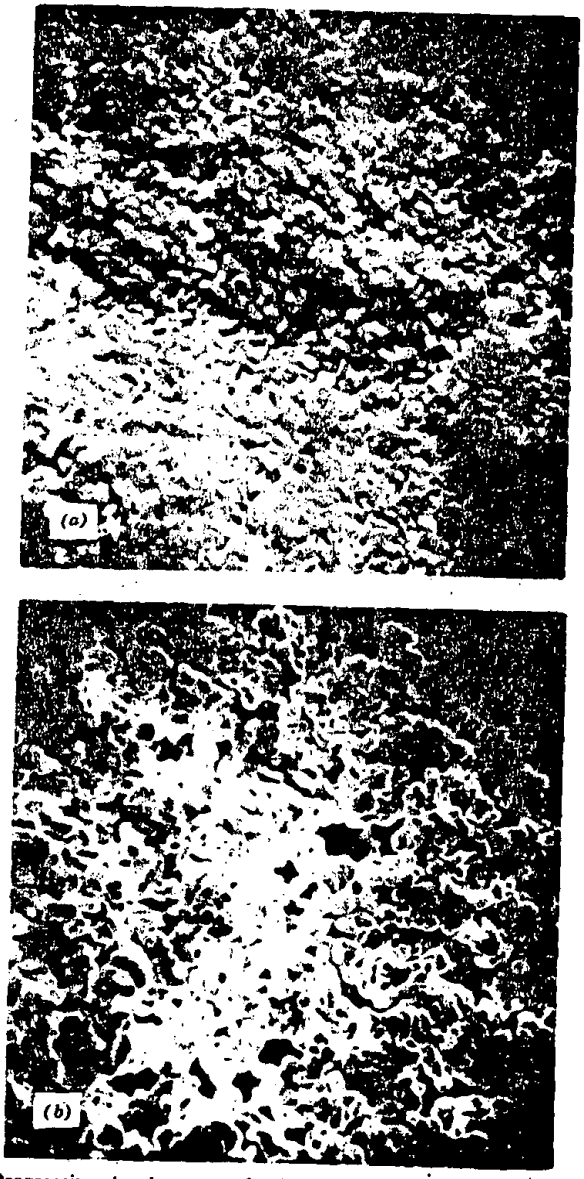

Fig. 10.27. Progressive development of microstructure in Lucalox alumina. Scanning electron micrographs of (*a*) initial particles in the compact (5000×), (*b*) after 1 min at 1700°C (5000×).

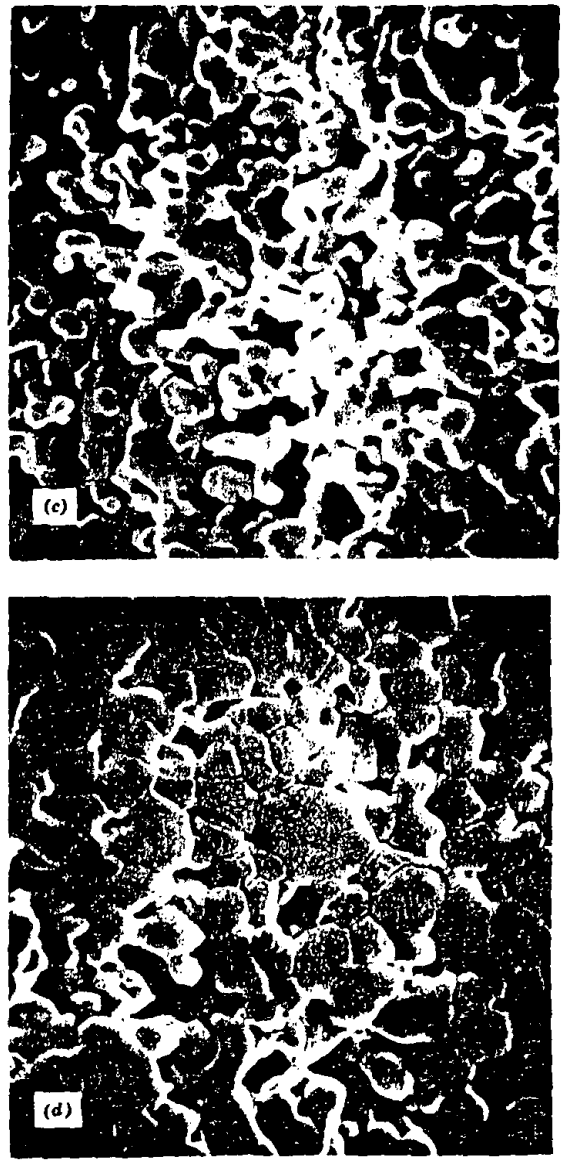

Fig. 10.27 (*Continued*) (*c*) Scanning electron micrographs after 2½ min at 1700°C (5000×), and (*d*) after 6 min at 1700°C (5000×). Note that pores and grains increase in size, that there are variations in packing and in pore size, and that pores remain located between dense grains.

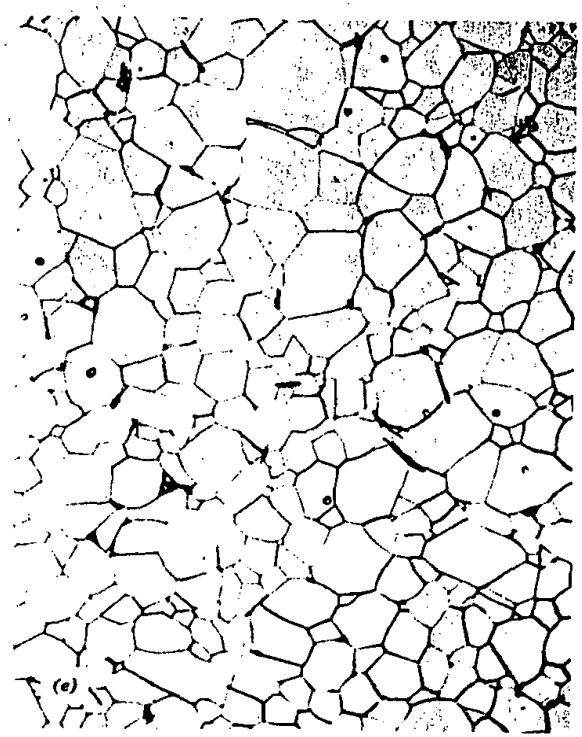

Fig. 10.27 (*Continued*) (*e*) The final microstructure is nearly porefree, with only a few pores located within grains (500×). Courtesy C. Greskovich and K. W. Lay.

of fine precipitated particles into clumps is severe, ball milling to break up the agglomerates leads to a remarkable increase in the sintering rate. Even minor variations in the original particle packing are exaggerated during the pore growth process; in addition, spaces between agglomerates and occasional larger voids resulting from the bridging of particles or agglomerates are present. As a result, during intermediate stages of the sintering process there is a range of pore sizes present, and the slower elimination of the larger pores leads to variations in pore concentration in the later stages of the sintering process, as illustrated in Fig. 10.28*c*.

In addition to local agglomerates and packing differences, pore-concentration variations in the later stages of sintering can result from particle-size variations in the starting material, from green density variations caused by die-wall friction during pressing, and from the more rapid elimination of porosity near surfaces caused by temperature gradients during heating, as shown in Fig. 10.28. The importance of local variations in pore concentration results from the fact that the part of the sample containing pores tends to shrink but is restrained by other porefree parts. That is, the effective diffusion distance is no longer from the pore to an adjacent grain boundary but a pore-pore or pore-surface distance many orders of magnitude larger. An example of residual pore clusters in a sintered oxide is shown in Fig. 10.29.

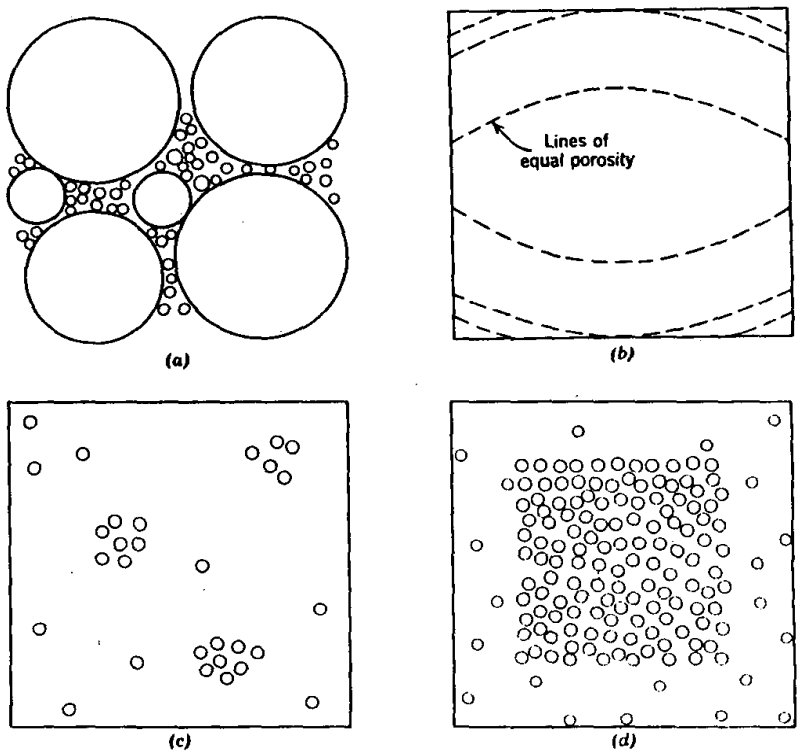

Fig. 10.28. Pore-concentration variations resulting from (*a*) a variation in grain sizes, (*b*) die friction, (*c*) local packing and agglomeration differences, and (*d*) more rapid pore elimination near surfaces.

Not only the kinetics of pore elimination can lead to "stable" and residual porosity, but it is also possible in some cases to have a thermodynamically metastable equilibrium pore configuration. In Fig.

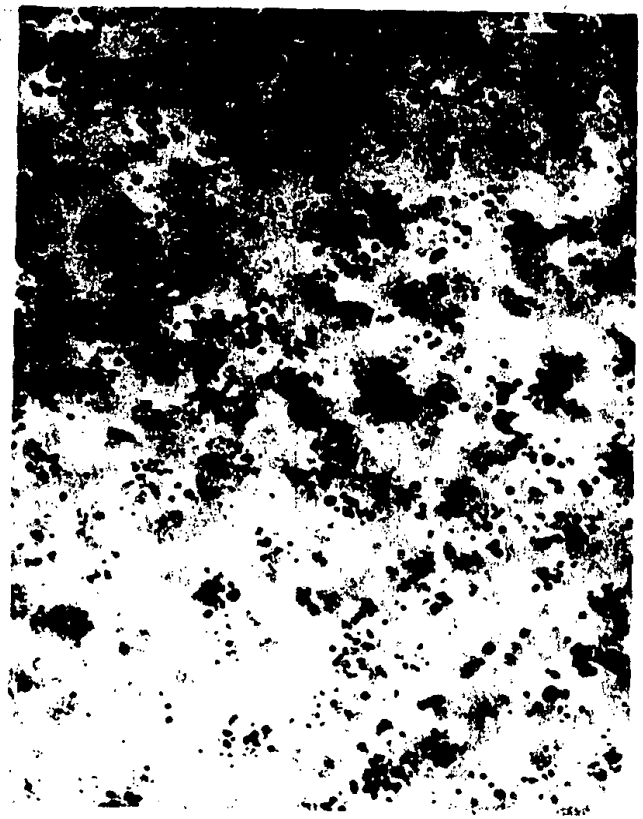

Fig. 10.29. Residual pore clusters resulting from improper powder processing in a sample of 90 mole % Y_2O_3–10 mole % ThO_2. Transmitted light, 137×. Courtesy C. Greskovich and K. N. Woods.

10.26 we have drawn spherical pores located on a grain boundary, the usual model description, but we know from our discussion of interface energies in Chapter 5 that there is a dihedral angle ϕ at the pore-boundary intersection determined by the relative interface energies;

$$\cos\frac{\phi}{2}=\frac{\gamma_{ss}}{2\gamma_s} \tag{10.30}$$

In most cases the dihedral angle for pure oxides is about 150°, and the spherical pore approximation is quite good; but for Al_2O_3 + 0.1% MgO the

value is 130°, for UO_2 + 30 ppm C the value is 88°, and for impure boron carbide the value is about 60°. For these materials the consequences of nonspherical pores have to be considered.

As discussed for discontinuous grain growth and illustrated in Figs. 10.4 and 10.11, the boundary curvature between grains or phases depends both on the value of the dihedral angle and on the number of surrounding grains. If we take r as the radius of a circumscribed sphere around a polyhedral pore surrounded by grains, the ratio of the radius of curvature of the pore surfaces ρ to the spherical radius depends both on the dihedral angle and on the number of surrounding grains, as shown in Fig. 10.30*a*. When r/ρ decreases to zero, the interfaces are flat and have no tendency

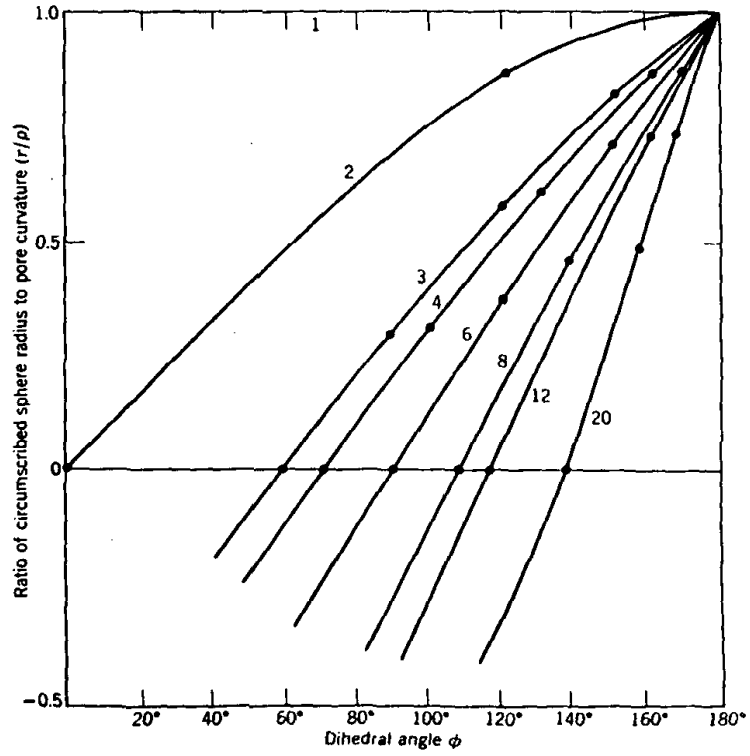

Fig. 10.30. (*a*) Change in the ratio (r/ρ) with dihedral angle for pores surrounded by different numbers of grains as indicated on individual curves.

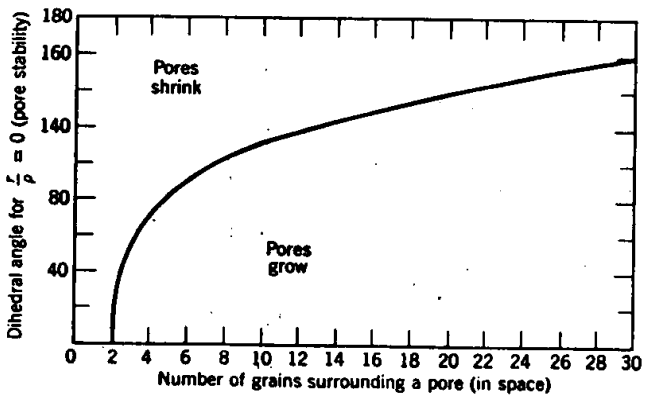

(*b*)

Fig. 10.30 (*Continued*). (*b*) Conditions for pore stability.

for shrinkage; when r/ρ is negative, the pore tends to grow. This is illustrated in Fig. 10.30*b*. For a uniform grain size the space-filling form is a tetrakaidecahedron with 14 surrounding grains. From an approximate relationship between the number of surrounding grains and the pore-diameter to grain-diameter ratio we can derive a relationship for pore stability as a function of dihedral angle and the ratio of pore size to grain size, as shown in Fig. 10.31. From this figure we can see why large pores present in poorly compacted powder such as shown in Fig. 10.32 not only remain stable but grow. It is also seen that an enormous disparity between

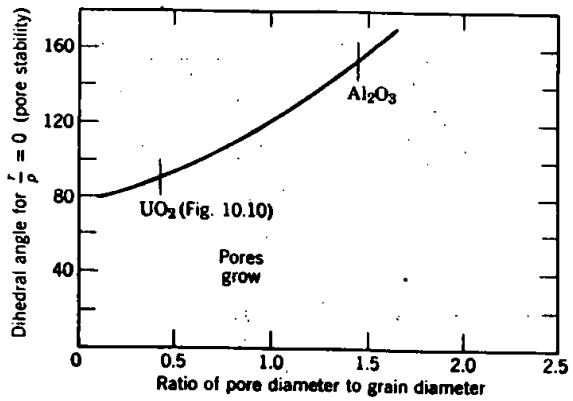

Fig. 10.31. Conditions for pore stability.

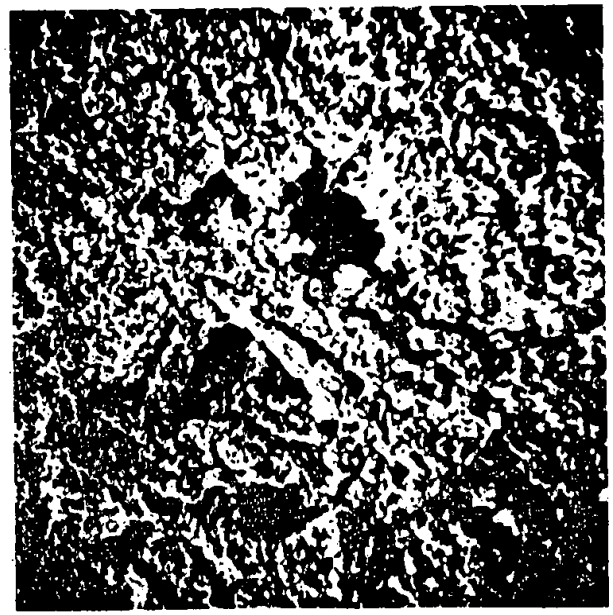

Fig. 10.32. Large voids formed by bridging of agglomerates in fine Al_2O_3 powder viewed with scanning electron microscope at 2000×. Courtesy C. Greskovich.

grain size and pore size is not necessary for pore stability. That is, the site and size of the porosity relative to the grain-boundary network not only affects the necessary distance for diffusion but also the driving force for the process.

The interaction of grain boundaries and porosity is, of course, a two-way street. When many pores are present during the initial stages of sintering, grain growth is inhibited. However, as discussed in Section 10.1, once the porosity has decreased to a value such that secondary grain growth can occur, extensive grain growth may result at high sintering temperatures. When grain growth occurs, many pores become isolated from grain boundaries, and the diffusion distance between pores and a grain boundary becomes large, and the rate of sintering decreases. This is illustrated in Fig. 10.16*b*, in which extensive secondary recrystallization has occurred, with the isolation of pores in the interior of grains and a reduction in the densification rate. Similarly, the sample of aluminum oxide shown in Fig. 10.33 has been sintered at a high temperature at which discontinuous grain growth occurred. Porosity is only removed near the grain boundaries, which act as the vacancy sink. The importance of

Fig. 10.33. Sintered Al_2O_3 illustrating elimination of porosity adjacent to grain boundaries with residual porosity remaining at grain centers. Courtesy J. E. Burke.

controlling grain growth as an integral part of controlling sintering phenomena cannot be overestimated. Consequently, the grain-growth processes discussed in Section 10.1 must be actively prevented in order to obtain complete densification. Usually densification continues by a diffusion process until about 10% porosity is reached; at this point rapid grain growth occurs by secondary recrystallization, and the rate of densification is sharply reduced. In order to obtain densification much beyond this level, prevention of secondary recrystallization is essential. The most satisfactory way of doing this is with additives which prevent or slow down boundary migration to a point at which it is possible to obtain pore elimination. Additions of MgO to Al_2O_3, ThO_2 to Y_2O_3, and CaO to ThO_2, among others, have been found to slow boundary migration and allow complete pore elimination by solid-state sintering in these systems. The porefree microstructure of a polycrystalline ceramic having optical transparancy suitable for use as a laser material is shown in Fig. 10.34.

10.3 Vitrification

To vitrify is to make glasslike and the vitrification process—densification with the aid of a viscous liquid phase—is the major firing process for the great majority of silicate systems. (In some current glossaries vitrification is defined as being identical to densification on firing, but the more specific usage is preferred.) A viscous liquid silicate is formed at the firing temperature and serves as a bond for the body. For

Fig. 10.34. Polished section of Y_2O_3 + 10 mole % ThO_2 sintered to porefree state. 100×. Courtesy C. Greskovich and K. N. Woods.

satisfactory firing the amount and viscosity of the liquid phase must be such that densification occurs in a reasonable time without the ware slumping or warping under the force of gravity. The relative and absolute rates of these two processes (shrinkage and deformation) determine to a large extent the temperature and compositions suitable for satisfactory firing.

Process Kinetics. If we consider two particles initially in contact (Fig. 10.21), there is a negative pressure at the small negative radius of

curvature ρ compared with the surface of the particles. This causes a viscous flow of material into the pore region. By an analysis similar to that derived for the diffusion process, the rate of initial neck growth is given as*

$$\frac{x}{r} = \left(\frac{3\gamma}{2\eta\rho}\right)^{1/2} t^{1/2} \tag{10.31}$$

The increase in contact diameter is proportional to $t^{1/2}$; the increase in area between particles is directly proportional to time. Factors of most importance in determining the rate of this process are the surface tension, viscosity, and particle size. The shrinkage which takes place is determined by the approach between particle centers and is

$$\frac{\Delta V}{V_0} = \frac{3\,\Delta L}{L_0} = \frac{9\gamma}{4\eta r} t \tag{10.32}$$

That is, the initial rate of shrinkage is directly proportional to the surface tension, inversely proportional to the viscosity, and inversely proportional to the particle size.

The situation after long periods of time can best be represented as small spherical pores in a large body (Fig. 10.35). At the interior of each pore

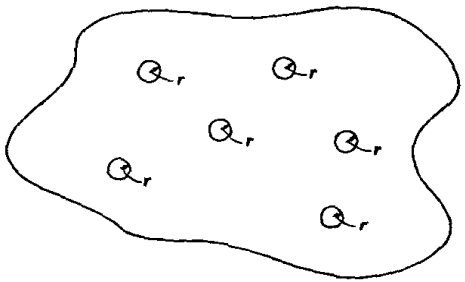

Fig. 10.35. Compact with isolated spherical pores near the end of the sintering process.

there is a negative pressure equal to $2\gamma/r$; this is equivalent to an equal positive pressure on the exterior of the compact tending to consolidate it. J. K. Mackenzie and R. Shuttleworth† have derived a relation for the rate of shrinkage resulting from the presence of isolated equal-size pores in a viscous body. The effect of surface tension is equivalent to a pressure of $-2\gamma/r$ inside all pores or, for an incompressible material, to the application of a hydrostatic pressure of $+2\gamma/r$ to the compact. The real problem is to deduce the properties of the porous material from the porosity and viscosity of the dense material. The method of approximation used gives an equation of the form

*J. Frenkel, *J. Phys (USSR)*, **9**, 385 (1945).
†*Proc. Phys. Soc. (London)*, **B62**, 833 (1949).

$$\frac{d\rho'}{dt} = \frac{2}{3}\left(\frac{4\pi}{3}\right)^{1/3} n^{1/3} \frac{\gamma}{\eta} (1-\rho')^{2/3} \rho'^{1/3} \tag{10.33}$$

where ρ' is the relative density (the bulk density divided by the true density or the fraction of true density which has been reached) and n is the number of pores per unit volume of real material. The number of pores depends on the pore size and relative density and is given by

$$n \frac{4\pi}{3} r^3 = \frac{\text{Pore volume}}{\text{Solid volume}} = \frac{1-\rho'}{\rho'} \tag{10.34}$$

$$n^{1/3} = \left(\frac{1-\rho'}{\rho'}\right)^{1/3} \left(\frac{3}{4\pi}\right)^{1/3} \frac{1}{r} \tag{10.35}$$

By combining with Eq. 10.33,

$$\frac{d\rho'}{dt} = \frac{3\gamma}{2r_0\eta} (1-\rho') \tag{10.36}$$

where r_0 is the initial radius of the particles.

The general course of the densification process is best represented by a plot of relative density versus nondimensional time, illustrated in Fig. 10.36 following Eq. 10.33. Spherical pores are formed very quickly to reach a relative density of about 0.6. From this point until the completion of the sintering process about one unit of nondimensional time is

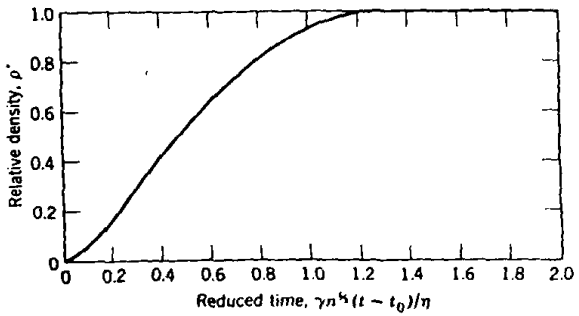

Fig. 10.36. Increase in relative density of compact with reduced time for a viscous material. From J. K. Mackenzie and R. Shuttleworth, *Proc. Phys. Soc. (London)*, **B62**, 833 (1949).

required. For complete densification

$$t_{sec} \sim \frac{1.5 r_0 \eta}{\gamma} \tag{10.37}$$

Some experimental data for the densification of a viscous body are shown in Fig. 10.37, in which the strong effect of temperature, that is, the viscosity of the material, is illustrated by the rapid change in sintering rates. The solid lines in Fig. 10.37 are calculated from Eq. 10.33. The

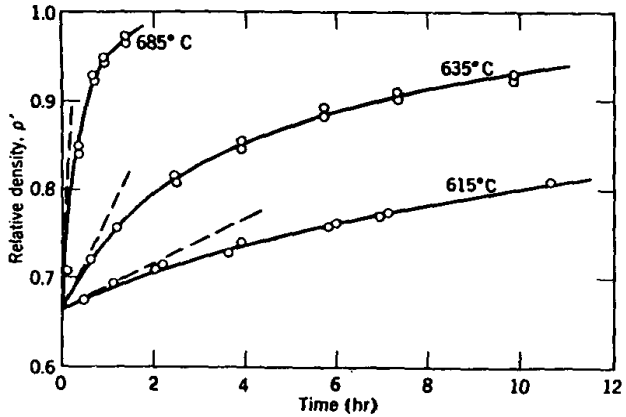

Fig. 10.37. Densification of a soda-lime-silica glass.

initial rates of sintering indicated by the dashed curves are calculated from Eq. 10.32. The good agreement of these relationships with the experimental results gives us confidence in applying them to vitrification processes in general.

Important Variables. The particular importance of Eqs. 10.31 to 10.37 is the dependence of the rate of densification on three major variables—the particle size, viscosity, and surface tension. For silicate materials the surface tension is not changed much by composition, although there are some systems for which surface energy is particularly low, as illustrated in Chapter 5. However, surface tension is not a variable that normally causes difficulty during the design of compositions or the control of processing. The particle size has a strong effect on the sintering rate and must be closely controlled if the densification process is going to be controlled. In changing from a 10-micron to 1-micron particle, the rate of sintering is increased by a factor of 10. Even more important for control

purposes is the viscosity and its rapid change with temperature. For a typical soda-lime-silica glass the viscosity changes by a factor of 1000 over an interval of 100°C; the rate of densification changes by an equal factor over the temperature range. This means that the temperature must be closely controlled. Viscosity is also much changed by composition, as discussed in Chapter 3. The rate of densification, then, can be increased by changing the composition to lower the viscosity of the glassy material. The relative values of viscosity and particle size are also important; the viscosity must not be so low that appreciable deformation takes place under the forces of gravity during the time required for densification. This makes it necessary for the particle size to be in such a range that the stresses due to surface tension are substantially larger than the stresses due to gravitational forces. Materials sintered in a fluid state must be supported so that deformation does not occur. The best means of obtaining densification without excessive deformation is to use very fine-grained materials and uniform distribution of materials. This requirement is one of the reasons why successful compositions in silicate systems are composed of substantial parts of talc and clays that are naturally fine-grained and provide a sufficient driving force for the vitrification process.

Silicate Systems. The importance of the vitrification process lies in the fact that most silicate systems form a viscous glass at the firing temperature and that a major part of densification results from viscous flow under the pressure caused by fine pores. Questions that naturally arise are how much liquid is present and what are its properties. Let us consider Fig. 7.26, which shows an isothermal cut at 1200°C in the K_2O–Al_2O_3–SiO_2 system; this is the lower range of firing temperatures used for semivitreous porcelain bodies composed of about 50% kaolin (45% Al_2O_3, 55% SiO_2), 25% potash-feldspar, and 25% silica. This and similar compositions are in the primary field of mullite, and at 1200°C there is an equilibrium between mullite crystals and a liquid having a composition approximately $75SiO_2$, $12.5K_2O$, $12.5Al_2O_3$, not much different in composition from the eutectic liquid in the feldspar-silica system (Fig. 7.14). In actual practice only a small part of the silica present as flint enters into the liquid phase, and the composition of the liquid depends on the fineness of the grinding as well as on the overall chemical composition. However, the amount of silica which dissolves does not have a large effect on the amount and composition of the liquid phase present. The liquid is siliceous and has a high viscosity; the major effect of compositional changes is to alter the relative amounts of mullite and liquid phases present. Since mullite is very fine-grained, the fluid flow properties of the body correspond to those of a liquid having a viscosity greater than the pure liquid phase. For

some systems the overall flow process corresponds to plastic flow with a yield point rather than to true viscous flow. This changes the kinetics of the vitrification process by introducing an additional term in Eqs. 10.33 and 10.36 but does not change the relative effects of different variables.

Although phase diagrams are useful, they do not show all the effects of small changes in composition. For example, a kaolinite composition should show equilibrium between mullite and tridymite at 1400°C with no glassy material. However, it is observed experimentally that even after 24 hr about 60 vol% of the original starting material is amorphous and deforms as a liquid. The addition of a small amount of lithium oxide as Li_2CO_3 has been observed to give a larger content of glass than additions of the same composition as the fluoride. Similar small amounts of other mineralizers can also have a profound effect in the firing properties of particular compositions. That fine grinding and intimate mixing reduce the vitrification temperature follows from the analysis in Eqs. 10.31 to 10.37. S. C. Sane and R. L. Cook* found that ball milling for 100 hr reduced the final porosity of a clay-feldspar-flint composition from 17.1 to 0.3% with the same firing conditions. This change is caused in part by increased tendencies toward fusion equilibrium and uniform mixing of constituents and in part by the smaller initial particle and pore size. In contrast to triaxial (flint-feldspar-clay) porcelains, which frequently do not reach fusion equilibrium, many steatite bodies and similar compositions which are prepared with fine-particle, intimately mixed material and form a less siliceous liquid reach phase equilibrium early in the firing process.

The time-temperature relationship and the great dependence of vitrification processes on temperature can perhaps be seen best in the experimental measurements illustrated in Fig. 10.38. As shown there, the time required for a porcelain body to reach an equivalent maturity changes by almost an order of magnitude with a 50° temperature change. There are changes in both the amount and viscosity of the glassy phase during firing, so that it is difficult to elucidate a specific activation energy for the process with which to compare the activation energy for viscous flow. However, the temperature dependence of the vitrification rate of a composition such as this (a mixture of clay, feldspar, and flint) is greater than the temperature dependence of viscosity alone. This is to be expected from the increased liquid content at the higher firing temperatures.

In summary, the factors determining the vitrification rate are the pore size, viscosity of the overall composition (which depends on amount of liquid phase present and its viscosity), and the surface tension. Equivalent

*J. Am. Ceram. Soc., 34, 145 (1951).

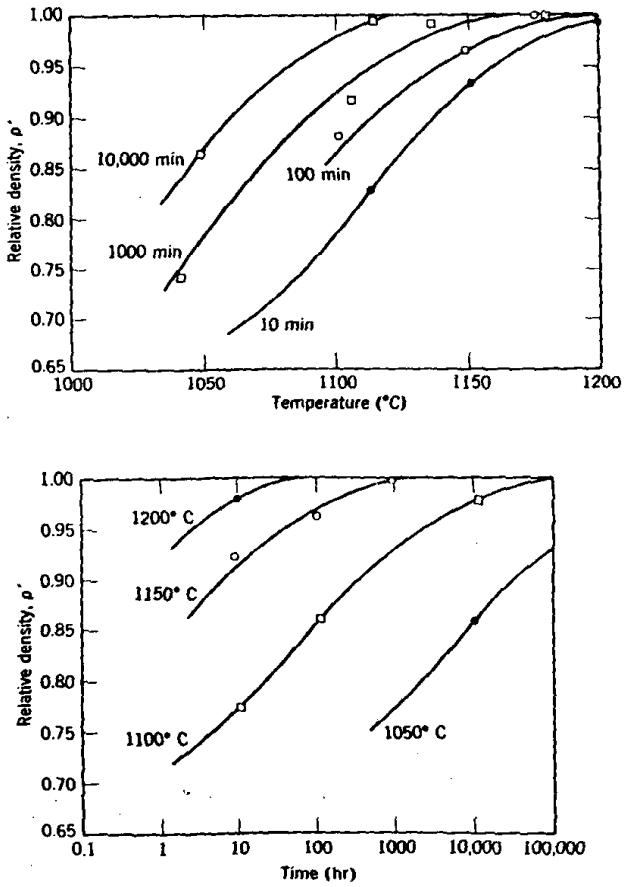

Fig. 10.38. Effect of time and temperature on the vitrification of a porcelain body. Data from F. H. Norton and F. B. Hodgdon, *J. Am. Ceram. Soc.*, 14, 177 (1931).

densification results from longer periods of time at the same temperature. In controlling the process, the temperature dependence is great because of the increase in liquid content and lowered viscosity at higher temperatures. Changes in processing and changes in composition affect the vitrification process as they affect these parameters.

10.4 Sintering with a Reactive Liquid

Another quite different process which leads to densification is sintering in the presence of a reactive liquid. Here we are referring to systems in which the solid phase shows a certain limited solubility in the liquid at the sintering temperature; the essential part of the sintering process is the solution and reprecipitation of solids to give increased grain size and density. This kind of process occurs in cermet systems such as bonded carbides and also in oxide systems when the liquid phase is fluid and reactive, such as magnesium oxide with a small amount of liquid phase present (Fig. 10.39), UO_2 with the addition of a small amount of TiO_2 (Fig. 7.11), and high-alumina bodies which have an alkaline earth silicate as a bonding material.

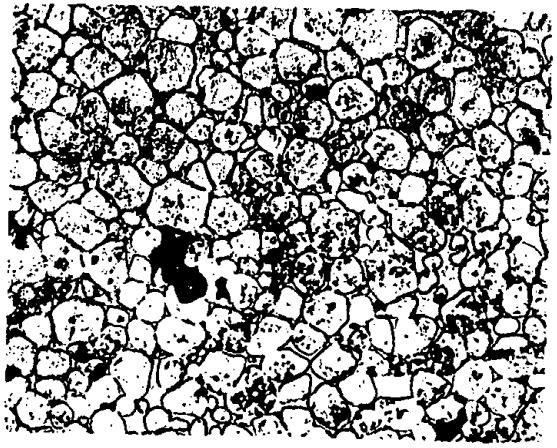

Fig. 10.39. Microstructure of magnesia—2% kaolin body resulting from reactive-liquid sintering (245×).

Studies of a large number of systems indicate that for densification to take place rapidly it is essential to have (1) an appreciable amount of liquid phase, (2) an appreciable solubility of the solid in the liquid, and (3) wetting of the solid by the liquid. The driving force for densification is derived from the capillary pressure of the liquid phase located between the fine solid particles, as illustrated in Fig. 10.40. When the liquid phase wets the solid particles, each interparticle space becomes a capillary in which a substantial capillary pressure is developed. For submicron particle sizes, capillaries with diameters in the range of 0.1 to 1 micron

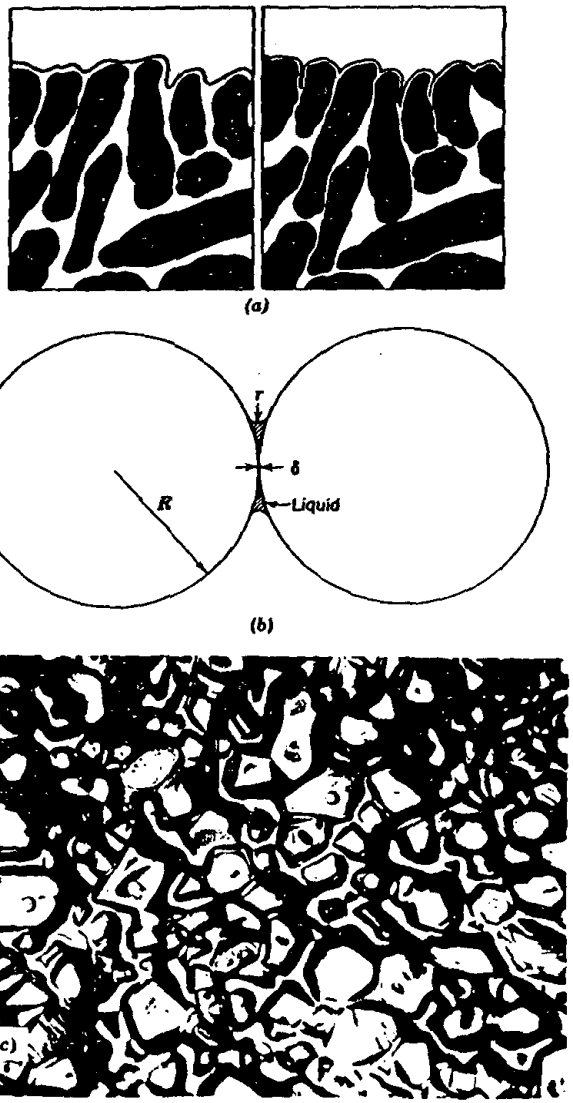

Fig. 10.40. (*a*) Surface of solid-liquid composite with varying amounts of liquid phase. (*b*) Drop of liquid between two solid spheres exerts pressure to pull them together. (*c*) Surface of forsterite ceramic showing liquid capillary depression between crystals.

develop pressures in the range of 175 to 1750 psi for silicate liquids and in the range of 975 to 9750 psi for a metal such as liquid cobalt (see discussion in Chapter 5 and Table 5.2).

The capillary pressure results in densification by different processes which occur coincidentally. First, on formation of a liquid phase there is a rearrangement of particles to give a more effective packing. This process can lead to complete densification if the volume of liquid present is sufficient to fill in the interstices completely. Second, at contact points where there are bridges between particles high local stresses lead to plastic deformation and creep, which allow a further rearrangement. Third, there is during the sintering process a solution of smaller particles and growth of larger particles by material transfer through the liquid phase. The kinetics of this solution-precipitation process have already been discussed in Chapter 9. Because there is a constantly imposed capillary pressure, additional particle rearrangement can occur during grain-growth and grain-shape changes and give further densification. (As discussed for vapor transport and surface diffusion in solid-state sintering, mere solution-precipitation material transfer without the imposed capillary pressure would not give rise to densification). Fourth, in cases in which liquid penetrates between particles the increased pressure at the contact points leads to an increased solubility such that there is material transfer away from the contact areas so that the particle centers approach one another and shrinkage results; the increase in solubility resulting from the contact pressure has been discussed in Chapter 5. Finally, unless there is complete wetting, recrystallization and grain growth sufficient to form a solid skeleton occur, and the densification process is slowed and stopped.

Perhaps even more than for the solid-state process, sintering in the presence of a liquid phase is a complex process in which a number of phenomena occur simultaneously. Each has been shown to occur, but experimental systems in which a single process had been isolated and analysed during sintering have not been convincingly demonstrated. Clearly, the process requires a fine-particle solid phase to develop the necessary capillary pressures which are proportional to the inverse capillary diameter. Clearly, the liquid concentration relative to the solid particle packing must be in a range appropriate for developing the necessary capillary pressure. Clearly, if and when a solid skeleton develops by particle coalescence, the process stops.

A critical and still controversial question is the degree of wetting required for the process to proceed. In some important systems such as tungsten carbide–cobalt and titanium carbide–nickel–molybdenum the dihedral angle is zero. In other systems such as iron-copper and magnesia-silicate liquids this is not the case at equilibrium; but the dihedral angle is

low, and the solid is wetted by the liquid phase, as required to develop the necessary capillary pressure. For grain growth of periclase particles in a silicate liquid, the dihedral angle has a large effect on the grain-growth process, as illustrated in Fig. 10.41. Although zero dihedral angle is not essential for liquid-phase sintering to occur, the process becomes more effective as this ideal is approached.

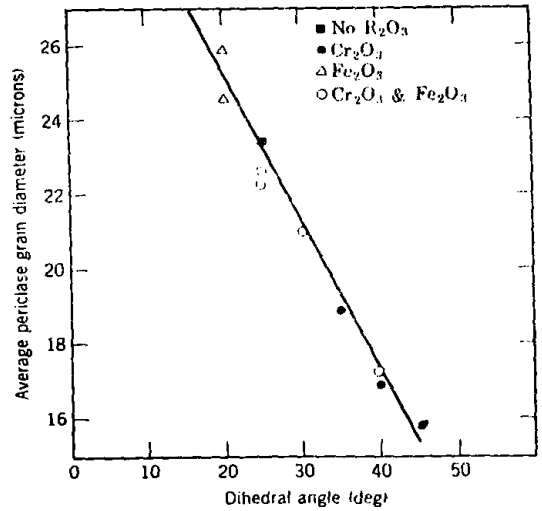

Fig. 10.41. Grain growth of periclase particles in liquid-phase-sintered periclase-silicate compositions as a function of dihedral angle. From B. Jackson, W. F. Ford, and J. White, *Trans. Brit. Ceram. Soc.*, 62, 577 (1963).

10.5 Pressure Sintering and Hot Pressing

The sintering processes thus far discussed depend on the capillary pressures resulting from surface energy to provide the driving force for densification. Another method is to apply an external pressure, usually at elevated temperature, rather than relying entirely on capillarity.* This is desirable in that it eliminates the need for very fine-particle materials and also removes large pores caused by nonuniform mixing. An additional advantage is that in some cases densification can be obtained at a temperature at which extensive grain growth or secondary recrystalliza-

*R. L. Coble, *J. Appl. Phys.* 41, 4798 (1970).

tion does not occur. Since the mechanical properties of many ceramic systems are maximized with high density and small grain size, optimum properties can be obtained by hot-pressing techniques. The effect of added pressure on the densification of a beryllium oxide body is illustrated in Fig. 10.42. The main disadvantages of hot pressing for oxide

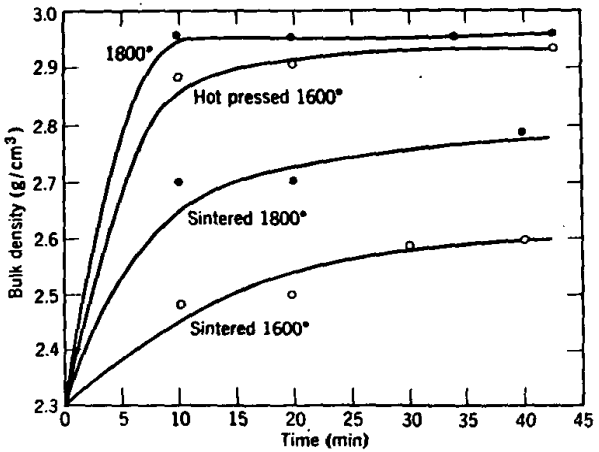

Fig. 10.42. Densification of beryllia by sintering and by hot pressing at 2000 psi.

bodies are the unavailability of inexpensive and long-life dies for high temperatures and the difficulty in making the process into an automatic one to achieve high-speed production. Both factors make the hot-pressing process an expensive one. For oxide materials which have to be pressed at temperature above 1200 or 1300°C (often at 1800 to 2000°C) graphite is the most satisfactory die material available; the maximum stress is limited to a few thousand pounds per square inch, and the life of dies is usually limited to seven or eight pieces. The entire die must be heated and cooled with the formation of each piece. Techniques for using high temperatures in a process in which the die is maintained cool with the material heated have shown some promise in laboratory tests but have not been developed for production.

For lower-temperature materials, such as glasses or glass-bonded compositions which can be pressed in metal dies at temperatures below 800 to 900°C, the hot-pressing process can be developed as an automatic and inexpensive forming method. This is similar to the normal pressing of

glass as a glass-forming method in which it is used to obtain the desired shape rather than as a means of eliminating porosity.

Densification during pressure sintering can occur by all the mechanisms which have been discussed for solid-state sintering, vitrification, and liquid-phase sintering. In addition, particularly during the early stages, when high stresses are present at the particle contact points, and for soft materials, such as the alkali halides, plastic deformation is an important densification mode. Since the grain-growth process is insensitive to pressure, pressure-sintering oxides at high pressures and moderate temperatures allows the fabrication of high-density–small-grain samples with optimum mechanical properties and with sufficiently low porosity to be nearly transparent. Covalent materials such as boron carbide, silicon carbide, and silicon nitride can be hot-pressed to nearly complete density. It is often advantageous to add a small fraction of liquid phase (i.e., LiF to MgO, B to silicon carbide, MgO to silicon nitride) to allow pressure-induced liquid phase, or liquid-film, sintering to occur.

10.6 Secondary Phenomena

The primary processes which occur on heating and are important in connection with the firing behavior of all ceramic compositions are grain growth and densification, as discussed in previous sections. In addition to these changes, there are a large number of other possible effects which occur during the firing of some particular compositions. These include chemical reactions, oxidation, phase transitions, effects of gas trapped in closed pores, effects of nonuniform mixing, and the application of pressure during heating. Although they are not processes of the most general importance, they frequently cause the main problems and the major phenomena observed during firing. Although we cannot discuss them in great detail, we should at least be familiar with some of the possibilities.

Oxidation. Many natural clays contain a few percent organic matter which must be oxidized during firing. In addition, varnishes or resins used as binders, as well as starches and other organic plasticizers, must be oxidized during firing, or difficulties result. Under normal conditions organic materials char at temperatures above 150°C and burn out at temperatures ranging from 300 to 400°C. Particularly with low-firing-temperature compositions, it is necessary to heat at a slow enough rate for this process to be completed before shrinkage becomes substantial. If the carbonaceous material is sealed off from the air by vitrification occurring before oxidation is completed, it acts as a reducing agent at higher temperatures. Sometimes this may merely affect the color, giving rise to

black coring of brick and heavy clay products whose interiors are in a reduced state, black in color. A typical example of a stoneware heated too rapidly for oxidation to be completed is illustrated in Fig. 10.43, which shows the central black core. Very often impurities present, particularly sulfides, may cause difficulties unless oxidized before vitrification. Sulfides in general react with oxygen in the temperature range of 350 to 800°C, forming SO_2 gas which escapes through open pores.

Fig. 10.43. Example of black core produced when time allowed for oxidation reactions was insufficient for completion of the reaction.

In ferrite and titania compositions control of oxidation reactions during firing is particularly important. As illustrated for the Ti–TiO_2 and Fe–O_2 systems (Chapter 7), the phases present depend on the oxygen pressure. In addition, as discussed in Chapter 4, the composition of these phases covers a substantial range of stoichiometry and depends on the oxygen pressure. It is common practice in the manufacture of ferrites to control the oxygen pressure during firing so that the composition of each phase present, and the overall phase composition of the body, is maintained to give the best magnetic properties.

Decomposition Reactions. Many of the constituents used in ceramic bodies are in the form of carbonates or hydrated compounds; these decompose during firing to form the oxide plus a gaseous product (CO_2, H_2O). Many impurities are also incorporated as carbonates, hydrates, and sulfates and decompose during firing (see Section 9.4).

Hydrates decompose over a wide temperature range between 100 and 1000°C, depending on the particular composition. Carbonates decompose over a temperature range from 400 to 1000°C, also depending on the particular composition. For each temperature there is, of course, an

equilibrium pressure of the gaseous product; if this pressure is exceeded, further decomposition does not take place, leading to the major problem encountered, the sealing of pores before complete dissociation. As the temperature is raised, the decomposition pressure increases and forms large pores, blistering, and bloating. (This is, of course, the method used to form cellular glass products in which the surface is intentionally sealed off before chemical reaction or decomposition takes place to form a gas phase that expands and produces a foamed product.) This kind of defect is particularly common when high heating rates are used, for then there is a temperature gradient between the surface and interior of the ware, and the surface layer vitrifies, sealing off the interior. This temperature gradient and the time required for oxidation of constituents or impurities are the two most important reasons for limiting the rate of heating during firing.

Sulfates create a particular problem in firing because they do not decompose until a temperature of 1200 to 1300°C is reached. Therefore they remain stable during the firing process used for burning many clay bodies. In particular, $CaSO_4$ is stable but slightly soluble in water, so that a high sulfate content leads to a high concentration of soluble salts in the burned brick. This causes efflorescence—the transport of slightly soluble salts to the surface, forming an undesirable white deposit. Addition of barium carbonate prevents the deposit from forming by reacting with calcium sulfate to precipitate insoluble barium sulfate.

Decomposition also occurs in some materials to form new solid phases. A particular example used in refractory technology is the decomposition of kyanite, $Al_2O_3 \cdot SiO_2$, to form mullite and silica at a temperature of 1300 to 1450°C. This reaction proceeds with an increase in volume, since both mullite and the silica glass or cristobalite formed have lower densities than kyanite. The reaction is useful, since the addition of kyanite to a composition can counteract a substantial part of the firing shrinkage if the other constituents are carefully selected. Similarly, reaction of MgO with Al_2O_3 to form spinel occurs with a decrease in volume. By incorporating magnesia and alumina in a refractory mix, or more commonly in a high-temperature ramming mix or cement, the shrinkage taking place on heating can be decreased.

Phase Transformations. Polymorphic transformations may be desirable or undesirable, depending on the particular composition and the anticipated use. If a large volume change accompanies the polymorphic transformation, difficulties result, owing to the induced stresses. Refractories cannot be made containing pure zirconium oxide, for example, since the tetragonal monoclinic transformation at about 1000° involves such a large volume change that the ware is disrupted. The source of these

stresses has been discussed in Chapter 5 in connection with boundary stresses caused by differential thermal expansion or contraction of different grains. The expansion or contraction of a crystal in a matrix leads to the same sort of stresses that may give rise to actual cracking, illustrated for quartz grains in a porcelain body in Fig. 10.44. The stresses in individual grains can be reduced if the grain size is reduced; properties of porcelains are improved if fine-grained flint is used rather than coarse material.

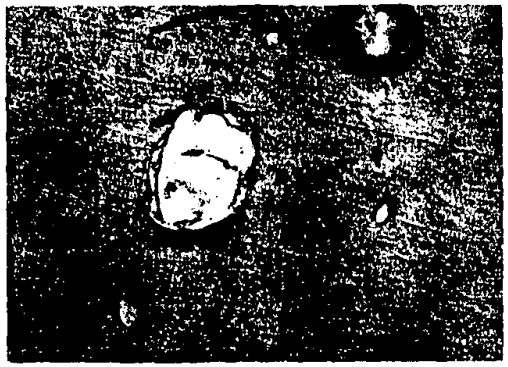

Fig. 10.44. Cracked quartz grain and surrounding matrix in a porcelain body. Differential expansion due mainly to the α-β quartz transition leads to cracking of larger grains but leaves small grains intact (500×).

Sometimes desirable phase transformations only occur sluggishly. This is what happens, for example, with the firing of refractory silica brick. The transition from quartz, the starting material, to tridymite and cristobalite, the desired end constituents, occurs only slowly. In order to increase the rate of transformation, calcium oxide is added as a mineralizer. The calcium oxide forms a liquid in which silica is soluble. Consequently the quartz dissolves and precipitates as tridymite, which is the more stable phase (Chapter 7). Some of the quartz transforms directly to cristobalite during the process as well. In general, mineralizers help in achieving equilibrium conditions by providing a mechanism of material transfer—solution or vaporization—that circumvents energy barriers to direct transformations. In silicate systems the addition of fluorides or hydroxyl ions is particularly helpful in this regard, since they greatly increase the fluidity of the liquid phase present.

Trapped Gases. In addition to the bloating occasioned by decomposition reactions, trapping of gases within closed pores imposes a limitation

on the ultimate density that can be reached during firing. Gases such as water vapor, hydrogen, and oxygen (to a lesser extent) are able to escape from closed pores by solution and diffusion. In contrast, gases such as carbon monoxide, carbon dioxide, and particularly nitrogen have a lower solubility and do not normally escape from closed pores. If, for example, spherical pores are closed at a total porosity of 10% and a partial pressure of 0.8 atm nitrogen, the pressure has increased to 8 atm (about 110 psi) when they have shrunk to a total porosity of 1%, and further shrinkage is limited. At the same time that the gas pressure is increasing, however, the negative radius of curvature of the pore becomes small so that the negative pressure produced by surface tension is increased proportional to $1/r$; the gas pressure builds up proportional to $1/r^3$. For sintering in air this factor usually limits densification; where very high densities are required, as for optical materials or dental porcelains requiring high translucency, vacuum or hydrogen atmosphere is preferred.

Nonuniform Mixing. Although not mentioned in most discussions of sintering, the most important reason why densification and shrinkage stop short of complete elimination of pores is that gross defects caused by imperfect mixing and compact consolidation prior to firing are usually present. Examination of typical production ceramics shows that they commonly contain upward of 10% porosity in the millimeter size range (that is, pores much larger than the particle size of the raw materials introduced in the composition). These pores are caused by local variations induced during forming, and there is no tendency for elimination of these pores during firing. Corrective treatment must be taken in the forming method.

Overfiring. Ware is commonly referred to as overfired if for any of a variety of reasons a higher firing temperature leads to poorer properties or a reduced shrinkage. For solid-state sintering, such as ferrites and titanates, a common cause is secondary recrystallization occurring at the higher temperature before the elimination of porosity. Consequently, there is some maximum temperature at which the greatest density or optimum properties are obtained. For vitreous ceramics the most common cause of overfiring is the trapping of gases in pores or the evolution of gases which cause bloating or blistering.

10.7 Firing Shrinkage

As formed, green ware contains between 25 and 50 vol% porosity. The amount depends on the particle size, particle-size distribution, and forming method (Chapter 1). During the firing process this porosity is removed; the volume firing shrinkage is equal to the pore volume

eliminated. This firing shrinkage can be substantially decreased by addition of nonshrinking material to the mix; fire-clay brick is commonly manufactured with grog (prefired clay) additions which serve to decrease firing shrinkage. Similarly, this is one of the functions of the flint in the porcelain body; it provides a nonshrinking structure which reduces the shrinkage during firing. Terra-cotta compositions, composed of mixtures of fired grog and clay, can be made in large shapes because a large part of the raw material has been prefired and the firing shrinkage is low.

If firing is carried to complete densification, the fractional porosity originally present is equal to the shrinkage taking place during firing. This commonly amounts to as much as 35% volume shrinkage or 12 to 15% linear shrinkage and causes difficulty in maintaining close tolerances. However, the main difficulties are warping or distortion caused by different amounts of firing shrinkage at different parts of the ware. Nonuniform shrinking can sometimes even cause cracks to open.

Warping. A major cause of warping during firing is density variations in the green ware. There are many reasons for differences in porosity in the green ware. The density after firing is nearly uniform, and there is higher shrinkage for the parts that had a low density than for the parts that had a high density in the green ware. In pressed ware, pressure variations in the die (Chapter 1) cause different amounts of compaction at different parts of a pressed piece; usually the shrinkage at the center is larger than the shrinkage at the ends, and an hourglass shape results from an initially cylindrical sample (Fig. 10.45*a*).

Another source of warping during firing is the presence of temperature gradients. If ware is laid on a flat plate and heated from above, there is a temperature difference between the top and bottom of the ware that may cause greater shrinkage at the top than at the bottom and a corresponding warping. In some cases the gravitational stresses may be sufficient to make the ware lie flat, even though shrinkage is nonuniform. The relationship between temperature distribution, warpage, and deformation under the stresses developed is complicated and difficult to analyze quantitatively. Another source of warpage in firing is preferred orientation of the platey clay particles during the forming process. This causes the drying and firing shrinkage to have directional properties.

Vitreous ware is also warped by flow under forces of gravity. This is especially true for large heavy pieces in which substantial stresses are developed. In the forming of vitreous sanitary ware, the upper surface of a closet bowl (Fig. 10.45*c*) or a lavatory (Fig. 10.45*d*) must be designed with a greater curvature than is desired in the end product so that the settling which occurs on firing produces a final shape that is satisfactory. A final contributor to warpage during firing is the frictional force or *drag*

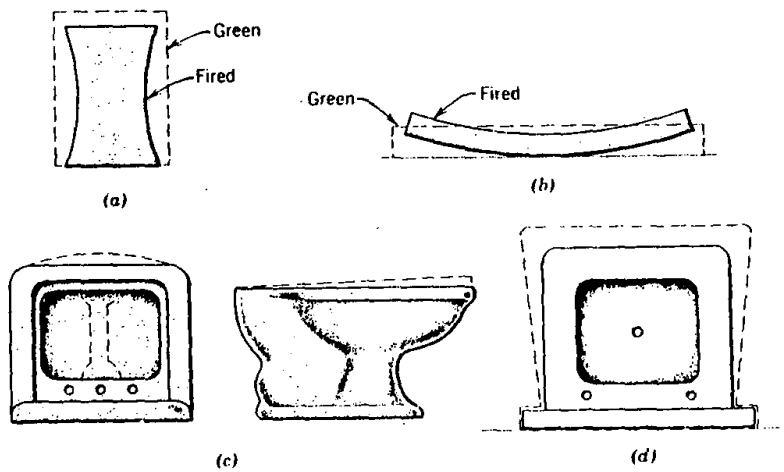

Fig. 10.45. Firing shrinkage of (*a*) pressed crucible with differential shrinkage due to green density variations, (*b*) tile with differential shrinkage due to temperature gradients, (*c*) ware with differential shrinkage due to gravity settling, and (*d*) differential shrinkage due to frictional force of setting.

of the ware against the setter. This means that the bottom surface tends to shrink less than the upper surface (Fig. 10.45*d*). Ware must be designed so that the final shape, including shrinkage, comes out to be rectangular.

Difficulties caused by differential firing shrinkage, resulting distortion, and warping can be eliminated in three ways: first, altering the forming method to minimize the causes of warping; second, designing shapes in a way that compensates for warping; and third, using setting methods in firing that minimize the effects of warping. One obvious improvement in forming methods is to obtain uniformity of the structure during initial forming. This requires elimination of pressure gradients, segregation, and other sources of porosity variation. Pressing samples that have long ratios of length to die diameter cause density variations. Extruded and pressed mixes that have low plasticity are particularly prone to large pressure variations and green density differences. Slip casting and extrusion both cause a degree of segregation and density differences during firing. Some settling may occur during the casting process, causing structural variations. During extrusion pressure differences at various parts of the die or an unsymmetrical setting for the die can cause variations.

Sometimes variations in firing shrinkage and difficulties from warping can be overcome by compensating the shapes. This is true, for example, in Fig. 10.45, in which the closet bowl and lavatory are designed in such a

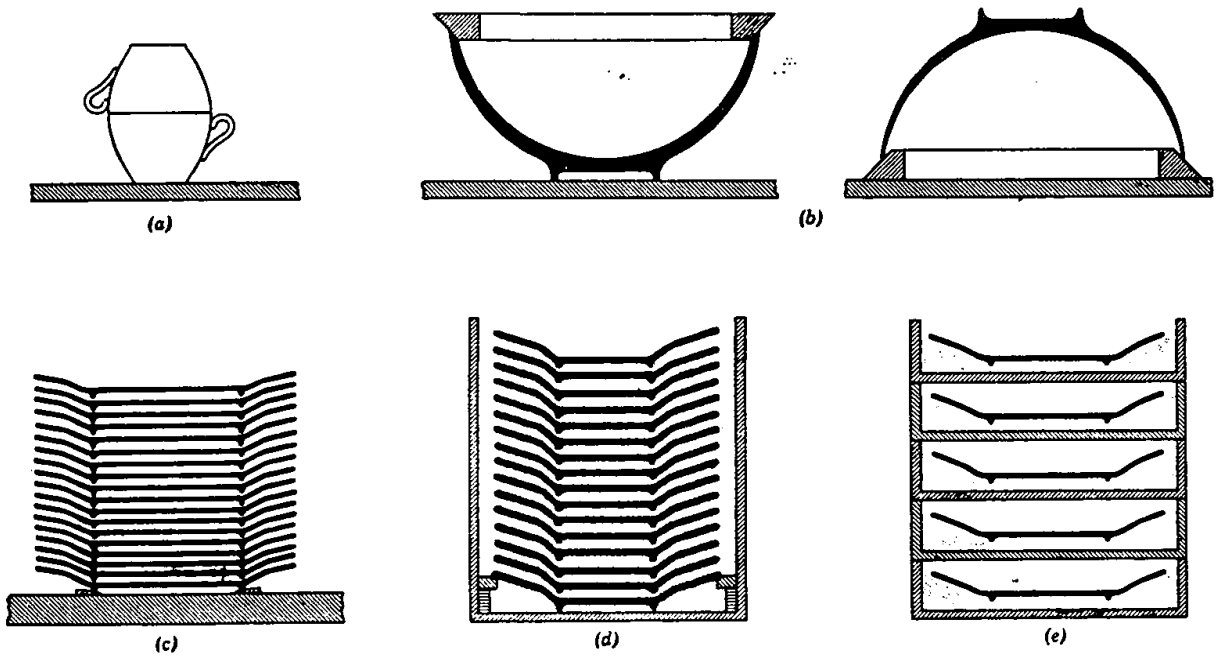

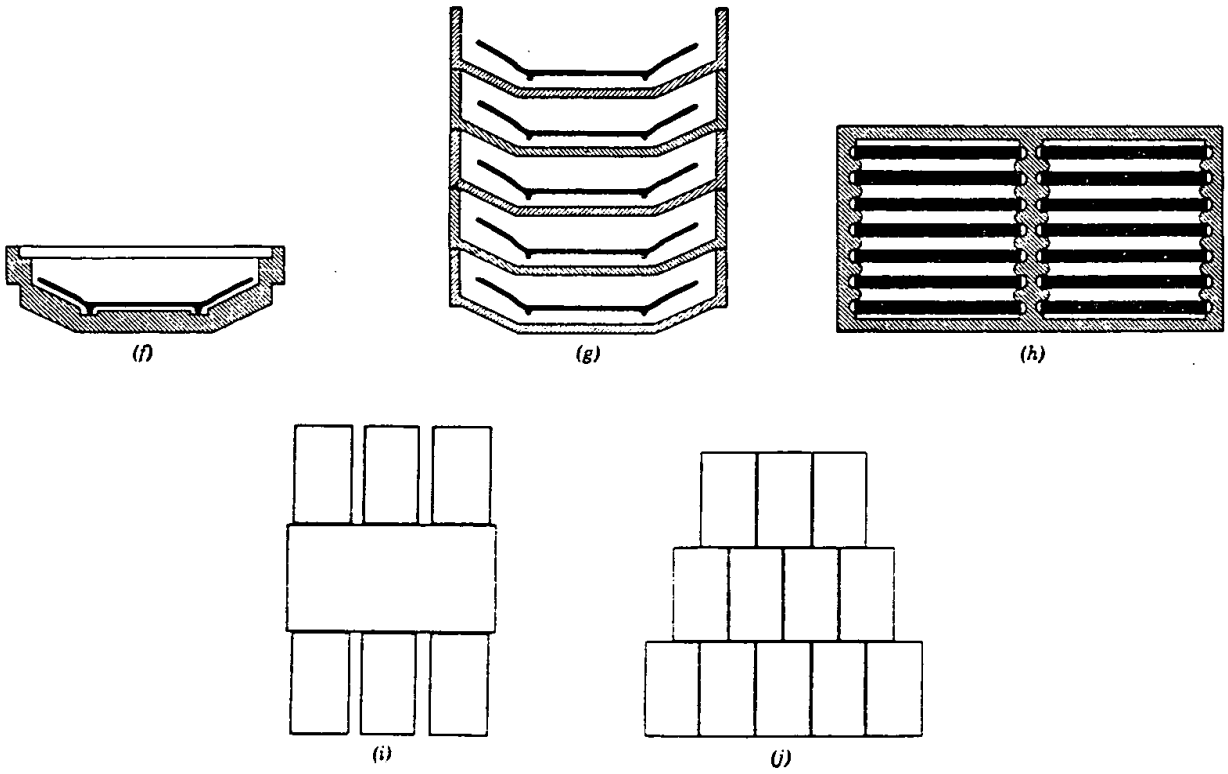

Fig. 10.46. Setting methods for (*a*) cups and bowls, (*b*) large bowls, (*c*) earthenware, (*d*) hotel china plates, (*e*) bone china plates, (*f*) frit porcelain plates, (*g*) hard porcelain plates, (*h*) tile, (*i*) brick checkerwork, (*j*) brick bench setting. From F. H. Norton.

way that the final shape is satisfactory. In the same way, when plates are fired in the horizontal position there is a tendency for the rims to settle; this can be compensated for by adjusting the shape of the initial piece.

Correct setting methods are important in eliminating difficulties caused by firing-shrinkage variations. These have been most extensively developed for porcelain compositions in which complete vitrification is desired and high shrinkages result. Some of the standard setting methods are illustrated in Fig. 10.46. Cups and bowls are commonly boxed as indicated in Fig. 10.46*a*. This keeps the rim circular, since warpage of one restricts warpage of the other; in addition, it prevents the thin rims from being too rapidly heated. For larger pieces, unfired setters are necessary as a means of controlling shrinkage and maintaining circular rims. A variety of methods is used for setting different kinds of plate compositions, depending on the amount of shrinkage expected. For ware fired to complete vitrification individual setting and support are essential. For ware fired to partial densification, plates can be stacked with no ill effects. In general, large tiles and brick do not cause much difficulty.

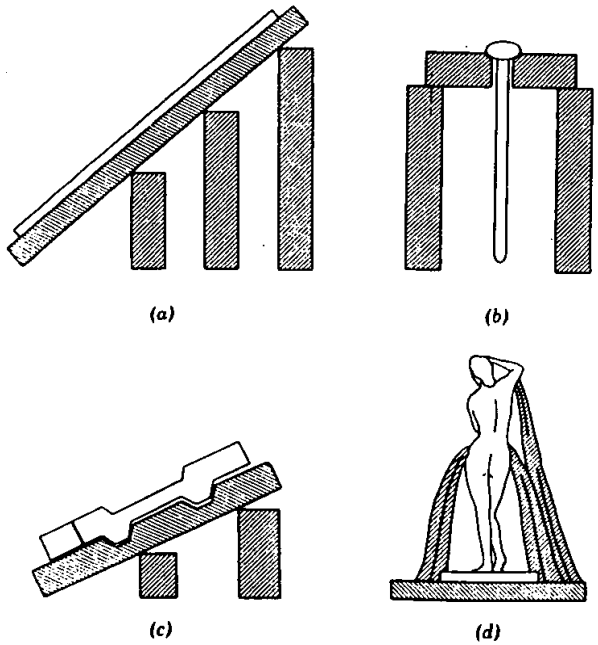

Fig. 10.47. Setting methods for special shapes. (*a*) Large tiles set an angle of repose; (*b*) slender rod supported by collar; (*c*) special shape; (*d*) sculptured piece. From F. H. Norton.

Special shapes may require special setting methods to eliminate adverse effects of firing shrinkage. Large refractory tile can be set at an angle of repose on a flat surface (Fig. 10.47*a*). This allows the tile to shrink without much stress. In the same way rods or tubes may be set in an inclined V groove or supported by a collar from the upper end (Fig. 10.47*b*). Gravitational forces keep the tubes straight up to lengths of several feet. Unique shapes can always be supported on special setters designed for the particular sample. Some experience is necessary to handle unique shapes efficiently. Small pieces of sculptured vitrified ware are particularly difficult. The safest setting provides complete support from unfired struts (Fig. 10.47*d*).

Suggested Reading

1. G. C. Kuczyuski, N. A. Hooton, and C. F. Gibson, Eds., *Sintering and Related Phenomena*, Gordon and Breach, New York, 1967.
2. G. C. Kuczyuski, Ed., "Sintering and Related Phenomena", *Materials Science Research*, Vol. 6, Plenum Press, New York, 1973.
3. R. L. Coble and J. E. Burke, *Progress in Ceramic Science*, Vol. III, J. E. Burke, Ed., Pergamon Press, 1963.
4. W. D. Kingery, Ed., *Ceramic Fabrication Process*, Part IV, Technology Press, Cambridge, Mass., and John Wiley & Sons, New York, 1958.
5. W. D. Kingery, Ed., *Kinetics of High-Temperature Process*, Part IV, Technology Press, Cambridge, Mass., and John Wiley & Sons, New York, 1959.
6. J. E. Burke and D. Turnbull, "Recrystallization and Grain Growth in Metals," *Prog. Met. Phys.*, 3, 220 (1952).
7. E. Schramm and F. P. Hall, "The Fluxing Effect of Feldspar in Whiteware Bodies," *J. Am. Ceram. Soc.*, 15, 159 (1936).
8. For additional papers on sintering see: R. L. Coble, *J. Appl. Phys.*, 41, 4798 (1970); D. L. Johnson and I. B. Cutler, *J. Am., Ceram. Soc.* 46, 541 (1963).

Problems

10.1. Distinguish between primary recrystallization, grain growth, and secondary recrystallization as to (*a*) source of driving force, (*b*) magnitude of driving force, and (*c*) importance in ceramic systems.

10.2. Explain why the activation energy for grain-boundary migration corresponds approximately with that for boundary diffusion, even though no concentration gradient exists in the former case.

10.3. Can grain growth during sintering cause compaction of ceramics? Explain. Can grain growth affect the sintering rate? Explain.

10.4. Which of the following processes can contribute increased strength to sintered articles without causing compaction? Explain.
(*a*) Evaporation condensation.
(*b*) Volume diffusion.
(*c*) Viscous flow.
(*d*) Surface diffusion.
(*e*) Solution reprecipitation.

10.5. Assuming the surface energy of $NiCr_2O_4$ is 600 erg/cm² and estimating diffusion data from Cr_2O_3 and NiO data given in Chapter 6, what would be the initial rate of densification for a compact of 1-micron particles at 1300°C? at 1400°C? at 1200°C?

10.6. If pores of 5-micron diameter are sealed off containing nitrogen at a pressure of 0.8 atm in a glass having a surface tension of 280 dyne/cm and a relative density of 0.85, what will be the pore size at which the gas pressure just balances the negative pressure due to the surface tension? What will be the relative density at this point?

10.7. Explain the mechanism of reactive-liquid sintering, such as occurs for Co–WC compositions. Identify two critical solid-liquid interaction characteristics in a system showing this behavior, and describe how you would quantitatively measure them.

10.8. From data collected during sintering of powder compacts of nominally pure simple phase materials at variable heating rates, the observed rates of density change analyzed on an Arrhenius plot frequently give activation energies higher in value than that for lattice self-diffusion. There are three sets of assumptions on which this behavior can be rationalized. Give two examples of suitable assumptions, and explain the behavior on a mechanistic basis.

10.9. During the normal grain growth of MgO at 1500°C, crystals were observed to grow from 1 micron diameter to 10 micron diameter in 1 hr. Knowing that the grain-boundary diffusion energy is 60 kcal/mole, predict the grain size after 4 hr at 1600°C. What effect would you predict impurities will have on the rate of grain growth of MgO? Why?

10.10. Suppose that in order to reduce sintering shrinkage you were to mix enough fine particles (about 30%), 1 micron in diameter, with coarse particles, 50 microns in diameter, so that all the interstices between the coarse particles were filled with fine particles. What would be the rate of shrinkage of this compact? Make a plot of $\log(\Delta L/L_0)$ versus $\log t$, and place the 1-micron powder and 50-micron powder shrinkage lines in their relative positions; then place the shrinkage curves for the composite material in its proper position with respect to the 1-micron and 50-micron curves. Justify your answer.

10.11. A certain magnetic oxide material is believed to follow the normal grain-growth equation. Magnetic-strength properties deteriorate when grain size increases beyond an average of 1 micron. The original grain size before sintering is 0.1 micron. Sintering for 30 min triples the grain size. Because of warping of large pieces, the superintendent of production wants to increase the sintering time. What is the maximum time you would recommend?

10.12. Alumina with MgO is sintered to nearly theoretical density in hydrogen to the point that the optical transmission in the visible range is almost 100%. Actually the material (Lucalox) is not transparent but translucent because of the hexagonal crystal structure of alpha alumina. It is used to contain sodium vapor (at pressures above atmospheric) for street lamps. An alternative candidate for this application is

CaO which is cubic and could be transparent if sintered to theoretical density. Outline your research program if you were to seek to make CaO transparent through sintering.

10.13. The time required to shrink 5% for a compact of 30-micron glass spheres is 209.5 min at 637°C and 5.8 min at 697°C. Compute the activation energy and viscosity of the glass on the basis that surface energy is 300 ergs/cm².